Experimental Studies on 1D Nanomaterials Incorporated Liquid Crystal Nanocomposites

THESIS

Submitted in partial fulfilment

of the requirements for the degree of

DOCTOR OF PHILOSOPHY

by

Mishra Shweta Ravindra

ID:2017PHXF0412P

Under the supervision of

Prof. V. Manjuladevi

BIRLA INSTITUTE OF TECHNOLOGY AND SCIENCE,

PILANI, (RAJASTHAN) INDIA-333031

2023

BIRLA INSTITUTE OF TECHNOLOGY AND SCIENCE, PILANI

CERTIFICATE

This is to certify that the thesis titled “Experimental Studies on 1D Nanomaterials Incorporated Liquid Crystal Nanocomposites” submitted by Mishra Shweta Ravindra, ID No. 2017PHXF0412P for award of Ph.D. of the Institute embodies original work done by her under my supervision.

(Prof. V. MANJULADEVI)
Professor, Department of Physics,
BITS Pilani, Pilani campus, Rajasthan, India

Date:

Dedicated

to

my family

ACKNOWLEDGEMENTS

The completion of this thesis work is a collective effort of people who always stood by me, supported me, and encouraged me on this indelible journey. I am heartily grateful to all and would like to acknowledge them as my token of respect and appreciation.

I am indebted to my supervisor, Prof. V. Manjuladevi, Professor, Department of Physics, Birla Institute of Technology & Science, Pilani for her constant support and guidance. I have learned, implemented, and experienced a whole new world of research under her mentorship. She has always been a kind support, provided generous ideas as well as feedbacks. It’s been a great pleasure of mine to work with her pursuing my doctoral degree.

I am obliged to receive support and rigorous feedbacks from my Doctoral Advisory Committee (DAC), Prof. Anshuman Dalvi and Prof. R K Gupta during the course of my work. Their insightful advice helped me a lot to improve on my research work. I would also like to thank Prof. Rakesh Choubisa, Head, Department of Physics, Birla Institute of Technology & Science, Pilani and previous HoDs, Prof. V. Manjuladevi, Convenor, Department Research Committee, and all previous convenors and all members of DRC for their official support and encouragement during the course of my doctoral degree.

I am thankful to DST-SERB (EMR/2016/005782) and BITS Pilani for the funding. I am thankful to different characterization facilities provided by SIF, CAL, BITS Pilani, Department of Physics, for providing the XRD facility created with the support from DST-FIST (No.:SR/FST/PS-I/2017/30) and Department of Chemical Engineering for providing various experimental facilities (DSC, TGA, ATR-FTIR). I am also thankful to Prof Anshuman Dalvi’s laboratory for allowing me to use some of the experimental facilities available.

I would like to extend my gratitude to Prof. V Ramgopal Rao, Vice-chancellor as well as Prof. Sudhirkumar Barai, Director, all Deans, Associate deans, and previous authorities to give me an opportunity to pursue my doctoral degree in BITS Pilani and for their official support.

I am thankful to our collaborator, Prof. Sandeep Kumar, Raman Research Institute, Bangalore for his support in my research work.

I am also thankful to office staff of Department of Physics, BITS Pilani, Mr Rajeev, Mr Shrikant, Mr Kundan for their official support.

I am thankful to Library, BITS Pilani, for providing support and facilities, literature and help during completion of my report.

I am thankful to Prof Rahul Singhal, MNIT, Jaipur for providing material characterization facilities (TEM).

I sincerely thank my lab-mates Prasoon, Preeti, Samarth, Mudit, Aksah, Amrit, Ashutosh, Dr Parul for their support. It’s a great pleasure for me to acknowledge, especially, my senior Dr Shivaraja S J for his guidance, support, encouragement, and advice. I am also thankful to my colleagues, Dr Dinachandra, Dr Rambabu, Dr Nikita, Khushboo, Aayushi, Anju, Chandrachud, Dhritabrata, Soumana for their constant support.

I would also like to specially acknowledge, Dr Geeta Sharma, UKRI Fellow at School of Chemical and Process Engineering, University of Leeds, Leeds, United Kingdom for her professional as well as personal teachings and lessons about the field of research and the opportunities lying within.

It’s a special mention for my family who have been pillars of my strength throughout my journey and are proud of me achieving new milestones. Sharing all love, care, and happiness with them. Words won’t be enough to express and share my happiness for them.

I would like to acknowledge all the people mentioned or not mentioned heartily to assist me to successfully accomplish one of the milestones of my life.

Mishra Shweta Ravindra

ABSTRACT

"Liquid Crystals" (LCs) are ‘mesomorphic phases’ having symmetries intermediate between those of liquids and crystals. LCs show interesting properties and have potential industrial applications. The shape anisotropy of the constituent molecules is one of the fundamental requirements for the formation of mesophases. The most widely developed application of LCs is in flat panel display technology which potentially uses nematic LCs (NLCs) as their main components. Liquid crystal display (LCD) devices have become indispensable part of modern life because of their wide-spread use in television displays, electronic book readers, digital photo frames, display panels of industrial appliances, personal computers (PCs), smart phones etc. The important properties that LCs offer from application point of view are low driving voltage, low power consumption, low melting point, high clearing point, modest birefringence, low viscosity, large bend to splay elastic constant ratio and low ionic transport number. The main disadvantages that affect the LCD device performance include difficulty in producing black and very dark greys resulting in low contrast ratio, restricted viewing angle, low resolution, slow response times and scan rate conversion resulting in severe motion artifacts and image degradation for moving or rapidly changing images. Nematic LCs (NLCs) cannot emit their own light; hence, backlight becomes an essential component in display devices which in turn increases the power consumption. To overcome the difficulties that emerge during fabrication of LCD devices, industry as well as researchers are taking serious efforts. Modification of physical properties of liquid crystal by dispersion of nanomaterials is widely investigated and the results indicate improvement of display device parameters. Based on the available literature, spherical NPs are observed to decrease the order parameter while elongated particles are expected to fit into liquid crystalline ordering and promote long-range molecular interactions. Also, in some of the reported investigations, spherical particles or quantum dots are observed to form chain-like structures in LC matrix under the influence of nematic orientational ordering which affects the order parameter and behaviour of isotropic-nematic phase transition. Theoretical investigations on nanocomposites of liquid crystal with different shapes and size of nanomaterials suggests that rod-shaped nanomaterials are expected to yield ameliorate long range orientation as compared to its spherical or disc-shaped counterparts. However, there is comparatively less literature available for the systematic experimental investigations for nanocomposites of 1D nanomaterials in NLC. In this thesis, an attempt has been made to experimentally investigate the effect of incorporation of 1D nanostructures on

physical properties of liquid crystals including dielectric anisotropy, elastic constants, threshold voltage, electro-optic response time and ionic conductivity.

To summarize the work presented in this thesis:

Introduction to liquid crystals, its properties, applications, and research background is presented in Chapter 1. The experimental techniques used for synthesis and characterization of the nanomaterials as well as various measurement techniques used to study the electro-optic and dielectric properties of liquid crystals and its nanocomposites are discussed in Chapter 2. The results on effect of incorporation of CdS nanowire capped with oleic acid on behaviour of isotropic-nematic (I-N) phase transition and physical properties of NLC, PCH5 are presented in Chapter 3. Results on effect of synthesized zinc oxide nanorods capped with oleic acid (ZOR) on physical properties of 8CB are presented in Chapter 4. The results of the study indicate that above a critical concentration of ZOR (0.3 wt%) in host LC, ZOR induces vertical alignment of LC molecules in planar/unaligned cells. To study the effect of shape of nanoparticles, further work is carried out in which zinc oxide (ZnO) nanoparticles of different shapes (sphere, rod, wire) are synthesized without any functionalization. The results on effect of these ZnO NPs on physical properties of PCH5 are presented in Chapter 5. The results of the study indicate that incorporation of ZnO nanorods and ZnO nanowires helps better dispersion, alignment and improved physical properties of nanocomposite samples as compared ZnO nanospheres in NLC. In continuation to this work, results on effect of size of ZnO nanorods with similar aspect ratio but different size (diameter: length), on physical properties of PCH5 are presented in Chapter 6. Results of the study indicate that properties of PCH5 can be tuned by variation in size as well as concentration of nanorods in NLC. The conclusion of the work done in the thesis followed by the future scope of the work is presented in Chapter 7.

TABLE OF CONTENTS

LIST OF SYMBOLS

$\hat{n}$	**Director**
$\Delta\varepsilon$	Dielectric Anisotropy
Δn	Birefringence
$\varepsilon_{\parallel}$	Parallel component of dielectric permittivity
$\varepsilon_{\perp}$	Perpendicular component of dielectric permittivity
σ_{ac}	Bulk ac conductivity
$\sigma_{\parallel}$	Parallel component of Bulk ac conductivity
$\sigma_{\perp}$	Perpendicular component of Bulk ac conductivity
S	Order parameter
V_{th}	Threshold Voltage
k_B	Boltzmann Constant
θ	Angle between long axis of the molecule and director
ε'	Real Part of complex dielectric permittivity
ε''	Imaginary Part of complex dielectric permittivity
f_R	Relaxation Frequency
E_A	Activation Energy
τ_r	Rise time
τ_d	Decay Time
τ	Total Response time
K_{11}	Splay Elastic Constant
K_{33}	Bend Elastic Constant
T_{IN}	Isotropic to nematic phase transition temperature
$T - T_{IN}$	Reduced temperature

LIST OF TABLES

LIST OF FIGURES

This page is intentionally left blank

CHAPTER 1

INTRODUCTION

Conventionally, the common states of condensed matter are distinguished as solid, liquid and gas. The liquid state has highest possible symmetry but no long-range order. The crystalline solid state has much lower symmetry than the liquid state but shows long-range positional and orientational order. Between these extremes, there exists systems that have symmetries intermediate between those of liquids and crystals. These ‘mesomorphic phases’ grouped together are called "Liquid Crystals" (LCs) [1,2]. The field of LCs have attracted many researchers due to their interesting properties and potential industrial applications. The history of the invention of these mesomorphic phases, experimental and theoretical advancements and their applications is summarized in Table1-1. The shape anisotropy of the constituent molecules is one of the fundamental requirements for the formation of mesophases. The important properties that LCs offer from application point of view are low driving voltage, low power consumption, low melting point, high clearing point, modest birefringence, low viscosity, large bend to splay elastic constant ratio (K_{33} /K_{11}) and low ionic transport number. The most widely developed application of LCs is in flat panel display technology which potentially uses nematic LCs (NLCs) as their main components. Liquid crystal display (LCD) devices have become indispensable part of modern life because of their wide spread use in television displays, electronic book readers, digital photo frames, display panels of industrial appliances, personal computers (PCs), smart phones etc. [3]. Apart from display, LCs also can be used for potential applications in the field of photovoltaics[4–6], organic light emitting diodes, organic field effect transistors, 2D optoelectronics and photonics[7] as well as biomedical applications such as drug delivery and sensing (Fig 1-1). The main disadvantages that affect the LCD device performance include difficulty in producing black and very dark greys resulting in low contrast ratio, restricted viewing angle, low resolution, slow response times and scan rate conversion resulting in severe motion artifacts and image degradation for moving or rapidly changing images. Nematic LCs (NLCs) cannot emit their own light; hence, backlight becomes an essential component in display devices which in turn increases the power consumption. Constant efforts are made by industry as well as researchers to overcome the difficulties that emerge during fabrication of LCD devices.

Table 1-1 History of evolution of liquid crystals (Theory and Applications)[2,8,9]

Year	Researcher	Research Area	Observation/ Research
1850-1888	R Virchow, C Mattenheimer, G Valentine	Biologist	Unusual effects under polarized light shown by nerve fibres
1877	Otto Lehmann	Physicist	Constructed Heating stage and added polarizers to microscope
	P Planer W Lobisch B Raymann		Striking colours on cooling of cholesterol compounds
	W Heintz		Unusual melting behaviour of stearin (fat)
1888	F Reinitzer	Biologist	Cholesterol Derivatives in plants show[1] • 2 melting points • Blue colour upon cooling from liquid phase • Blue-violet colour near crystal transition
	Otto Lehmann		Coined term “LIQUID CRYSTALS”
	L Gattermann A Ritschke		Synthesis of first LC (p-azoxyanisole, PAA)
	G Tammann W Nerst	Chemist Physicist	Suggested that LC maybe a mixture/emulsion
	O Lehmann R Schenk		LC is a Single Phase
1900	D Vorlander	Chemist	Synthesized many new LCs Single LC material possessing many LC phases Suggested that molecules with linear shape are more likely to be liquid crystalline
	E Bose	Physicist	Attempted to give complete theory of LCs base on molecular structure
	M Born		Separation of charges causes basic interaction in linear molecules leads to LC phase
1922	G Freidel	Minerologist	Proposed classification using words Nematic, Smectic, Cholesteric Molecular ordering Defect structures Layer structure of Smectic LC Orientation of LC by electric field
1922-1942			Theoretical work on elastic properties of LC
1925	C Oseen	Physicist	Continuum theory (Oseen’s theory of nematics)
			X-ray Experiments to prove that order in LCs is more than liquids but less than solids Effect of electric and magnetic field on LC Light scattering properties of LCs
1927 1933	Zocher Freedericksz & Zolina	Physicist Physicist	Freedericksz transition[10]
1942-1945			Flow properties of LCs in high electric and magnetic fields
1949	Onsager	Physical Chemist	Statistical theory of nematics[11]
1957	G Brown		Published: Review of LC phase
1958			Faraday Society of London held a conference

1958	F C Frank	Physicist	Developed Oseen’s theory of nematics (Oseen-Frank theory)
1950-1959			the development of LC thermometers using cholesteric LC.
1961	Ericksen		Generalization of static theory of nematics
1962	G Gray	Chemist	Published a book: Molecular structure and properties of LCs
	Brown		Establishment of Liquid crystal Institute @ Kent State University
			Series of International conference (ICLC)
			the switchable orientation of LC molecules was first utilised in laser devices
	W Maier A Saupe	Physicist	Microscopic Theory of Liquid crystals No separation of charges
1964	Scientists @RCA		Switching of Thin layer of LC on application of voltage (first LCD)
1965	George H. Heilmeier	Engineer	the first prototype LCD was developed [12]
1966-1968	Leslie		Dynamic theory for NLCs
1969	Fischer & Fredrickson		Experiment on unusual scaling law of Poiseuille’s flow
1970	Atkin		Theoretical prediction of unusual scaling law of Poiseuille’s flow
Late 1960s	Leslie		Dynamic theory for cholesterics
1971			LC turns clear to black by application of voltage Improved display quality and low power consumption
1969-1971			the first twisted nematic cell displays were developed from the initial work of Martin Schadt and incorporated in display devices
1971			LC turns clear to black on application of voltage Improved display quality and low power consumption
1974	W MacMillan R Meyer		proposed a mean-field theory for smectic.
1977	S Chandrasekhar	Physicist	reported the existence of discotic liquid crystals[13]
1980-1990			LCDs found widespread application in small mobile devices as the display of choice
Late 1990s	Leslie Carlson Laverty		Proposed biaxial nematic theory
1991	Leslie Stewart Nakagawa		Nonlinear static and dynamic theory for non-chiral SmC LCs
1991	PG de Gennes		Nobel Prize Landau - de Gennes theory

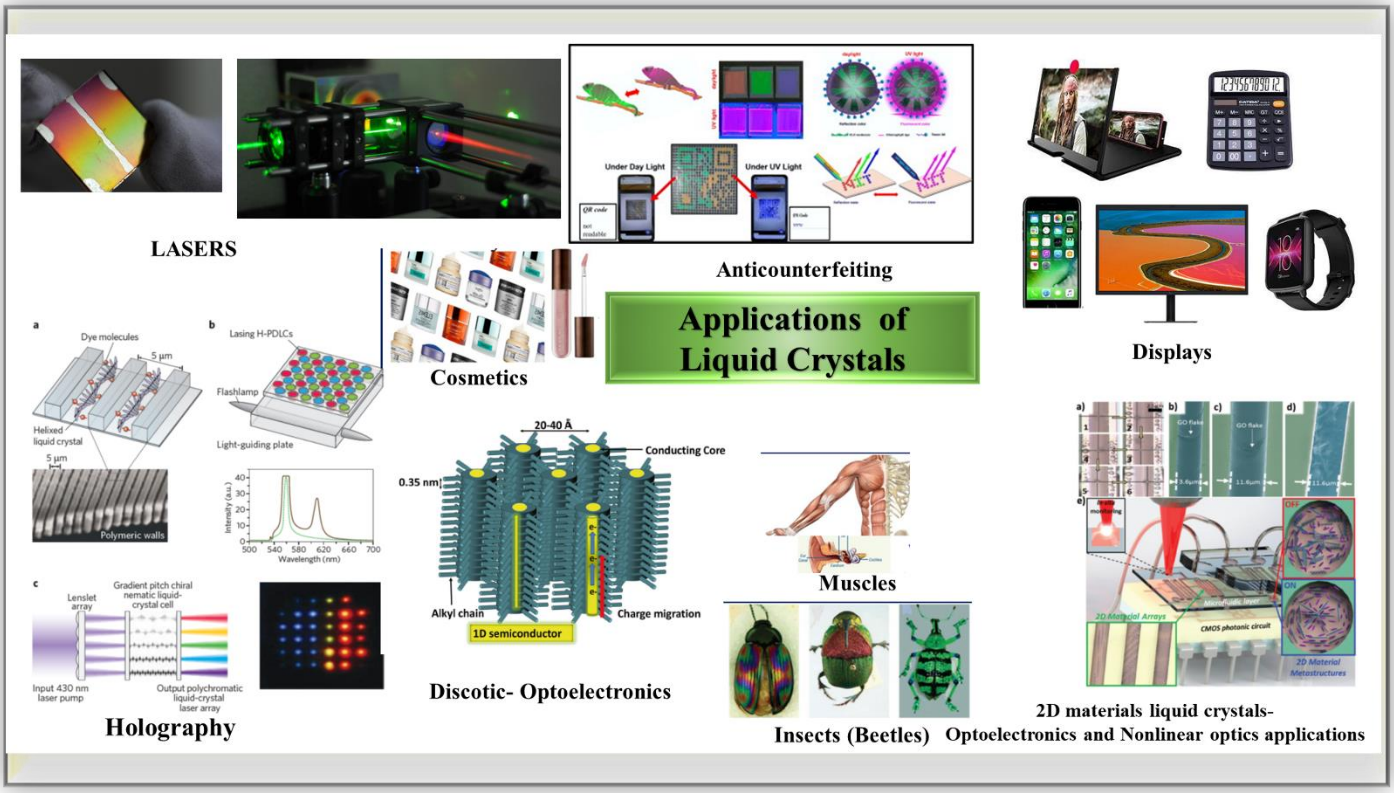

Figure 1-1 Applications of liquid crystal (**Collage is prepared using Images taken from the reports cited in the text)*

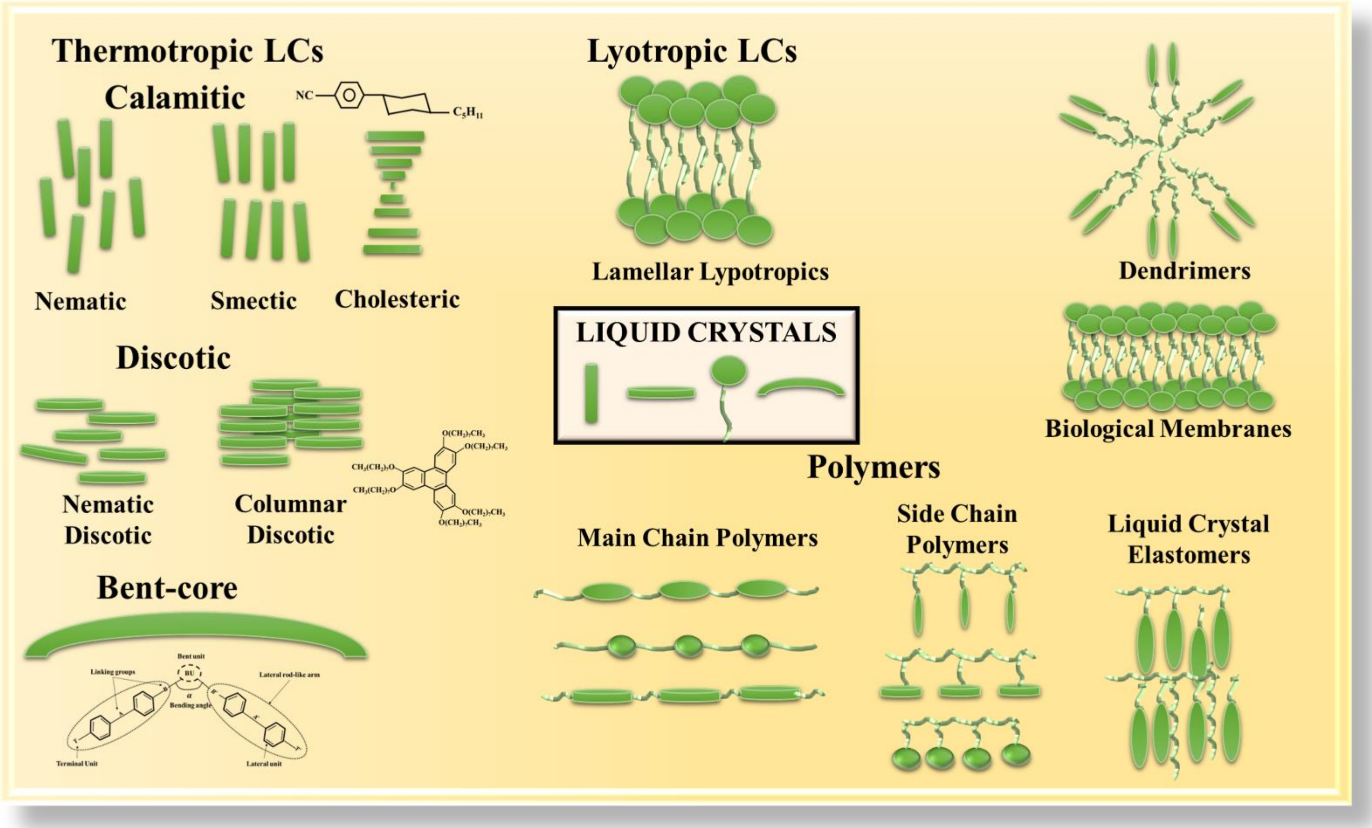

Figure 1-2 Classification of liquid crystal phases

1.1 CLASSIFICATION OF LIQUID CRYSTALS

Based on various shapes and external stimuli (temperature, concentration etc.) responsible for formation of mesophases, liquid crystal phases are classified as shown in the Fig 1-2. Based on the parameter governing phase transition, liquid crystals can be classified as follows:

Thermotropic liquid crystals:

Thermotropic liquid crystals are the liquid crystal compounds that show phase transition with the variation of temperature. These compounds exhibit liquid crystalline mesophases in defined temperature range. If the formation of mesophases is stable with increasing as well as decreasing temperature, i.e., heating, and cooling cycles, then such LCs are termed as enantiotropic LCs. If the mesophase formation is observed only during cooling cycles, then these mesophases are termed as monotropic LCs. Generally, thermotropic LC phases are exhibited by low molecular weight compounds.

Lyotropic liquid crystals:

Lyotropic liquid crystals are formed by dissolving amphiphilic mesogens in solvent under appropriate conditions of concentration, pressure, and temperature. In lyotropic LCs, constituent molecules are observed to form aggregates with well-defined geometries such as lamellar, cubic, hexagonal etc.

Polymer liquid crystals:

Some of the high molecular weight polymeric compounds are also observed to exhibit LC mesophases. These are called polymer liquid crystals. They can be further classified into main chain polymers and side chain polymers.

Thermotropic LCs are further classified based on the shape of constituent molecules as follows:

Calamitic liquid crystals

Calamitic liquid crystals are made up of elongated, rod-shaped molecules. Generally, they are composed of three main structural elements: rigid ring systems, connective linkage groups, and flexible terminal groups. Based on the orientational and positional order present, they can be classified further as nematic, smectic and cholesteric.

Discotic liquid crystals

Discotic liquid crystals are made up of disc-shaped molecules. Generally, they are composed of central rigid aromatic core and numerous flexible alkyl chains in the periphery. These molecules can form columnar assemblies and show unique functional properties like unidimensional charge conduction and aggregation-induced emissive/quenching phenomenon.

Bent-core liquid crystals

Bent core liquid crystals are made up of molecules having bent-shaped rigid core instead of a linear one. There are three main groups of such materials: (i) molecules containing a rigid bent aromatic core (ii) mesogenic dimers with an odd-numbered non-cyclic spacer unit and (iii) hockey-stick molecules, where an alkyl chain is attached at one end of an aromatic core. Bent-core liquid crystals show polar order and chiral superstructures in their LC mesophases, despite the constituent molecules of these mesophases being achiral.

Based on the symmetry of the medium, Calamitic LCs are further classified as:

Nematic liquid crystal

Nematic liquid crystals (NLC) are the most common and simplest form of LCs. NLCs made up of rod-shaped molecules exhibit long range orientational order but no translational order. The average direction of orientation of long axes of the molecules is known as director ($\hat{\boldsymbol{n}}$). NLCs are the least ordered thermotropic LC phases. Some of the characteristic properties of NLCs are:

- The isotropic to nematic phase transition is weakly first order discontinuous phase transition.
- The director ($\hat{\boldsymbol{n}}$) is dimensionless apolar unit vector, i.e., $\hat{\boldsymbol{n}}\ and - \hat{\boldsymbol{n}}$ are equivalent
- Due to long range orientational order of constituent molecules, NLCs show anisotropy in its different physical properties such as dielectric, optical and conductivity properties.
- NLCs can be deformed easily with weak external perturbations.

Smectic liquid crystals

Smectic liquid crystals are characterized by presence of quasi-long range 1D or 2D translational order along with the orientational order. Among all the known smectic LC phases, smectic A and smectic C are least ordered in which constituent molecules show quasi-long range 1D order.

Cholesteric liquid crystals

Cholesteric phase is observed in nematic LCs made up of optically active molecules. Hence, it is also termed as chiral nematic LC phase. The direction of average orientation of molecules (director) rotates in a helical fashion. The distance along the helix over which complete 360° rotation of director is observed is called helical pitch.

The current thesis work is mainly focused on the modifications of the properties of calamitic nematic liquid crystals.

1.2 PROPERTIES OF NEMATIC LIQUID CRYSTALS

The physical properties of NLCs such as dielectric, optical, conductivity properties are anisotropic. These anisotropic properties of NLCs are highly sensitive to the changes in the external stimuli such as temperature, pressure, electric and magnetic fields. Hence, the basic understanding of the changes in the physical properties of NLCs with external stimuli is important.

1.2.1 Order Parameter

NLCs are characterized by the presence of long range orientational order. Orientational order can be described as the extent to which the long axis of the molecules is aligned in a particular direction. The average direction of preferred orientation of long axes of the molecules in NLCs is known as director ($\hat{\boldsymbol{n}}$). The degree of order can be quantified by orientational order parameter (S) given as

$$\mathrm{S} = \frac{1}{2}\langle 3cos^2\theta - 1\rangle$$

where, θ denotes the angle made by long axis of the molecule with $\hat{\boldsymbol{n}}$ (Fig 1-3). For isotropic liquid S =0 whereas S=1 for perfectly aligned nematic. Generally, the value of S varies from 0.3 to 0.8 in NLCs. The value of S is temperature dependent, and it decreases as the temperature of the system increases. It can be correlated with experimentally measured parameters such as dielectric anisotropy and birefringence[14,15].

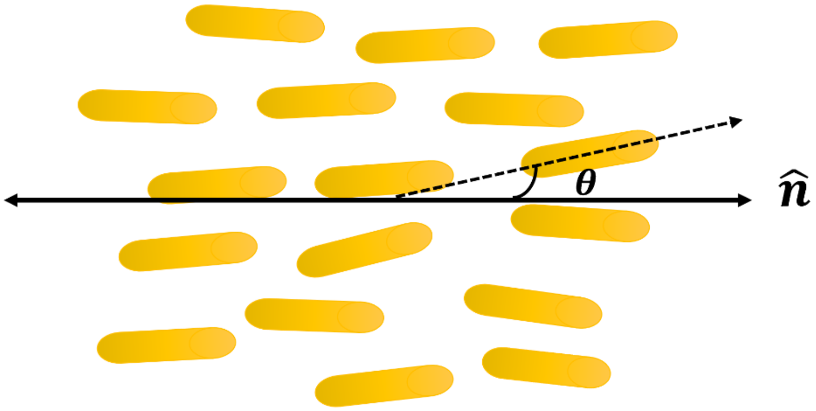

Figure 1-3 Schematic representation of nematic phase of calamitic LCs: $\hat{\boldsymbol{n}}$ denotes director; θ denotes the angle made by long axis of the molecule with $\hat{\boldsymbol{n}}$

1.2.2 Dielectric Properties

Measure of a response of the material on the application of external electric field is termed as dielectric permittivity (ε). Generally, for NLCs, the variation of ε with temperature and frequency gives the information on molecular polarizability, dipole moments, intermolecular interactions, and relaxation processes.

The dielectric anisotropy ($\Delta\varepsilon$) is defined as

$$\Delta\varepsilon = \varepsilon_{\parallel} - \varepsilon_{\perp}$$

where, $\varepsilon_{\parallel}$ is the dielectric permittivity measured when the applied external electric field is in the direction parallel to that of the director and $\varepsilon_{\perp}$ is the dielectric permittivity measured when the applied external electric field is in the direction perpendicular to that of the director. For positive dielectric anisotropy NLCs, $\Delta\varepsilon > 0$, i.e., $\varepsilon_{\parallel} > \varepsilon_{\perp}$ whereas for negative dielectric anisotropy NLCs, $\Delta\varepsilon < 0$, i.e., $\varepsilon_{\parallel} < \varepsilon_{\perp}$.The description of both positive and negative $\Delta\varepsilon$, the observed temperature dependence of the principal dielectric constants $\varepsilon_{\parallel}$ and $\varepsilon_{\perp}$ and the existence of a special $\varepsilon_{\parallel}$-dispersion is given by Maier-Meier theory[16]. Maier- Meier theory is a hybrid theory which considers the Onsager's theory of static dielectric polarization of a dipole along with the anisotropy of the molecular polarizability, the orientation of the permanent dipole moment in the molecule and the long-range nematic order. They introduced an additional contribution to the interaction energy of the system dependent on the orientation of the molecules, the nematic potential U_i. The orientation distribution of the permanent dipoles determining part of the potential energy is given by Onsager theory as

$$U_i = -h(\overline{\mu^*}\bar{E})$$

where, h- cavity field factor, $\overline{\mu^*}$- dipole moment and $\bar{E}$ is applied electric field vector.

In a simplified version neglecting internal field and polarization effects, the mean square dipole moments parallel $\langle\mu_{\parallel}^2\rangle$ and perpendicular $\langle\mu_{\perp}^2\rangle$ to the director

$$\langle\mu_{\parallel}^2\rangle = \frac{\mu^2}{3k_BT}\,[1-(1-3cos^2\Psi)S]\,E$$

$$\langle\mu_{\perp}^2\rangle = \frac{\mu^2}{3k_BT}\left[1+\frac{1}{2}(1-3cos^2\Psi)S\right]\,E$$

is obtained where Ψ is the angle between the direction of dipole moment and the long axis of the molecule (k_B is the Boltzmann constant and T the temperature). The difference in the quasi static permittivities parallel ($\varepsilon_{s,\parallel}$) and perpendicular ($\varepsilon_{s,\perp}$) to the director based only on the orientation is

$$\delta\varepsilon = \varepsilon_{s,\parallel} - \varepsilon_{s,\perp} = -\,\frac{\mu^2}{2k_BT\varepsilon_0}\frac{N}{V}\,(1-3cos^2\Psi)S$$

where N is the number of dipoles/ number density of molecules, V the volume of the system and ε_0 is the permittivity of free space. With the addition of molecular polarizability, a shift component (based on polarizability anisotropy) is added to the total anisotropy function. Hence, the total dielectric anisotropy ($\Delta\varepsilon$) of the system can be described as

$$\Delta\varepsilon = \frac{NhF}{\varepsilon_0}\left[\Delta\alpha - \frac{F}{2k_BT}\,\mu^2\,(1-3cos^2\Psi)\right]S$$

The sign of the dielectric anisotropy $\Delta\varepsilon$ is positive if Ψ is small. Generally, for $\Psi > 55°$, the sign of $\Delta\varepsilon$ is observed to be negative.

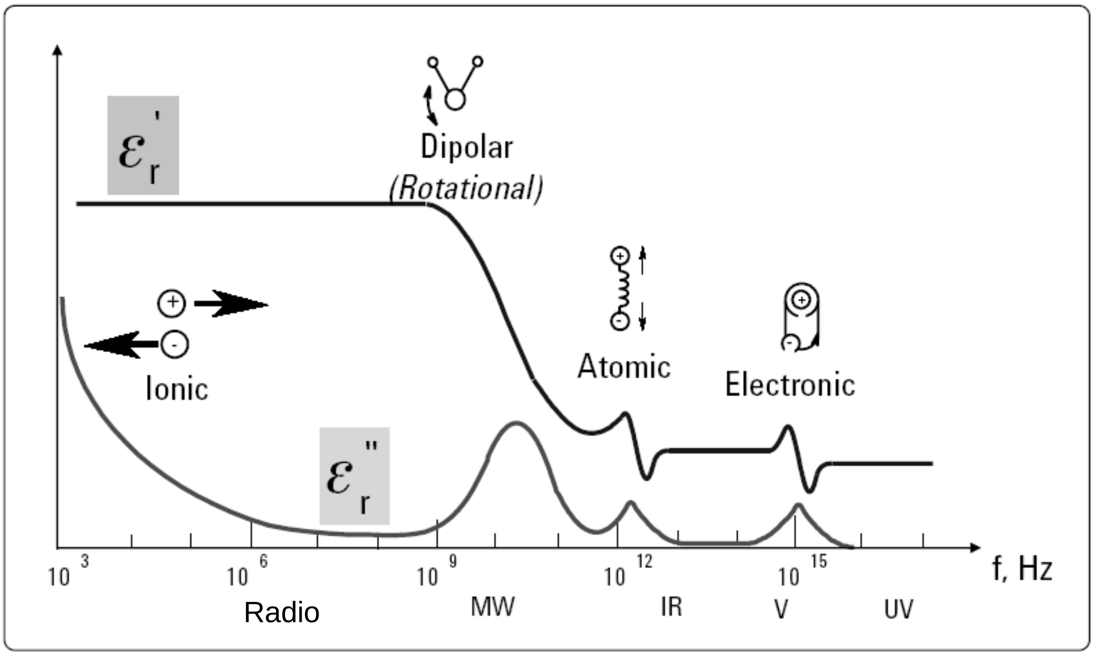

Figure 1-4 Frequency response of relaxation mechanisms of a dielectric material (Reprinted from Ref 14)

The response of a sample to an external applied electric field of varying frequency is studied by dielectric spectroscopy (DS) also known as impedance spectroscopy [17]. The relaxation processes in a typical dielectric material are categorized as shown in Fig1-4 [18]. DS can provide information on the structure of matter, ion displacement, valence cloud distortion, defect displacement, state and local space-charge electric moment orientation, etc.[18,19]. The highlight of this technique is the measurement of various dielectric parameters in a range of frequencies from10^{-6} Hz to10^{12} Hz. These measurements can also be performed under different temperatures, pressures, and environmental conditions, permitting one to observe a large variety of mechanisms at very different timescales. In this experimental window, molecular and collective dipolar fluctuations, charge transport, and polarization effects occur, and these effects help, in turn, to determine the dielectric response of the material of interest. The complex dielectric function (ε^*) has its foundation in Maxwell's equations. It describes – within the regime of linear response – the interaction of electromagnetic waves with matter and underlying molecular mechanisms. The variation of ε^* as a function of frequency can be described by a generalised relaxation function[20,21]

$$\varepsilon^*(\omega) = \varepsilon_\infty + \frac{\delta\varepsilon}{((1+i\omega\tau)^\alpha)^\beta} - i\frac{\sigma}{2\pi\varepsilon_0 f^n}$$

where f denotes frequency, ω denotes angular frequency, α and β are the shape parameters describing the asymmetry and broadness of the dielectric dispersion curve at higher frequencies. For $\alpha = \beta = 1$, the famous Debye function [21] is obtained. The third term accounts for the contribution of conductivity (σ) in very low frequency region ($\mathrm{mHz} - \mathrm{few\ Hz}$), with n as fitting parameter. The plot of imaginary part (ε") $vs\ real\ part$ (ε') of dielectric permittivity showing Debye type relaxation mechanism is Cole-Cole plot. The measured dispersion of ε' in Cole-Cole plot can be described by [22]

$$\varepsilon' = \varepsilon_\infty + [\varepsilon_s - \varepsilon_\infty/(1 + \omega^2\tau_1^2)]$$

where, low frequency limit of the Cole-Cole plot is static dielectric permittivity, ε_s, whereas high frequency limit is ε_∞ and τ_1 is relaxation time. The difference ($\delta\varepsilon = \varepsilon_s - \varepsilon_\infty$) is known as dielectric strength. Meier and Saupe [23] correlated τ_1 with the ordinary Debye relaxation time τ_0 by a retardation factor $g = \frac{\tau_1}{\tau_0}$ which can be calculated approximately as $g = k_B\tau_1 W \exp\left(\frac{W}{k_B T}\right)$, where, W is the height of the potential barrier due to intermolecular forces hindering the reorientation of the molecules in the parallel direction.

The relaxation processes generally observed in NLCs follow an Arrhenius type dependence

$$f_r = f_\infty \exp(-E_A/k_B T)$$

where, k_B is the Boltzmann constant, and E_A is the activation energy corresponding to the flip-flop motion of molecules about their short axes. f_∞ corresponds to the relaxation rate in the high temperature limit.

The salient features of measured variations of $\varepsilon_\parallel(\omega)$ and $\varepsilon_\perp(\omega)$ using aligned samples of NLCs, over a wide frequency range (radio($\sim 10^6 Hz$) and microwave($\sim 10^9 Hz$) frequencies) are [2]:

i. Both $\varepsilon_\parallel(\omega)$ and $\varepsilon_\perp(\omega)$ usually show a Debye type relaxation at microwave frequencies ($10^9 Hz$). Similar relaxation is also found in isotropic phase.

ii. In the measurement of parallel component of dielectric constant $\varepsilon_\parallel(\omega)$ which determines component of electric dipole along long axis of a molecule, an additional relaxation process is observed at lower frequencies (radio frequencies). The effect was discovered by Maier and Meier and interpreted by Meier and Saupe in terms of a 180° rotation of a molecule around one of the short axes of the molecule. For a long molecule, such a rotation is obviously difficult in the nematic phase and the resulting relaxation rate is comparatively slow- typically 10^3times slower (in MHz) than the rotations around the long axis.

1.2.3 *Fréedericksz transition and Elastic constants*

External applied electric field ($\vec{\boldsymbol{E}}$) couples to the NLC medium through its dielectric anisotropy ($\Delta\varepsilon$). The orientational part of the energy density is given by $-\varepsilon_0 \Delta\varepsilon\ (\hat{\boldsymbol{n}} \cdot \vec{\boldsymbol{E}})^2/2$. Applying external field to uniformly aligned sample, orientation due to surface anchoring competes with that due to applied field causing a distortion in the original director field. In a planar aligned LC sample, when strength of applied electric field exceeds threshold electric field (E_{th}) which is slightly higher than or comparable to surface anchoring energy, distortion in the orientation of the director is observed. This is known as Fréedericksz transition (Fig 1-5b) [10]. The free energy of the distorted state is described initially by Oseen& Zocher[24] which was further elaborated by Frank[25]. Free energy density due to distortion in $\hat{\boldsymbol{n}}$ is given as

$$F_d = \frac{1}{2} K_{11}\ (div\, \hat{\boldsymbol{n}})^2 + \frac{1}{2} K_{22}\ (\hat{\boldsymbol{n}} \cdot curl\, \hat{\boldsymbol{n}})^2 + \frac{1}{2} K_{33}\ (\hat{\boldsymbol{n}} \times curl\, \hat{\boldsymbol{n}})^2$$

This free energy density is known as the Frank-Oseen free energy density and is the fundamental formula for continuum theory for nematics. The elastic constants K_{ii} (i = 1, 2, 3) are respectively associated with three types of deformations shown in Fig 1-5.

K_{11} : conformation with $div\, \hat{\boldsymbol{n}} \neq 0$ (splay)

K_{22} : conformation with $\hat{\boldsymbol{n}} \cdot curl\, \hat{\boldsymbol{n}} \neq 0$ (twist)

K_{33} : conformation with $\hat{\boldsymbol{n}} \times curl\, \hat{\boldsymbol{n}} \neq 0$ (bend)

Generally,

1. $K_{33} > K_{11} > K_{22}$;
2. $K_{ii} \propto S^2$;
3. the value of K_{ii} decreases with increasing T;
4. their ratio is nearly independent of T.

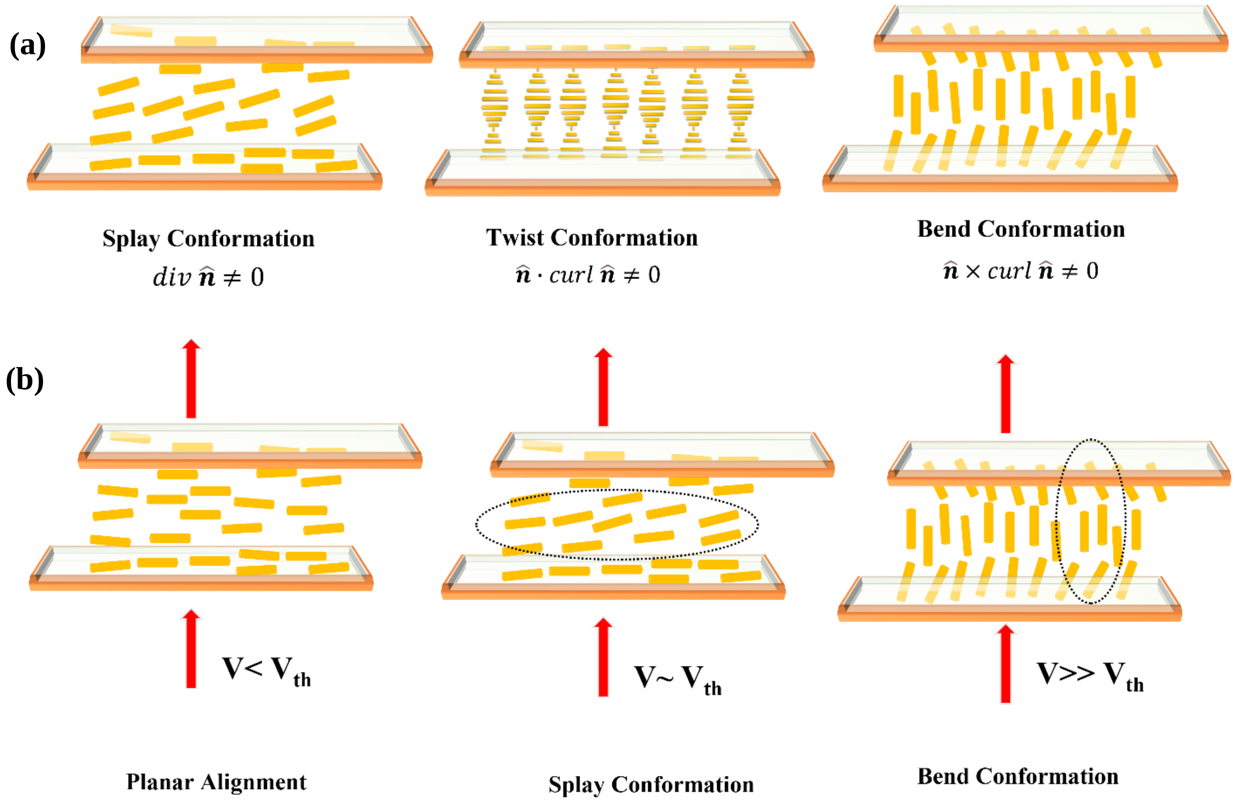

Figure 1-5 Schematic showing (a) different deformations (b) splay and bend deformations as a function of applied field for calamitic nematic liquid crystal filled in planar aligned cell

The use of LCs in devices require modification in their characteristic properties because, generally, single LC material is observed not to exhibit all the desired properties. In view of this, many researchers have been trying to synthesize new LC materials with different structures which can exhibit optimized properties required for device application. This approach seems to be tedious and time-consuming. One of the approaches for modification of properties of LCs is mixing of several LCs to enhance the characteristic features of the mixture which is commercially used technology in present days. With the emergence of nanotechnology, the research on the composite systems of nanomaterials in the LC hosts has shown promising results with improved physical properties for device applications[26]. This approach seems to be promising as compared to the ones mentioned above for modification of properties of LC host.

1.3 NANOSCIENCE AND NANOTECHNOLOGY

Nanotechnology [27,28] has emerged as one of the most promising technologies of the 21st century. The study, manipulation and engineering of matter, particles, and structures on the nanometre scale is referred to as ‘Nanoscience’. With the dominance of quantum mechanical effects, nano-structures differ in various properties from their bulk counterparts. This scientific field stands at the interface between physics, chemistry, materials science, microelectronics, biochemistry, and biotechnology which thus requires a multidisciplinary scientific exploration.

Two approaches have been developed for the synthesis of nanostructures: top-down and bottom-up approach (Fig1-6). The top-down approach is the breaking down of bulk material to get nano-sized particles achieved by using advanced techniques such as precision engineering and lithography which have been developed and optimized by industry during recent decades. Top-down approach consists of various methods, including mechanical milling, electrospinning, lithography, sputtering, arc discharge, and laser ablation methods. Next, the bottom-up approach refers to the build-up of nanostructures atom-by-atom or molecule-by-molecule by physical and chemical methods which are in a nanoscale range using controlled manipulation of self-assembly of atoms and molecules. This includes chemical vapor deposition (CVD), solvothermal and hydrothermal, sol–gel, and reverse micelle methods. Chemical synthesis is a method of producing materials used either directly in product in their bulk disordered form or as the building blocks of more advanced ordered materials. Self-assembly is a bottom-up approach in which atoms or molecules organize themselves into ordered nanostructures with the help of physico-chemical interactions.

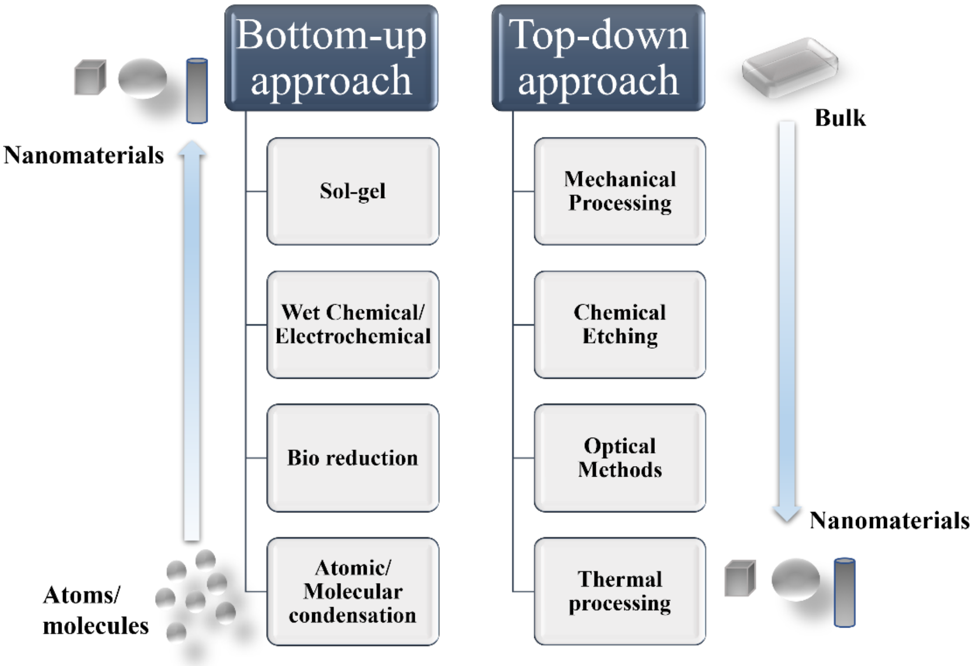

Figure 1-6 Different methods used generally for synthesis of nanomaterials.

The nanomaterials family includes metal-based nanomaterials, carbon-based nanomaterials, ultrathin 2-dimensional nanomaterials, nanoporous materials and core–shell materials. Carbon-based nanomaterials are a fascinating class of nanomaterial, consisting of fullerenes, carbon nanotubes, carbon-based quantum dots and graphene. After isolation of graphene in 2004 from graphite, large interest in applications of ultrathin 2D materials is witnessed due to their numerous exceptional features. Several ultrathin nanomaterials including silicene, borophene, antimonene, MXenes, 2D MOF nanosheets, and boron nitride nanosheets have been reported. Currently, more efforts are being made on producing nanomaterials with controlled morphologies and nanoscale dimensions to achieve the desired outcomes because of well-organized nanostructures. By using nanotechnology, some commercial devices have already been introduced. Submicron-sized tin oxide particles are a key component of white paints. Zinc oxide and tin oxide nanoparticles are used in commercial sunscreens.

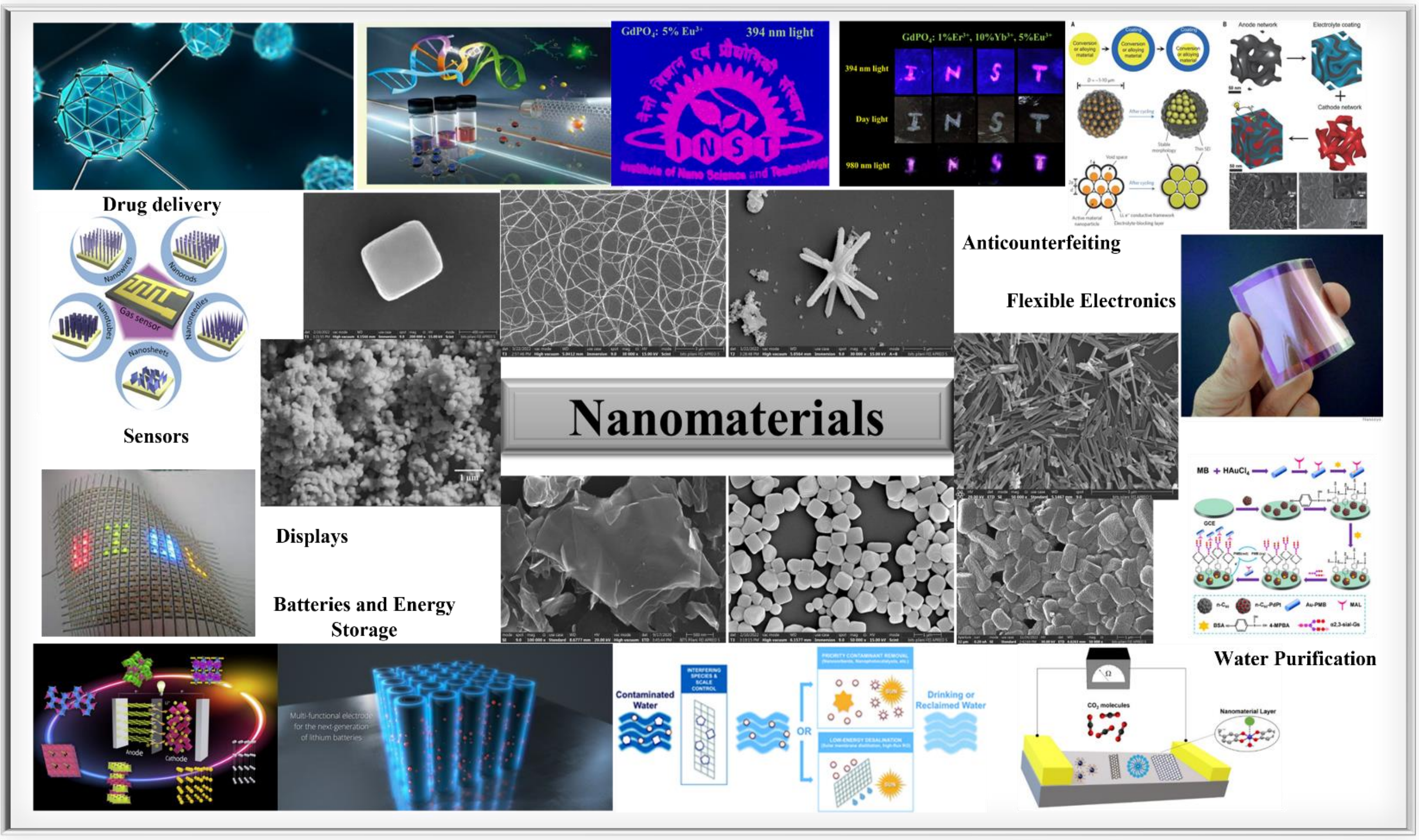

Figure 1-7 Nanomaterials and its applications

*Collage is prepared using Electron microscopy images from our work and Images showing various applications taken from reports cited in the text

In commercial LCDs, colour pigments with crystalline sizes of < 40 nm are introduced to provide better colour purity, brightness, and contrast for high-definition display-based applications.

The properties of matter at the nanoscale level are substantially distinct compared to their bulk counterparts as size-dependent effects become more prominent at the nanoscale. Tuning the nanomaterial size provides a pathway to tune the properties of nanomaterials. Among a range of unique properties, the following key properties can be obtained upon tuning the sizes and morphologies of nanomaterials.

i. High surface area to volume ratio
ii. High thermal and electrical conductivity
iii. Excellent mechanical properties
iv. Dominant quantum mechanical effects
v. Rich surface textural features
vi. Enormous number of binding sites
vii. Discretization of band structure

Currently, researchers are concentrating on the development of randomly shaped nanomaterials as well as rational design of materials with controlled nano-architectures for boosting their performances for specific applications. As particle morphology is a crucial factor in the performance of nanomaterials for specific applications. The same materials with different morphologies can produce different outcomes. In the literature, many nanostructured materials[29–31] such as nanotubes [32–34], nanorods[35–37], nanoflowers[38], nanosheets[39], nanowires[40–42], nanocubes[43,44], nanospheres[45], nanocages have been reported for a range of applications (Fig 1-7). Currently, huge numbers of theoretical and experimental studies of nanomaterials and their applications have been witnessed. Most nanomaterials are being engineered for lab scale applications, and serious efforts are being made to bring them to the commercial market. Future technologies depend upon effective manipulation of nanoscale materials for various applications. However, the development and effective utilization of nanomaterials involve many challenges. To mention a few:

i. The presence of defects in nanomaterials can affect their performance and their inherent characteristics can be compromised.

ii. The synthesis of nanomaterials through cost-effective routes is another major challenge. High-quality nanomaterials are generally produced using sophisticated instrumentation and harsh conditions which limit their large-scale production.
iii. The agglomeration/ aggregation of particles at the nanoscale level is an inherent issue that substantially damages performance of devices in relevant fields. The process of agglomeration may be due to physical entanglement, electrostatic interactions, or high surface energy.

1.4 NANOCOMPOSITES OF LIQUID CRYSTALS

Nanomaterial assisted improvements in the characteristics of liquid crystals (LCs) have attracted a great deal of interest from researchers worldwide [26,27]. The extreme size-dependent characteristics of nanomaterials provide an easy pathway to tailor their properties. In the composite systems of nanomaterials and LCs, both size and shape of NPs affect the properties of LCs. Generally, spherical NPs are observed to decrease the order parameter while elongated particles fit into liquid crystalline ordering and promote long-range molecular interactions[46]. In the present thesis work, calamitic LC hosts comprising of rod-shaped molecules are used. The addition of 1D nanomaterials which has similar shape anisotropy as that of the host LC under investigation is expected to be a good choice amongst the nanomaterials. Further, the miscibility of the nanomaterial with the host LC along with its aspect ratio is expected to play a major role in the alteration of properties of host LC.

Various research groups have tried doping metallic (e.g. Ag, Au) [47], ferroelectric (e.g. BaTiO3)[48], semiconducting (e.g. ZnS, ZnO, PbS, TiSiO4, etc.)[49–52], magnetic (e.g. Fe3O4) nano particles in LC matrix which showed improvement in physical parameters such as switching time, threshold voltage, elastic constant, contrast ratio etc. Dispersion of ferroelectric nanoparticles in NLC leads to enhancement in the dielectric anisotropy and the orientational order of NLC [53]. Dispersions of ultrasmall magnetic needles or platelets results in ferronematic domains, which can be reoriented by weak magnetic fields and allow thresholdless optical switching in electric fields [54,55]. Anisotropic nanostructures such as nanorods, nanowires, nanotubes, nano platelets, nanoflowers etc. have also been used as dopants in LCs by few research groups. Apart from these, incorporation of carbon-based nanomaterials such as single- and multiwalled carbon nanotubes (S/MWCNTs) [56,57], graphene flakes [58,59], graphene QDs (GQDs), fullerenes, carbon dot [60] have also been immensely investigated. Switching behaviour of cylindrical shaped LC molecules plays a crucial role in display devices. Nematic phase exhibited by calamitic liquid crystals is the most useful of all the LC phases for display devices because of their long range orientational order, low viscosity, and large elastic constant ratio. NLCs composed of cylindrical shaped molecules are easy to align and switch at low strengths of electric fields as compared to their other shape anisotropic counterparts, discotic and bent core nematic. NLC with unidirectional orientational order are naturally suited for hosting 1D nanoparticles (1D-NPs), such as nanorods, nanowires and nanotubes [50–52,61–65]. For composite system of NP in NLC, Osipov et al.[66], Egorov et al.[67], and recently Orlandi et al. [68] predicted that the shape of NPs strongly affects the interactions between NP and host LC molecules. [35,36]. Uniaxial deformed particles such as rods and discs are expected to stabilise the nematic order and widen the nematic temperature range. Spherical particles on the contrary are expected to destabilise the nematic order, which manifests as a decrease of phase transition temperatures. Classical Onsager theory predicts the stable nematic phase for a system consisting of rod shaped particles [11]. The simplest explanation for these reported results could be the similarity of shape anisotropy of LC molecules with 1D-NPs. Dispersions of rod-shaped particles in isotropic fluids are known to exhibit spontaneous formation of orientationally ordered phases by themselves. Therefore, composites of 1D-NPs with LC host are expected to exhibit synergetic orientational ordering. However, the mixing behaviour is observed to be quite complex. Addition of a relatively small amount (≤1 wt%) of 1D-NPs to the nematic LC host can alter the orientational order of the host medium. This effect perhaps depends on various factors such as the diameter and aspect ratio of the dispersed 1D-NPs with respect to that of the LC molecules, the interaction between the NPs and the interfacial interaction between the NPs and the LC molecules, which may alter the surface anchoring conditions. These dispersions are interesting to study as they allow investigating pure interactions between added nanomaterial and host LC molecules, without overlaying additional effects. However, even in the simplest case of nanoparticle doping, surface and bulk parameters get altered. The effect of addition of 1-D nanostructures such as nanorods, nanowires and nanotubes on physical parameters of NLCs has been studied by different research groups [49,52,66,69–72]. Among the 1D nanomaterials, CNTs are known to exhibit fascinating properties. The variation of dielectric and electro-optic properties of NLCs with the dispersion of CNTs is most extensively studied [56,65,73].

1.4.1 Carbon Nanotubes (CNTs) in NLCs

Modification in physical properties of LCs with the incorporation of CNTs is widely studied by researchers [65,74]. The incorporation of functionalized single-walled CNT (SWCNT) in the NLC host shows the reduced threshold voltage and enhanced nematic ordering of host NLC in the composite medium [62]. The addition of functionalized multi-walled CNT (MWCNT) in the NLC host media shows reduction in threshold voltage of host NLC, fast response, reduction in ionic impurities and increase in thermal stability, and better alignment of NLC molecules. One of the main conclusions drawn from several investigations is that alignment of CNTs in thermotropic LCs is feasible, but in practice very difficult to be achieved because of difficulties with CNT dispersibility and dispersion stability. If surfactants are added to improve the dispersion properties, the resulting surface anchoring modifications are typically such that they contradict requirements for good alignment. On incorporation of CNTs in LC, some of the device parameters improve but with deterioration of other key parameters. Therefore, an optimized control of modifications in properties of NLC with the incorporation of CNTs is yet to be reached.

1.4.2 Inorganic nanorods in NLCs

Dispersion of inorganic nanorods in liquid crystals is still a challenging task for researchers working in this field. Over the years, there are comparatively very few reports on the investigation of physical properties of composite systems of liquid crystals with nanorods. Zhang et al [47] demonstrated that molecular-colloidal organic-inorganic composites formed by liquid crystals and relatively dilute dispersions of orientationally ordered anisotropic gold nanoparticles (rods and platelets) can be used in engineering of switchable plasmonic polarizers and colour filters. The use of metal nanoparticles instead of dichroic dyes allows for obtaining desired polarizing or scattering and absorption properties not only within the visible but also in the infrared parts of an optical spectrum. Effect of dispersion of gold nanorods on properties of liquid crystals has been studied by few researchers [75–77]. Gold nanorod dispersion are observed to increase dielectric permittivity of LC host but also increases the conductivity[77] Wu et al. [51] reported a novel nanocomposite device based on liquid crystals and CdS nanorods where polarization of the emission from semiconductor nanorods can be controlled by an external bias. This offers new possible applications for one-dimensional semiconductor nanostructures in smart optoelectronic applications, including optical switches, integrated photonic devices, and electrochromatic gadgets. Kundu et al. demonstrated that dispersion of ultranarrow PbS nanorods[50] or ZnS nanorods[78] encapsulated by a fluidlike soft organic layer in the NLC results in a novel, highly miscible soft matter type blend where local ordering of nanorods significantly affects the global ordering of the blend allowing a more rapid response of the electro-optic properties.

Gap in the research

LC field has seen a rapid growth in industry as well as in research due to its potential applications, especially in display devices. Different functionalities of LCs offer large number of opportunities for their use in various fields along with display. Use of LC in photo-voltaic, switchable smart windows, holography, flexible electronics, sensors as well as bio-medical applications is gaining interest and advancing research in this direction. State of the art of research in LCs in display device applications is more intended to address following issues:

Minimizing ionic impurities: Presence of ionic impurities limits the device performance to larger extent. In display devices, these ionic impurities cause the accumulation of residual charges in the defect regions which leads to effects such as image sticking, flickering and slow response time. Impurity ions sometimes get adsorbed on inner polyimide layer while driving the LC cell causes residual image or ghost image. These impurity ions also induce the screening effects across LC layers which further decreases the effective voltage applied across the LC layers resulting in the increase of threshold voltage.

Control of long range of alignment is also one of the important issues to be addressed. The defect regions in alignment layer are the main sources for accumulation of impurity ions. Defect regions can arise from various mechanical treatments of substrate surface in industrial fabrication processes. Incorporation of 1D anisotropic nanomaterials may help in the control of long-range alignment of cylindrical shaped NLC molecule without need for such mechanical treatments.

Slow response times and scan rate conversion results in severe motion artifacts and image degradation for moving or rapidly changing images. Decreasing response times to an extent to achieve nearly zero motion blur in display devices is one of the important aspects to work on. Composites of nanorods with liquid crystals may be helpful to meet subcomponent manufacturing standards and offer fabrication possibilities for faster polarization-sensitive devices with wide viewing angles and improved contrast ratios.

Miscibility of nanomaterial in LC matrix plays a crucial role in determining the physical properties of the LC. If the nanomaterial is immiscible in LC matrix, it is observed to accumulate at the interfaces leading to alteration of boundary conditions and increase in the ionic conductivity. Also, the concentration of nanomaterial added into the host LC is a critical factor. The optimization of concentration of nanomaterial in LC matrix is very important to observe the desired properties.

Although, research in the composite system of LC and nanomaterials has progressed a lot in recent years, most of the studies are confined to the use of spherical nanoparticles. The most probable reason could be the ease and control on synthesis of nanomaterials of spherical shape and easy dispersion of spherical NPs in LC matrix. Miscibility of NPs in host NLC is one of the important factors to investigate the effect of NP on properties of NLC. However, a thorough investigation on the effect of incorporation of various 1D nanomaterials on the physical properties of LC is much required. CNTs show great potential as one of the only nanomaterials for the composite systems with NLC. But the challenge is to control the aggregation of CNTs in host matrix. Also, the simple procedure to synthesize high quality of CNTs and control over morphology is still a major challenge for material scientists. Hence, the composite systems of other 1D nanomaterials and a systematic investigation on incorporation of these 1D NPs in host NLC is required to be explored. As discussed above, it has been predicted theoretically that rod shaped NPs could greatly improve the properties of LC host starting from classical Onsager theory[11] to the recent theoretical investigations [66–68,79].

Objective of the Proposed Research:

- Selection of nanomaterials, Synthesis and characterization of nanoparticles of various aspect ratios based on its compatibility with liquid crystal host, solubility in solvents
- Optimization of concentration of nanoparticles in liquid crystal matrix so as to achieve the enhancement in the physical properties and avoid aggregation or accumulation of nanoparticles in liquid crystal matrix.
- Investigation on effect of concentration, size, and aspect ratio of nanoparticles on the physical parameters such as dielectric anisotropy, birefringence, and elastic constants of nematic liquid crystals
- Electro-optical response time, ion transport and conductivity measurements of pure and nanocomposites of nematic liquid crystals

The work done presented in this thesis is laid out as follows:

Introduction to liquid crystals, properties of nematic liquid crystals, applications, and research background is presented in Chapter 1. The experimental techniques used for synthesis and characterization of the nanomaterials as well as various measurement techniques used to study the electro-optic and dielectric properties of liquid crystals and its nanocomposites are discussed in Chapter 2. Fabrication of LC cells with different alignment configurations and preparation of nanocomposite samples is also discussed in Chapter 2. The results of study on effect of incorporation of CdS nanowire capped with oleic acid on behaviour of isotropic-nematic (I-N) phase transition and physical properties of NLC, PCH5 are presented in chapter 3. Results on effect of synthesized zinc oxide nanorods capped with oleic acid (ZOR) on physical properties of 8CB are presented in Chapter 4. The results of the study indicate that above a critical concentration of ZOR (0.3 wt%) in host LC, ZOR induces vertical alignment of LC molecules in planar/unaligned cells. To study the effect of shape of nanoparticles, further work is carried out in which zinc oxide (ZnO) nanoparticles of different shapes (sphere, rod, wire) are synthesized without any functionalization. The results on effect of these different shaped ZnO NPs on physical properties of PCH5 are presented in Chapter 5. The results of the study indicate that incorporation of ZnO nanorods and ZnO nanowires helps better dispersion, alignment and improved physical properties of nanocomposite samples as compared ZnO nanospheres in NLC. Also, isotropic particles tend to self-assemble in chains/strands to minimize the free energy of the nanocomposite system. In continuation to this work, results on effect of size of ZnO nanorods with similar aspect ratio but different size (diameter: length), on physical properties of PCH5 are presented in Chapter 6. Results of the study indicate that properties of PCH5 can be tuned by variation in size as well as concentration of nanorods in NLC according to the application. the conclusion of the work done is presented followed by the future scope of the work in Chapter 7.

CHAPTER 2

EXPERIMENTAL TECHNIQUES

Physical properties of NLCs with the variation of external stimuli such as temperature, frequency, and electric field are studied using different techniques. The electrical and optical properties of NLCs are interdependent and can be measured simultaneously. In the present chapter, various experimental techniques used for measurement of electro-optic and dielectric properties of pure and nanocomposites of liquid crystal are described. Also, the synthesis and characterization techniques for the 1D nanomaterials that are used for the preparation of various nanocomposites are explained.

2.1 SYNTHESIS OF NANOMATERIALS

The synthesis of nanomaterials presented in the following thesis is mainly done by bottom-up approaches viz., solid state decomposition and wet chemical synthesis methods. The detailed procedures for synthesis of nanomaterials are presented in the relevant chapters.

2.2 CHARACTERIZATION TECHNIQUES

The basic properties of synthesized nanomaterials such as crystal structure, morphology and thermal properties are studied using different techniques. Some of these techniques are also used to characterize the liquid crystals and its nanocomposites.

2.2.1 X-Ray Diffraction

X-ray diffraction is the technique for crystal structure analysis. X-ray diffractometer is conceptually simple and allows quite an accurate determination of crystal structure of polycrystalline samples, thin films, and nanoparticles. The XRD used for measurement in this thesis is Rigaku SmartLab II. It consists of X-ray generator (40 kV, 50 mA) with a monochromatic source of X-rays, (a copper target giving $\mathrm{Cu}K_\alpha(\lambda = 1.54\text{Å})$ after passing through nickel filter), sample holder and an X-ray detector. Detector (D/teX Ultra 250) is a 1D silicon strip detector with a higher capture angle and a larger active area. The diffracted rays make an angle $2\theta°$ at the detector with respect to incident beam direction. A plot of intensity (counts) as a function of angle $2\theta°$ gives the diffraction pattern. The interlayer spacing (d) is calculated by simple Bragg's reflection law,

$$2d \sin\theta = n\lambda$$

and crystallite size(D) is calculated by Debye-Scherrer formula,

$$D = \frac{0.9\lambda}{\beta \cos \theta}$$

where, β is full width at half maximum of specific XRD peak by subtracting instrumental broadening and θ is corresponding Bragg reflection angle.

2.2.2 Fluorescence Confocal Microscopy

The principle of imaging using Fluorescence Confocal Microscopy (FCM) imaging is based on the confocal microscopy (CM) (Fig 2-1b). Principal elements of a CM include a special objective with a high numerical aperture (NA) and a pinhole in front of the detector that functions as a spatial filter to reduce the signal emerging from outside the selected volume. Light rays from the focal point of the microscope pass through the pinhole, but rays from other points focus somewhere behind or in front of the screen and thus are effectively blocked by the aperture. The tightly focused light beam scans the sample to obtain a complete image. The scanning is usually performed by one focused beam traveling in the horizontal plane and then by mechanical or piezo element refocusing at different depths of the sample. The image is saved as a stack of thin (submicron) horizontal optical slices in the computer memory. The data can then be presented in a variety of forms, as a 3D pattern formed by images of all scanned volumes, or as horizontal or vertical ‘cross-sections’ of the sample.

If the composition of sample under investigation consists of high-quantum-yield fluorescent particles that strongly absorb at the wavelength of the exciting beam, FCM can be used. The difference between the fluorescence and absorption wavelengths is known as the Stokes shift. If the Stokes shift is sufficiently large, the exciting and fluorescence signals can be efficiently separated by filters so that only the fluorescence light would reach the detector. The concentration of the fluorescent probe becomes coordinate dependent, giving a high-contrast image if the sample is heterogeneous. FCM (Zeiss LSM880) is used for the characterization in current thesis work. The pure and nanocomposites of LC filled in cells (planar/ homeotropic) can be directly probed under this microscope.

2.2.3 Field Emission Scanning Electron Microscopy

In field emission scanning electron microscope (FE-SEM), a cold cathode emitting electrons on the application of a very high electric field known as field emitter is used. In FE-SEM, secondary electrons emitted from the sample are commonly used for imaging (Fig 2-1a). In an

FE-SEM, the electron beam is focussed to a very small spot size using electromagnetic lenses. The fine beam is scanned or rastered on the sample surface using a scan generator and secondary electrons are collected by an appropriate detector. Signal from scan generator along with amplified signal from the electron collector generates the image of sample surface. The schematic of working principle of FE-SEM is shown in Fig 2-1c. To avoid the oxidation and contamination of filament as well as to reduce the collisions between air molecules and electrons, filament and sample are housed in a vacuum chamber. Usually vacuum 10^{-2}–10^{-3} Pa or better is necessary for a normal operation of scanning electron microscope. FE-SEM used for the imaging of nanomaterials used in the current thesis work has following specifications: FEI Apreo LoVac with retractable STEM 3+ Detector and DBS Detector along with Aztec Standard EDS system having resolution 127 eV on Mn-k_{α}. For imaging, powder samples are dispersed in appropriate solvent and drop casted on silicon wafer. After complete evaporation of solvent, thin layer of gold is coated on the sample using sputtering (Leica Ultra Microtome EM UC7) technique to avoid accumulation of charges on sample surface.

2.2.4 Transmission Electron microscopy

Transmission electron microscope is ideal for investigating the nanomaterials at very high resolution (~0.5 nm). Here, the electrons are transmitted through the sample in this microscope. Electrons of very high energy (typically >50 keV) are used which pass through a series of magnetic lenses. The basic components of TEM include electron source, condenser lens, sample, objective lens, diffraction lens, intermediate lens, projector lens and a fluorescent screen in the given order (Fig 2-1d). There may be some additional lenses in different microscopes in order to improve the image quality and resolution. The lenses are electromagnetic with varying focal lengths to obtain optimized images. Similar to SEM, the components (and sample) of a TEM have to be housed in a chamber having high vacuum 10^{-3} to10^{-4} Pa for its proper functioning. The specifications of the TEM used for characterization of nanomaterials in current thesis work are: FEI Tecnai G2 20 S-TWIN (200 kV) with a point resolution of 0.24 nm and line resolution of 0.14 nm. For TEM imaging, samples are dispersed in appropriate solvent and drop cast on carbon coated copper grids.

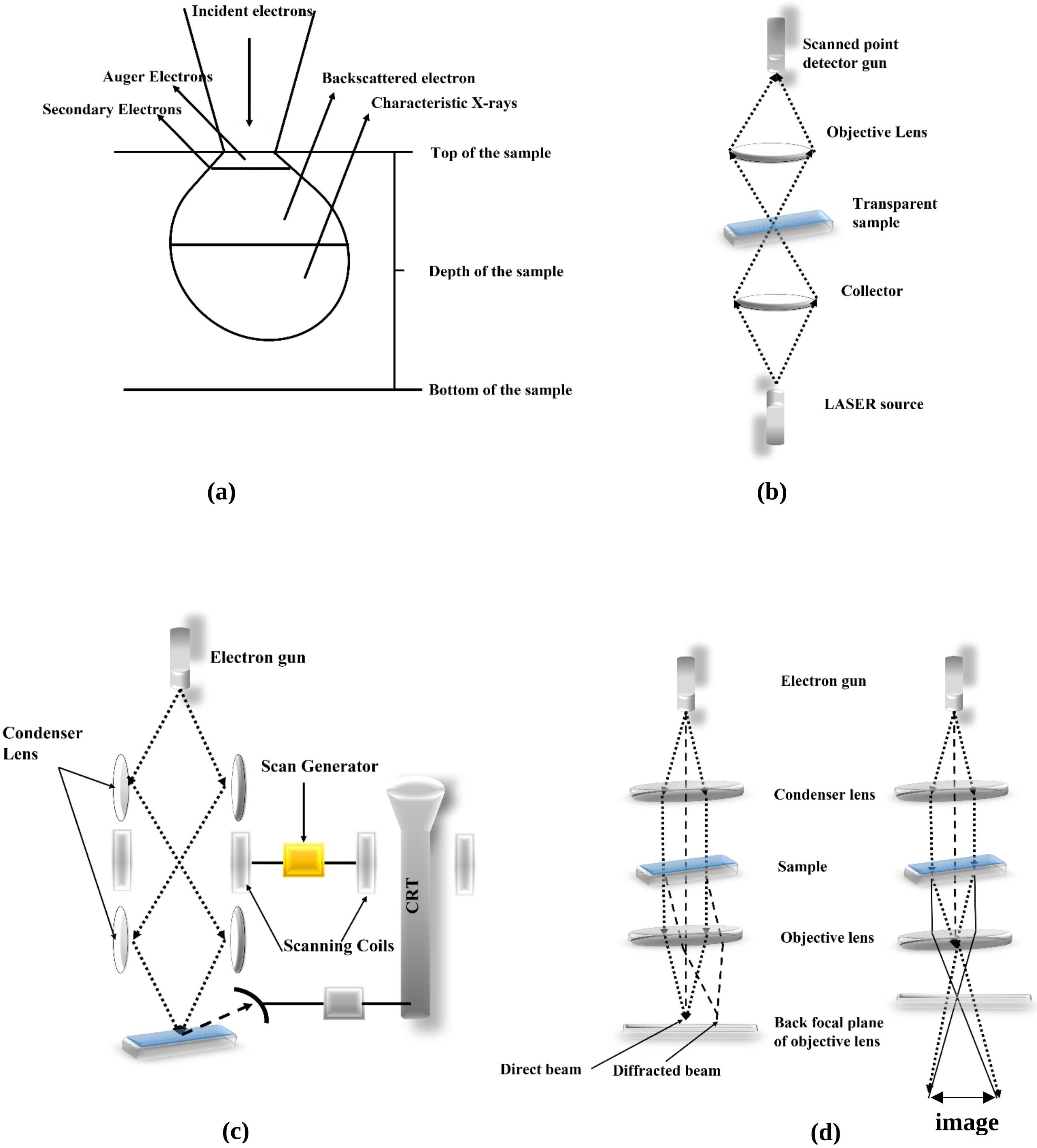

Figure 2-1 Schematic showing (a) Interaction of high energy electron with matter; working principle of (b) Confocal Microscope; (c) Scanning Electron Microscope; (d) Transmission electron microscope

2.2.5 Fourier Transform Infra-Red Spectroscopy

Liquid crystal phases are exhibited generally by organic compounds. Many functional groups like –OH, –SH, =C=O, $-CH_2$, $-NH_2$ etc. have some characteristic absorption bands in the Infra-Red (IR) regions. The transmitted light from the sample produces a spectrum in which certain characteristic frequencies are absorbed by molecules present in the sample. Fourier Transform IR (FTIR) spectrometer is mainly used to simultaneously record a spectrum for entire IR wavelength range in time domain and present the data in Fourier domain.

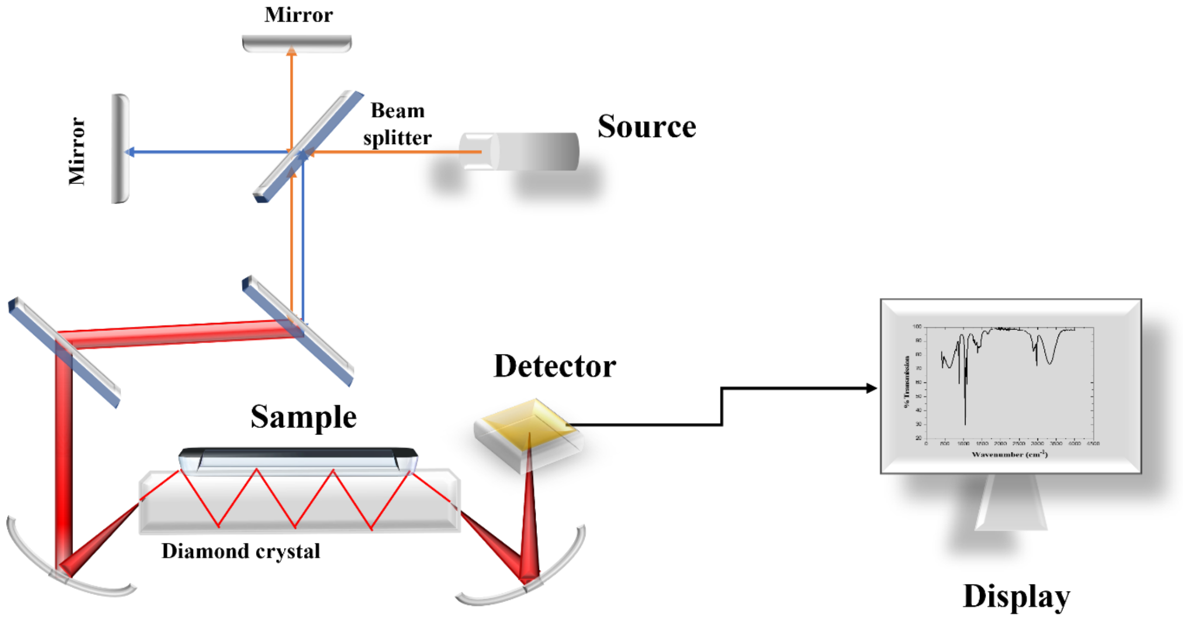

Figure 2-2 Schematic showing working principle of ATR-FTIR spectroscopy

Attenuated total reflectance (ATR) based on total internal reflection is one of the common sampling techniques in FTIR spectroscopy. In ATR-FTIR spectroscopy the sample is in contact with the ATR crystal. The IR radiation travels through the crystal and interacts with the sample on the surface in contact with the ATR crystal. The differences in refractive indices of both materials causes total internal reflection. This reflection forms an evanescent wave which extends into the sample. Based on the sample’s composition, a small part of the infrared light is absorbed when the evanescent wave interacts with the sample, resulting in a slightly attenuated total reflection. Schematic of working principle of ATR-FTIR is shown in Fig 2-2. To study the dipolar interactions of the nanomaterials with LC molecules in current thesis work, FTIR is performed using Perkin Elmer spectrophotometer equipped with ATR accessory (GladiATR).

2.2.6 Ultraviolet-Visible (UV-Vis) Spectroscopy

Optical absorption spectroscopy is a very useful technique to study metallic, semiconducting and insulating materials in bulk, colloidal, thin film and nanostructure forms. Semiconducting as well as some insulating materials have an energy gap corresponding to optical frequency of electromagnetic spectrum. The excitation of electron from valence band to conduction band minimum of a sample under investigation can be detected by absorption of typical wavelength (or energy) over a wide range of incident wavelengths. The absorbed (or reflected) intensity as a function of wavelength is useful to understand electronic structure and transitions between valence and conduction band of materials. UV-VIS spectrophotometer (Thermo Scientific EVOLUTION 201) is used for acquiring absorption spectra of nanomaterials. The powder samples are dispersed in appropriate solvents and this solution filled in quartz cuvette is used to record absorption spectra.

2.2.7 Differential Scanning Calorimetry

Technique for the measurement of the release or absorption of heat during chemical reactions, phase transitions, and other physical changes is termed as ‘calorimetry’ in which thermodynamic properties such as changes in enthalpy or entropy can be investigated. In differential scanning calorimetry (DSC), the difference in heat flow between two pans, one containing the sample and the other, a reference material, is determined. The sample and reference pans are heated independently such that the temperature difference is monitored and maintained at zero. When the material undergoes a phase transition, the amount of heat needed to maintain a constant sample temperature varies. The difference in energy needed to match the sample temperature to the reference is the amount of excess heat released or absorbed as a result of phase transitions. Basically, the information from DSC can be described by

$$\frac{dH}{dt} = mC_p \frac{dT}{dt}$$

where, dH/dt - DSC heat flow signal; m - sample mass; C_p - sample heat capacity; dT/dt - the heating rate. Physical changes in the material, such as melting, crystallization, and glass transitions can be observed using DSC. For the measurement of phase transition temperature of pure and nanocomposites of LC, Perkin Elmer DSC-4000 is used. A schematic of typical DSC thermograph is shown in Fig 2-3a.

2.2.8 Thermo-gravimetric Analysis

Thermogravimetric analysis (TGA) refers to the process in which the sample mass is monitored as it is heated at a controlled rate in a controlled atmosphere (reactive, e.g., oxygen, air or inert, e.g., argon, nitrogen, or vacuum). The sample is loaded onto a balance within a furnace and heated using a specific temperature program. As a result of the heating, the sample mass changes due to desorption of an adsorbed species such as water, oxidation of metal species, decomposition via pyrolysis or combustion in case of carbonaceous materials. First and second derivatives of thermogram of weight loss vs temperature is commonly used for analysis. A key TGA measurement parameter is the residual mass (M_{res}) of the sample at a given temperature, usually given as a percentage of the original sample mass:

$$M_{res}(\%) = M_r \times T \times M_s \times 100\%$$

where, M_r is the mass remaining at a specific temperature (T) and M_s is the initial mass of the sample. Temperatures of importance can be determined by differentiating the thermogram with respect to temperature or time followed by identification of the peaks. Hence, features that may not be easily detected or quantified in the thermogram (e.g., shoulders) can be easily identified and the onset temperature at which major transitions occur can also be quantified. Perkin Elmer TGA-4000 is used for measurements in current thesis work. A schematic of typical TGA thermograph is shown in Fig 2-3b.

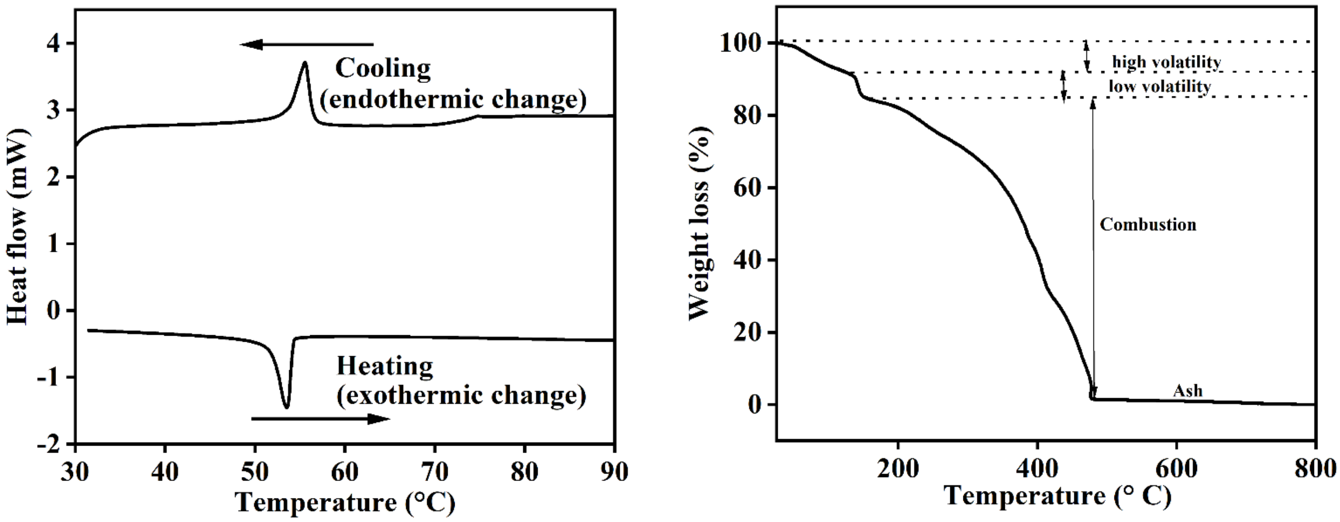

Figure 2-3 Typical (a) DSC thermograph (b)TGA thermograph

2.3 ALIGNMENT OF LC MOLECULES IN A CELL

The variety of applications that emerge utilizing liquid crystals require the very basic and most important quality control, i.e., the alignment of LC molecules. Widely used technique to control the alignment of the LC molecules is the use of sandwich cell made up of transparent and conducting indium tin oxide (ITO) coated glass plates of specific thickness coated with a polymer layer responsible for initial alignment of molecules. Glasses are excellent material for substrates because it has a flat surface, high transparency, high corrosion resistance for chemicals, very low moisture but lacks flexibility and are brittle. Although, plastic substrates may be another choice being light weight, flexible and not easy to break, but they have poor thermal resistance and moisture can pass through it easily. ITO is commonly used as electrode in LCD, and it is coated on the glass substrate by sputtering. It is smooth, conductive, and transparent, can be etched easily to make the desired pattern and it is thermally stable to go through processes at high temperature during fabrication. Measurement of different properties of LC and its composites can be easily done by applying external stimuli. Nowadays, nanoparticle induced alignments are also reported which require no pre-treatment of substrates and are also helpful for applications in flexible substrate-based technologies. In this section, various types of basic alignment modes and the preparation of classic sandwich LC cell is discussed.

2.3.1 Alignment of LC molecules

Nematic LCs are composed of rod-shaped molecules and hence are easiest to align making them most widely used in the device applications, especially, displays. Depending on the direction of molecular orientation, specifically, director with respect to the plane of the substrate surface, there exists three basic types of configurations viz., planar, homeotropic and twisted. Fig 2-4 depicts the schematic representing arrangement of molecules in these configurations. In planar configuration, director is aligned parallel to the plane of substrate while it is perpendicular in case of homeotropic configuration. Twisted configuration, which is used in commercial display applications, has the arrangement of molecules from bottom substrate to top substrate of the cell such that director rotates by 90°. The NLC filled sample cell when placed between the crossed polarizers show varying intensity pattern based on the configuration of cell. Homeotropic cell is observed to be completely dark at all angles of rotation of sample stage. Optical texture of LC filled in planar cell is completely bright and completely dark under crossed polarizers when rubbing direction of the cell is at an angle of 45° and 0°, respectively to either polarizer.

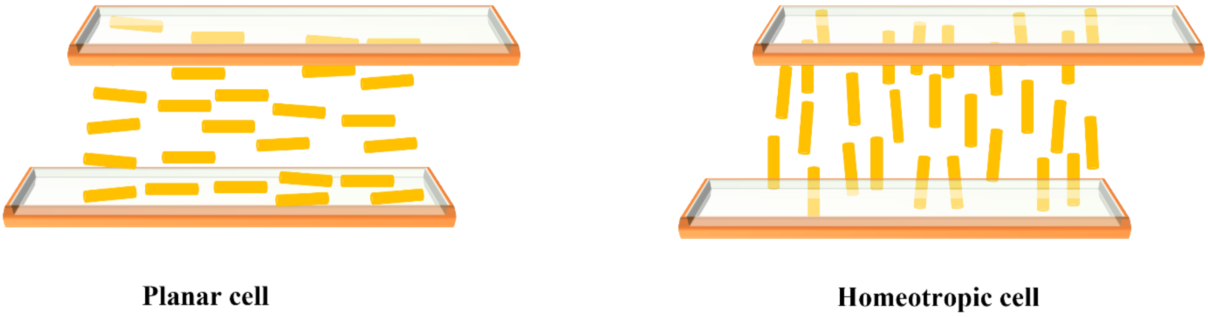

Figure 2-4 Schematic showing arrangement of LC molecules in planar and homeotropic cells

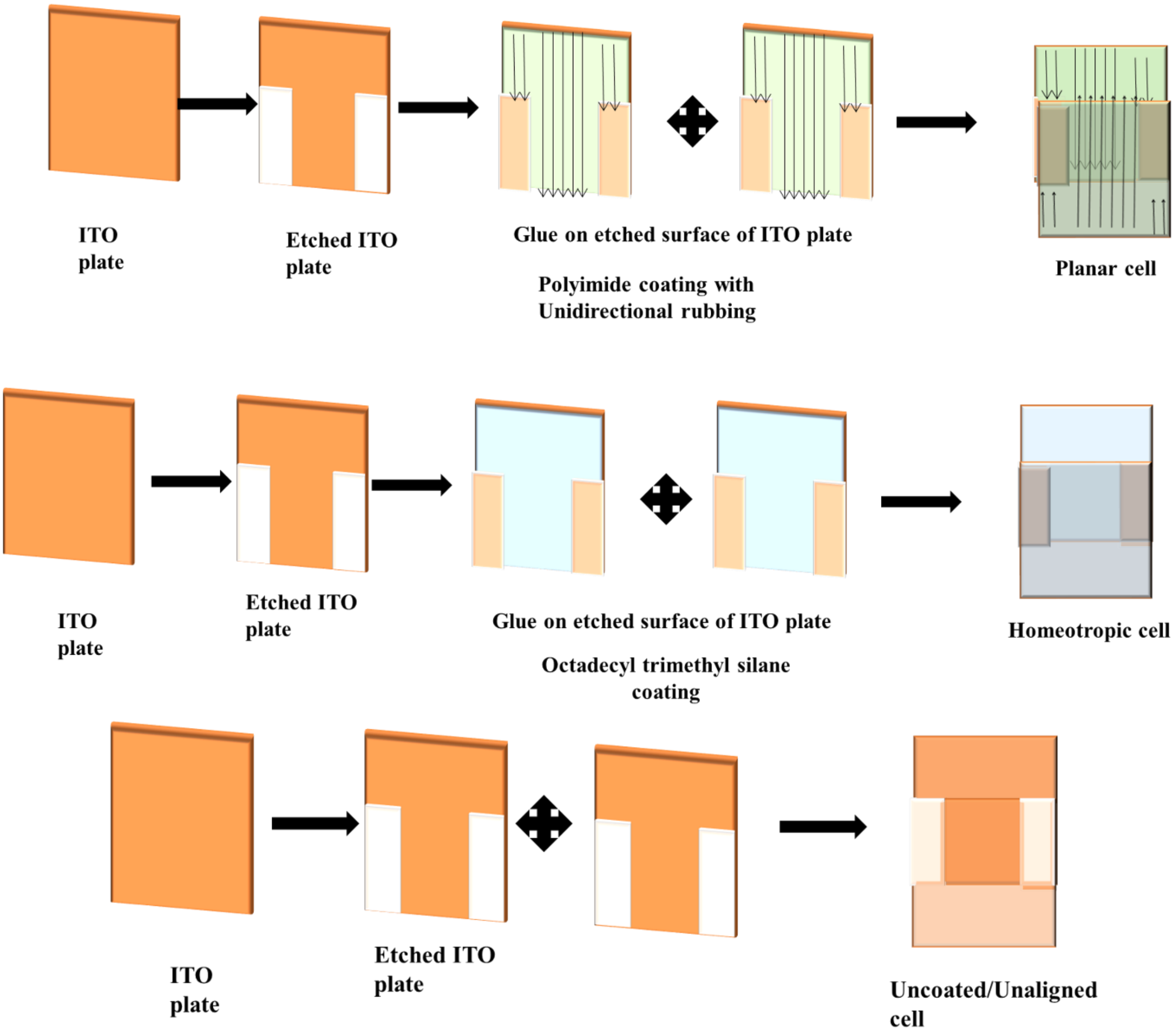

Figure 2-5 Schematic showing procedure for fabrication of LC cells

2.3.2 Fabrication of LC sample cells

The physical property measurement of LCs is performed by filling them in sandwich cells as mentioned earlier. The sample cells are prepared in planar and homeotropic configurations according to the standard procedure as shown in Fig 2-5. The ITO coated glass substrates are etched using 10% HCl in water followed by the thorough cleaning using soap water solution. Afterwards, these are ultrasonicated in 10% aqueous solution of ethanol and then completely dried in ambient. The cleaned substrates are treated further to obtain desirable configuration.

a. **Planar Cells:**

   The cleaned substrate is coated with Polyimide (PI2555) using spin-coating method. Afterwards these substrates are heated at 250℃ for 1 hour on a hotop (REMI 2MLH) to facilitate polymerization. After cooling to room temperature naturally, the polyimide coated substrates are unidirectionally rubbed using a soft cloth which helps making microgrooves on the substrate. Two such substrates are placed anti-parallel and glued together using epoxy glue mixed with glass spacers of desired thickness. This assembly is heated at 100℃ for 1 hour on hotop to obtain planar aligned cell.

b. **Homeotropic Cells:**

   Homeotropic cells are prepared by similar method as described above. Here, instead of polyimide, substrates are spin coated using octadecyl trimethyl silane (OTMS) and heated at 150℃. No mechanical rubbing is required for the preparation of homeotropic cells. The glued substrates after heating at 100℃ and cooling down naturally to room temperature gives the homeotropically aligned cells.

c. **Uncoated/Unaligned Cells:**

   For few of the studies presented in this thesis, we have also used uncoated cells. The cleaned ITO substrates are glued together without coating any layer of polymer and heated at 100℃ to obtain uncoated or unaligned cells.

2.4 MEASUREMENT TECHNIQUES

Various physical properties of pure and nanocomposites of liquid crystals are measured by different techniques as described below.

2.4.1 Thickness and capacitance of empty cell

Initially, the thickness and capacitance of the cells before filling liquid crystal sample are measured. The thickness of the empty cells is measured by interferometric technique using fibre-optic spectrometer (Ocean-Optics USB4000-XR1-ES). The corresponding wavelengths

(λ_m and λ_n) of the mth and nth maxima are measured, and thickness (d) is calculated using equation

$$d = \frac{(m-n)}{2} \frac{\lambda_m \lambda_n}{\lambda_m - \lambda_n}$$

Empty cells can be considered as a parallel plate capacitor filled with air as a dielectric material. Geometrical empty capacitance (C_0) of cell is simply a ratio of area (A) to thickness(d) times the permittivity of free space (ε_0).

$$C_0 = \frac{\varepsilon_0 A}{d}$$

After the parameters of the empty cell are recorded, cells with similar thickness and area are chosen for a set of an experiment. The pure and nanocomposites of liquid crystals are filled in the cells of desired configuration with the help of capillary action in their isotropic phase. Then, these sample filled cells are allowed to cool down to room temperature slowly and can be used for further measurement.

2.4.2 Polarizing Optical Microscopy

The observation of optical textures of the sample filled LC cells is the most important step before measuring any of its physical properties. The optical textures show the alignment of LC sample in the cell which is recorded using polarizing optical microscope (POM; Olympus BX53M). The sample filled LC cell is mounted on the hot stage (Microptik MTDC400) with a temperature control of 0.1℃. This assembly is placed between the crossed polarizers of the POM. White light is used as an optical source and transmitted light is detected using camera. The schematic of working principle of POM is shown in Fig 2-6. The sample cells that show uniform and homogeneous alignment of LC sample in accordance with the configuration of the cell are further used to measure the various physical properties. The representative images of the optical textures observed under POM in various cell configurations are shown in Fig 2-7. Variation of optical textures by varying temperature, applied electric field, angle between polarizer and analyser can also be recorded and analysed.

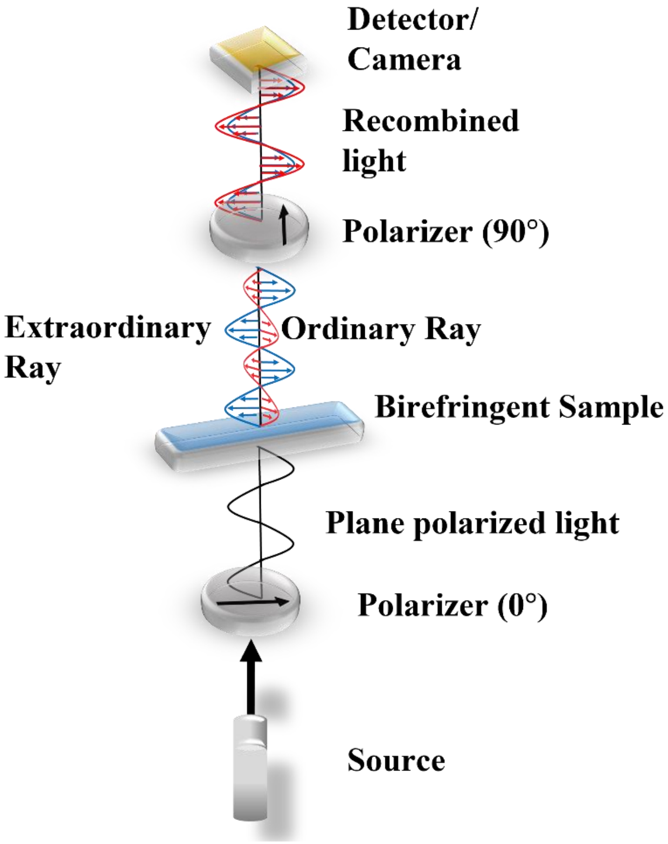

Figure 2-6 Schematic showing working principle of polarizing optical microscope.

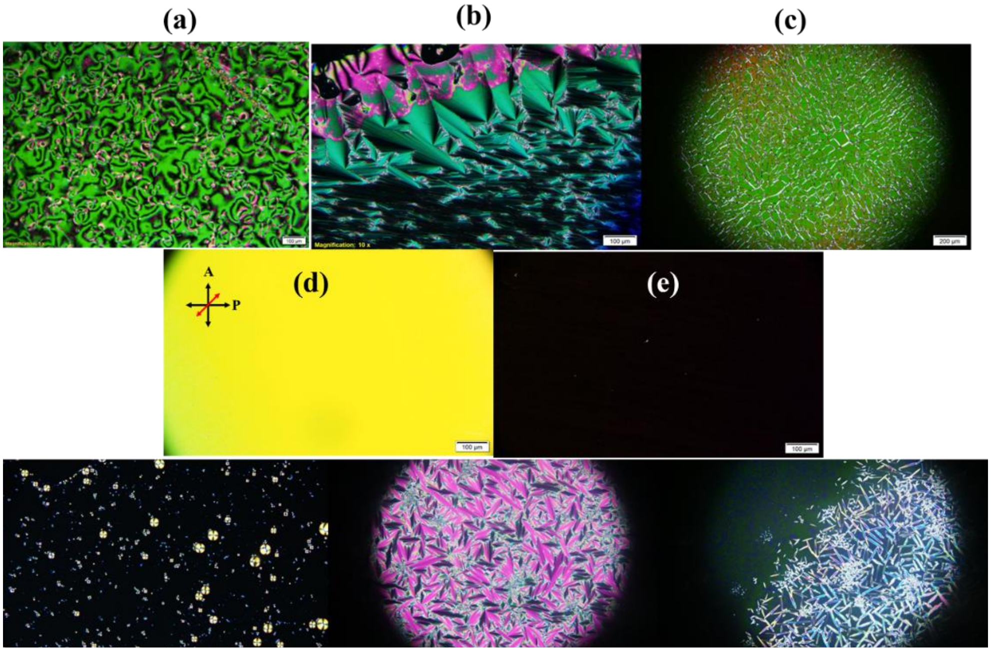

Figure 2-7 Polarizing optical microscope images (a) Schlieren texture of liquid crystal in nematic phase; (b) focal conic texture of liquid crystal in smectic A phase; (c) fingerprint texture of liquid crystal in cholesteric phase; (d) uniform alignment of nematic liquid crystal in planar cell (bright texture); (e) uniform alignment of nematic liquid crystal in homeotropic cell (dark texture); (f) nematic liquid crystal- water composite; (g) Liquid crystal with TGB$_A$ phase; (e) Evolutuion of TGB$_A$ phase from blue phase of a liquid crystalline material

2.4.3 Electro-optic properties

The electro-optic properties such as optical transmittance, birefringence, response time are some of the important characteristics for display device applications. The schematic of the set-up for the measurement of various electro-optical properties is shown in Fig 2-8.

a. Estimation of birefringence

The planar cell filled with LC sample is mounted on the hot stage. This assembly is placed between crossed polarizers in a way to obtain maximum intensity (I_{max}), i.e., the angle between rubbing direction of sample cell to either of the polarizers is 45°. The laser of wavelength ($\lambda = 633\ nm$) is passed through the sample cell kept between crossed polarizers and transmitted intensity is recorded using a photodetector (Thorlabs) connected to multimeter (Keysight 34461A). The variation in the transmitted intensity (I_{trans}) of the cell by varying the temperature is recorded which is used to measure the birefringence (Δn) of the sample using equation,

$$\Delta n = \frac{\lambda}{2\pi d}\,\Delta\phi$$

where, $\Delta\phi$ is the phase retardation calculated from equation

$$\Delta\phi = \cos^{-1}\left[1 - 2\left(\frac{I_{trans} - I_{min}}{I_{max} - I_{min}}\right)\right] + 2m\pi \qquad m = 0,1,2,\ldots$$

where, I_{max} and I_{min} are observed intensities at maxima and minima, respectively. Error in the measurements of I_{trans} is observed to be $< \pm 2\%$. The typical graph of variation of intensity as a function of temperature and variation of birefringence as a function of temperature are shown in Fig 2-9a and 2-9b, respectively.

b. Estimation of electro-optic response time

A digital storage oscilloscope (EDUX1002G; Keysight) is used to apply the voltage of fixed frequency (square wave signal of 60 Hz) to the sample filled LC cell. The output of the photodetector is connected to the DSO which records the response of the LC filled sample cell to the input signal. This data is analysed to calculate the rise time (τ_r) and decay time (τ_d) of the LC sample as shown in Fig 2-9 (c). Total response time (τ) of the sample is simply the sum of rise time and decay time.

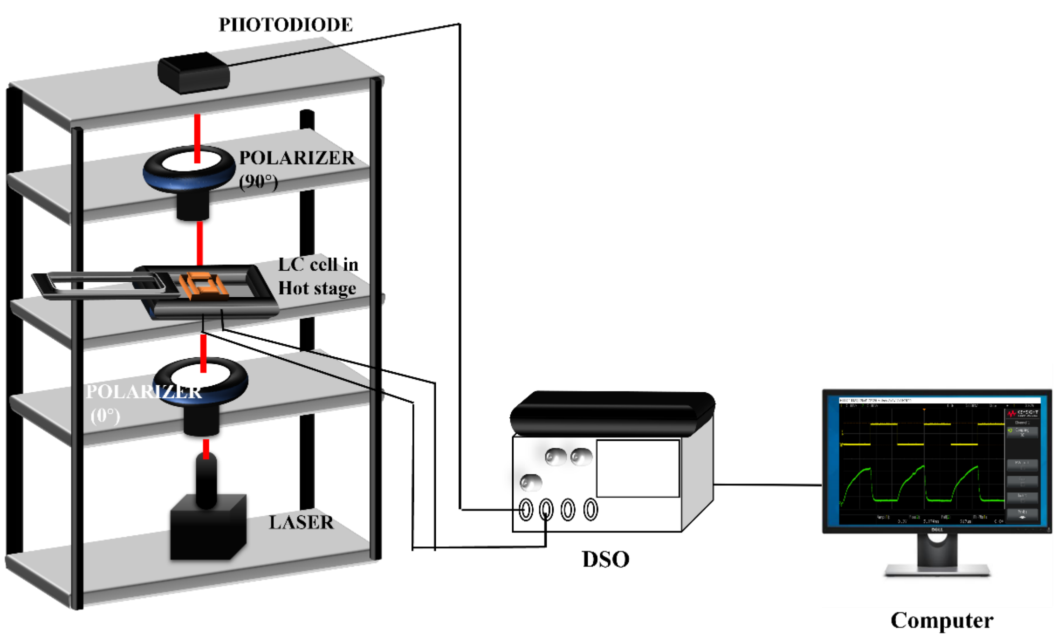

Figure 2-8 Schematic of setup for measurement of electro-optic properties of liquid crystal

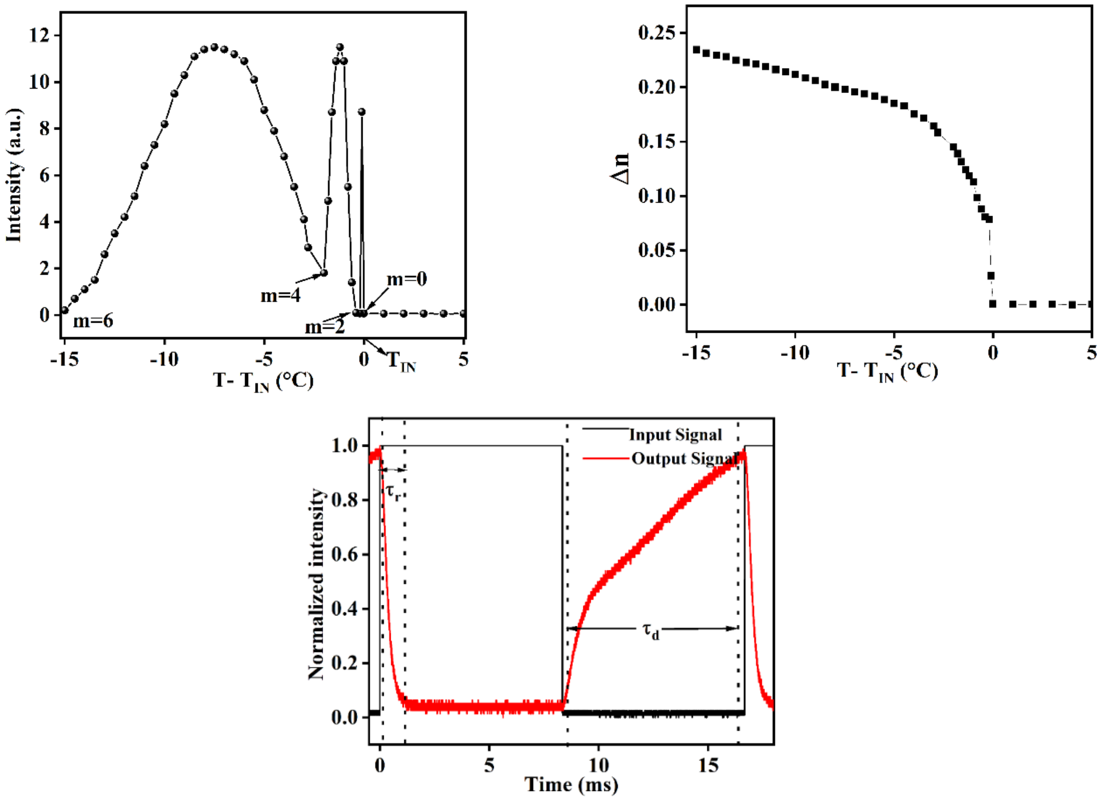

Figure 2-9 Typical graph showing (a) variation of transmitted intensity of light as a function of temperature; (b) variation of birefringence of a nematic liquid crystal as a function of temperature; (c) Electro-optic response by applying square wave signal; for LC sample filled in planar cell

Switching times of the LC sample depend on different properties of the LC given by equation,

$$\tau_r = \frac{\gamma}{\left(\Delta\varepsilon \frac{E^2}{4\pi}\right) - \left(\frac{K_{11}\pi^2}{d^2}\right)}$$

$$\tau_d = \frac{\gamma d^2}{K\pi^2}$$

where, γ –rotational viscosity, $d-$ thickness of sample, $V_{on}-$ driving voltage, $\varepsilon_0 -$ permittivity of free space, $\Delta\varepsilon$ –dielctric anisotropy of sample, $K\left(= K_{11} - \frac{K_{22}}{2} + \frac{K_{33}}{4}\right) -$ effective elastic constant of the sample.

2.4.4 Dielectric properties

Properties including dielectric permittivity, conductivity, elastic constants of an LC sample are crucial for device applications. Calamitic liquid crystals being made up of rod-shaped molecules, the properties are measured with respect to long-axis of the molecule. These properties show change with variation in external stimuli such as temperature, frequency and electric field.

a. Estimation of dielectric permittivity and conductivity

Thermotropic LCs show phase transition as a function of temperature which implies that the dielectric properties vary as a function of temperature. Sample filled LC cell is depicted as a simple circuit: a capacitor in parallel with a resistor. Schematic of a setup used to measure the dielectric properties of the sample filled LC cell is shown in Fig 2-10. An LC filled sample cell mounted in heating stage is connected to a lock-in amplifier (SRS830) which is used to apply an electric field at a defined frequency (AC field). A capacitor with comparatively higher capacitance value ($C \approx 1\mu F$) as compared to sample cell (< 2nF) is connected in series with sample cell. A computer-controlled programme is used to obtain the values of capacitance and resistance as a function of applied voltage to the pure and nanocomposites of LCs. The values of capacitance (C_p) and resistance (R_p) of the sample filled cell is calculated using standard method [80]. Error in the measurements of C_p and R_p are observed to be $< \pm 1\%$. The dielectric permittivity (ε) of the sample can be easily calculated as a ratio of capacitance after filling LC sample (C_p) to the one before filling (C_0).

$$\varepsilon = \frac{C_p}{C_0}$$

The typical graph of variation of ε as a function of temperature is shown in Fig 2-11a. The bulk ac conductivity (σ) can be calculated form the measured value of R_p using equation,

$$\sigma = \frac{d}{R_p A}$$

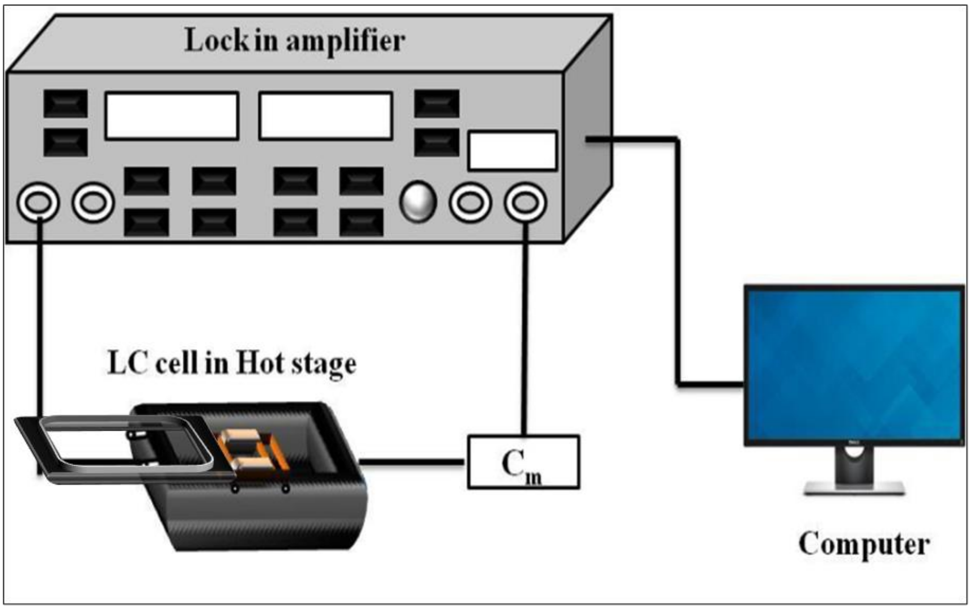

Figure 2-10 Schematic of setup for measurement of dielectric properties

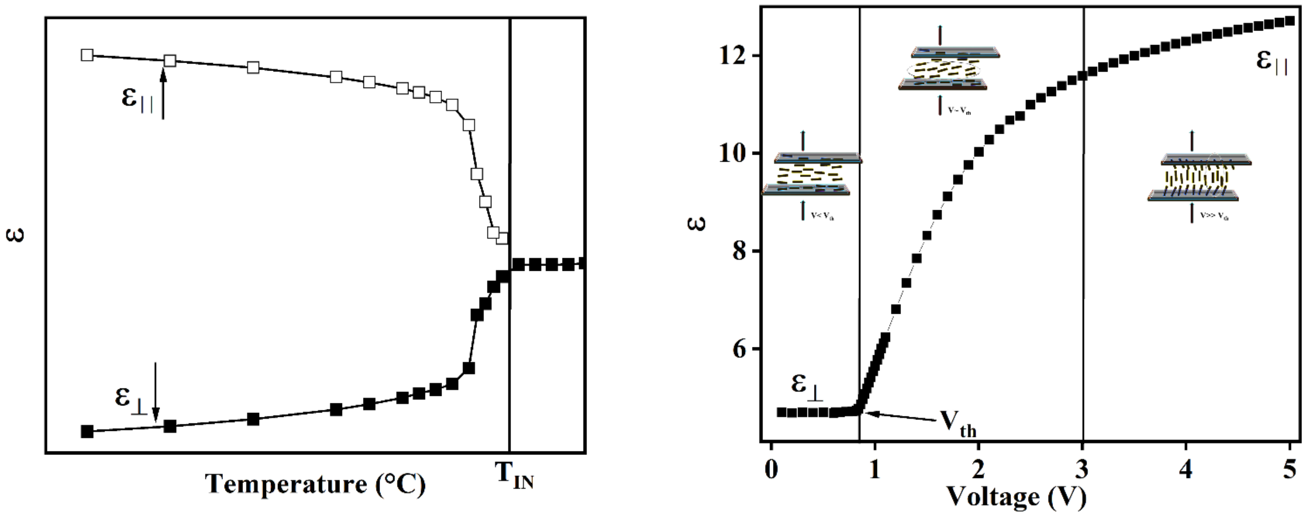

Figure 2-11 Typical graphs showing variation of dielectric permittivity as a function of (a) temperature and (b) voltage.

b. Estimation of threshold voltage and elastic constants

The same setup as described above can be used to measure the dielectric properties of LC samples as a function of varying electric field. The typical graph of ε vs voltage (V) for a positive dielectric anisotropy LC filled in planar cell is shown in Fig 2-11(b). In the planar cell, LC molecules are aligned parallel to the substrate surface and the field is applied across the cell, hence perpendicular to the long axis of the LC molecule. The component of ε measured at voltage less than threshold voltage (V_{th}) ($V < V_{th}$) is $\varepsilon_{\perp}$.The capacitance and hence, ε, of the LC sample starts changing as soon as the applied field overcomes the anchoring energy of the surface of the substrate and the long axis of the LC molecule starts to align in the direction of applied field. The voltage at which this change takes place is V_{th}. When the long axes of most of the LC molecules become almost parallel to that of the applied field, the value of C_p saturates and shows no change with further increase in the voltage. The component of ε measured at $V \gg V_{th}$ is $\varepsilon_{\parallel}$. The difference between both the components of dielectric permittivity is known as dielectric anisotropy ($\Delta\varepsilon = \varepsilon_{\parallel} - \varepsilon_{\perp}$). Dielectric anisotropy is one of the important parameters which relates to order parameter of the system.

Due to the application of electric field, the competition between anchoring energy of the surface of the substrate and applied field leads to the deformation viz., splay, bend and twist as explained in Section 1.1.3. In planar cells filled with LC sample, the splay deformation is prominent near the threshold voltage whereas bend deformation can be observed at higher applied voltages. The splay elastic constant (K_{11}) can be estimated using equation,

$$V_{th} = \pi \sqrt{\frac{K_{11}}{\varepsilon_0 . \Delta\varepsilon}}$$

For estimation of bend elastic constant (K_{33}) using data of variation of C_p as a function of applied voltage in the range of 2-5 V, a formulation given by Uchida et. al. (K_{33}) is used.

$$\frac{C(V) - C_{\perp}}{C_{\perp}} = \gamma - \frac{\alpha}{V}$$

where, $\alpha = \frac{2\gamma}{\pi} V_{th}\sqrt{1+\gamma} \int_0^{\frac{\pi}{2}} \left\{\frac{(1+k sin^2\phi)}{(1+\gamma sin^2\phi)}\right\}^{\frac{1}{2}} cos\phi \, d\phi$

C. Dielectric spectroscopy

Impedance analyser (KeysightE4990A) is used to measure the complex dielectric permittivity (ε^*), complex impedance (Z^*), and bulk conductivity of the LC sample (σ). It provides information about molecular dynamics as well as some important material parameters such as the static dielectric permittivity (ε) and DC electrical conductivity (σ_{dc}). The real part of the permittivity or dielectric constant (ε'), imaginary part of permittivity ($\varepsilon^{''}$) and loss factor ($\tan\delta$), subjected to an alternative (AC) sinusoidal supply voltage, can be determined from the following equations:

$$\varepsilon' = \frac{C_p d}{\varepsilon_0 A} \quad and \quad \tan\delta = \frac{\varepsilon^{''}}{\varepsilon'} = \frac{1}{R_p C_p \omega}$$

where, 'ε_0' represents the dielectric permittivity of free space, 'd' represents the thickness of the sample material, 'A' is the area of the electrode, 'ω' indicates the angular frequency, and C_p and R_p represent the measured values of capacitance and the resistance. At low frequency, the static (DC) conductivity can be estimated from the AC conductivity measurement data using the formula:

$$\sigma_{ac}(\omega) = \sigma_{dc}(\omega) + K\omega^n = \omega\varepsilon_0\varepsilon^{''}(\omega)$$

where 'K' represents an empirical parameter and 'n' represents the high-frequency slope of the AC conductivity ranging from 0 to 1.

Over broad frequency range (Hz-MHz), the variation of ε^* as a function of frequency can be fitted using Havriliak-Negami (H-N) function,

$$\varepsilon^*(\omega) = \varepsilon_\infty + \frac{\delta\varepsilon}{((1 + i\omega\tau)^\alpha)^\beta} - i\frac{\sigma}{2\pi\varepsilon_0 f^n}$$

where α and β are the shape parameters describing the asymmetry and broadness of the dielectric dispersion curve at higher frequencies. The third term accounts for the contribution of conductivity (σ) in low frequency region, with n as fitting parameter. Generally, liquid crystals show Debye type relaxation behaviour. The measured dispersion of ε' in Cole-Cole plot can be described by

$$\varepsilon' = \varepsilon_\infty + [\varepsilon_s - \varepsilon_\infty/(1 + \omega^2\tau_1^2)]$$

where, low frequency limit of the Cole-Cole plot is static dielectric permittivity, ε_s, whereas high frequency limit is ε_∞ and τ_1 is relaxation time. The difference ($\delta\varepsilon = \varepsilon_s - \varepsilon_\infty$) is known as dielectric strength. The molecular dynamics in the frequency range from 10^2 to 10^6 Hz corresponds to relaxation processes which take place on a local scale and follows an Arrhenius type of dependence

$$f_r = f_\infty \exp(-E_A/\mathrm{k_B}T)$$

where, $\mathrm{k_B}$ is the Boltzmann constant, and E_A is the activation energy corresponding to the flip-flop motion of molecules about their short axes. f_∞ corresponds to the relaxation rate in the high temperature limit for the dynamic glass transition. The dielectric spectroscopy measurements at low applied voltage are performed for LC samples filled in homeotropic cells. In homeotropic geometry, the observed peak in ε" vs frequency plot is due to flip-flop motion of LC molecules about their short-axes. However, the peak observed in the variation of ε" vs frequency plot for samples filled in planar cells is due to pseuodo-relaxation processes [62]. Hence, in the current thesis work, dielectric spectrscopy measurements are performed for pure and nanocompsoite samples of LC filled in homeotropic cells.

To summarize, we have discussed various characterization techniques used to estimate the properties of synthesized nanomaterials as well as to measure dielectric and electro-optic properties of pure and nanocomposites of liquid crystals. Using these measurement techniques, various properties of LCs incorporated with different nanomaterials are estimated. The characterization and measurement techniques used for investigation of different nanocomposite systems of LC are described in the relevant chapters.

CHAPTER 3

EFFECT OF INCORPORATION OF FUNCTIONALIZED CdS NANOWIRE ON PROPERTIES OF NEMATIC LIQUID CRYSTAL

A basic introduction to liquid crystals, properties of nematic liquid crystals, research background and experimental techniques used for the measurements of properties of nanomaterials as well as pure and nanocomposites of LCs used in the current thesis work are discussed in previous chapters. In this chapter, we present the results of investigation of NLC, on incorporating oleic acid functionalized CdS nanowires (CdS nanowires). As discussed in the Chapter 1, calamitic NLC generally exhibit a discontinuous weakly first order isotropic-nematic (I-N) phase transition. With the incorporation of CdS nanowires in NLC at concentration of 0.02 wt% and 0.05 wt%, the measurements of parallel and perpendicular components of dielectric permittivity and bulk conductivity of nanocomposites are found to follow second order continuous I-N phase transition in contrast to the discontinuous weakly first order transition of the pure host NLC. This was further confirmed from scattered intensity measurements on the CdS nanocomposite samples of nematic liquid crystal in homeotropically aligned cells. Such measurements indicate a continuous second order phase transition for the nanocomposites of NLC having concentrations less than 0.2 wt% of CdS nanowires in NLC. The dielectric anisotropy, birefringence, threshold voltage of nanocomposites of CdS nanowire in PCH5 with varying concentration of the nanowire have been measured. The ionic conductivity of nanocomposites of CdS nanowires of NLC increases with increasing concentration of CdS nanowires. The conductivity and relaxation behaviour with the incorporation of CdS nanowire in NLC enclosed in homeotropic cells is also studied using dielectric spectrosocpy measuremets. The dielectric strength as well as conductivity are observed to increase with the incorporation of CdS nanowires in PCH5.

Key findings of this study are published in

- Experimental evidence of continuous isotropic-nematic phase transition in CdS nanowire nanocomposites of a nematic liquid crystal, **S Mishra**, V Manjuladevi, RK Gupta, S Kumar, Liquid Crystals 48 (8), 1151-1161, 1, 2021

3.1 INTRODUCTION

The isotropic-nematic (I-N) phase transition exhibited by calamitic liquid crystals (LCs) is well known to be a first order phase transition phenomenon. This transition phenomenon is very well explained by Onsager[11,81] using the statistical mechanical theory of system of hard rods. Further, the theory of Landau-de-Gennes [2] using free energy expansion as a function of order parameter contains the third order term proving the I-N phase transition in LCs to be first order. However, the nature of I-N phase transition is only weakly first order [82] with a very small discontinuity in the order parameter at the phase transition temperature. The I-N phase transition can be transformed to second order continuous phase transition using suitable fields of high strength [83–85]. The density functional theory (DFT) followed by Monte Carlo simulation [86] of the system of hard ellipses of sufficiently large aspect ratio has proven the existence of second-order I-N phase transition. The phenomenon of continuous I-N phase transition is well studied both theoretically and experimentally for the polymer/lyotropic systems containing semiflexible chains of large aspect ratio > 4 [69,87]. DFT and molecular dynamics studies performed by Egorov et. al. on the lyotropic solutions of semiflexible polymers gives a thorough insight of the I-N phase transition as a function of chain length, flexibility of chain and monomer density[67]. They have reported for longer chain polymers, stiffer the polymer chain, the I-N phase transition occurs at lower monomer concentrations. Experimental investigations on nematic elastomers support the theoretical ideas of a continuous nematic-isotropic transition in contrast to the discontinuous first-order transition expected by the Landau-De Gennes mean field theory[88,89]. According to Petridis *et.al.*[88], the presence of network crosslinks in nematic elastomers act as sources of quenched orientational disorder. The addition of weak random anisotropy reduces the first-order discontinuity in order parameter and for sufficiently high disorder strength the jump disappears and the phase transition becomes continuous. The addition of crosslinks in liquid single crystal elastomers was shown to make the nematic transition smooth and to slightly reduce order [90]. The phase transition behaviour is found to be modified when there is a spatial confinement of LC molecules on micro- and nano- scales [91,92]. Using NMR studies, continuous I-N phase transition behaviour is observed in submicron size LC droplets (< 0.035 μm)[91]. This result is consistent with the Sheng's prediction that I-N coexistence terminates at critical enclosure size[93]. The continuous paranematic to nematic transition is observed in the NLCs confined in array of tubular silica nanochannels having mean diameter of 10 nm and 300μm long[92]. The theoretical calculations based on mean field theory[66] predicts a considerable softening of the first-order I-N phase transition in the presence of anisotropic nanoparticles.

Incorporation of nanomaterials into LC host not only affects the phase transition but also it can lead to improved electro-optic response of NLCs. The effect of addition of 1-D nanostructures such as nanorods and nanotubes on physical parameters of NLCs has been studied by many research groups[47,51,94] The addition of 1-D nanostructures to the NLCs shows better polarization control and switchable assembly [50,51], enhancement in the electro-optic switching properties of host NLCs, and orientation control [78]. The variation of dielectric and electro-optic properties of NLCs with the dispersion of carbon nanotube (CNT) is most extensively studied owing to the fascinating properties exhibited by the CNTs [95,96] The incorporation of single-walled CNT (SWCNT) in the NLC host shows the reduced threshold voltage and enhanced nematic ordering of host NLC in the composite medium [97] The addition of functionalized multi-walled CNT (MWCNT) in the NLC host media shows reduction in threshold voltage of host NLC, fast response , reduction in ionic impurities and increase in thermal stability , and better alignment of NLC molecules [60]. These studies indicate the potential of the field of nanocomposite systems consisting of NLC and nanowires. A systematic studies on such system is important which can address several aspects including the nature of I-N phase transition due to incorporation of nanomaterials in NLC host. In this article, we report that I-N phase transition which is weakly first order in a pure NLC evolves as a continuous second order phase transition in CdS nanowire nanocomposites of NLC.

3.2 EXPERIMENTAL

For this experimental study, we have taken 4-(trans-4’pentylcyclohexyl)-benzonitrile (PCH5) as NLC host material procured from TCI chemicals. The NLC host PCH5 exhibits the phase transition sequence: Isotropic (55.3 ° C) Nematic (30 ° C) Crystal. NLC nanocomposites were prepared using CdS nanowires functionalized with oleic acid (CdS nanowires) synthesized in the laboratory[98]. The image of CdS nanowires captured using field emission scanning electron microscope (FEI Apreo LoVac) is shown in Figure 3-1. As synthesized, CdS nanowire is 40-50 nm wide with the aspect ratio of ~200. CdS nanowire is dissolved in chloroform and this solution is ultrasonicated for about two hours to get a homogeneous dispersion. Calculated quantity of this solution is added into host NLC to obtain nanocomposites of various concentrations viz., 0.02, 0.05, 0.1, 0.2 and 0.5 wt% of CdS nanowire in PCH5. Sufficient time is allowed for the solvent to evaporate from the nanocomposites.

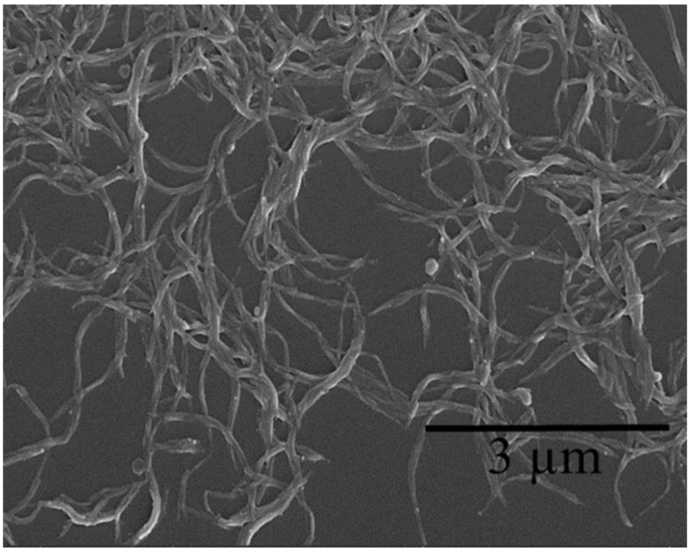

Figure 3-1 Field emission scanning electron microscope image of functionalized CdS nanowires

The I-N phase transition temperature is recorded using Differential Scanning Calorimeter (DSC; Shimadzu DSC60). For the electro-optic and dielectric measurements, we have used planar as well as homeotropically aligned cells of thickness ~7.5 μm. Thickness of the sample cells is measured using an interferometric fibre-optics spectrometer (Ocean-optics USB4000-XR1-ES). Optical texture of the LC filled sample cells is observed under polarizing optical microscope (POM; Olympus BX53M) at room temperature. The sample cell is placed inside the hot stage (Micro-optik MDTC600) with temperature control of 0.1 ℃ having a small hole in the middle to allow light to pass through. This assembly was then kept on the rotating stage of the POM between crossed polarizers. A laser beam of wavelength 633 nm passes through the sample placed between crossed polarizers. The planar aligned cell is kept between crossed polarizers with a rubbing direction at an angle of 45˚ to either of the polarizers. The transmitted intensity (I) as a function of temperature is recorded and used to estimate the birefringence of the nematic samples. The transmitted intensity through homeotropic cell is expected to be zero in this geometry as the incident beam is along the optic axis of the sample. However, thermal fluctuations of the director $\hat{n}$ can lead to strong scattering of light. A schematic representation of the scattering geometry in homeotropically aligned cell kept between crossed polarizers is shown in Figure 3-2. The propagation direction of the incident wave vector k_0 is along the optic axis $\hat{n}$ of the nematic sample. The directions of electric vectors of the incident beam and the scattered beam are denoted by i and f. In this geometry [2] the scattered intensity I will be given by

$$I \propto \frac{\varepsilon_{ai}^2}{K_{22}q_\perp^2 + K_{33}q_\parallel^2}$$

where K_{22} and K_{33} are twist and bend elastic constants respectively and ε_{ai} is the anisotropy of optical susceptibility. $q_\perp$ and $q_\parallel$ denote the perpendicular and parallel components of the scattering vector $\vec{q}$, respectively. For $\vec{q} = \overrightarrow{k_0} - \overrightarrow{k_1} \approx 0$ the scattered intensity is large. We have conducted measurements on the samples in the orthoscopic configuration of the microscope (parallel beam observation).

For $\overrightarrow{k_0} \approx \overrightarrow{k_1}$ the scattered intensity is given by,

$$I \propto \frac{\varepsilon_{ai}^2}{K_{22}q_\perp^2}$$

The scattered intensity in the forward direction in a narrow range of angles with $\vec{q} \approx 0$ is detected using a photo-detector.

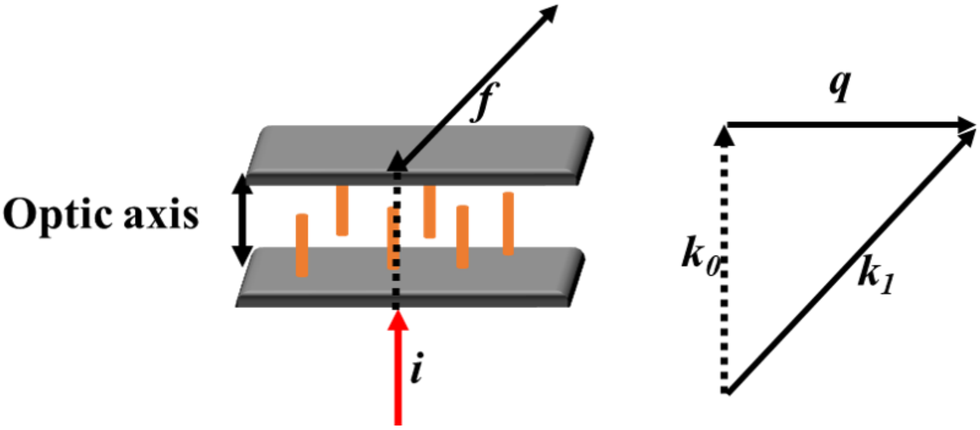

Figure 3-2 Schematic of scattering geometry; ***i*** and ***f*** denote polarization vectors of the incident and scattered beam respectively; $\boldsymbol{k_0}$ and $\boldsymbol{k_1}$ denote wave vectors of incident and scattered beam respectively and ***q*** is scattering vector

The dielectric permittivity ($\boldsymbol{\varepsilon}$) measurements as well as ac conductivity ($\boldsymbol{\sigma}$) measurements as a function of voltage are performed at an applied frequency of 4 kHz. Planar aligned cells filled with pure PCH5 as well as CdS nanowire nanocomposites of PCH5 are subjected to varying electric field to obtain both parallel ($\boldsymbol{\varepsilon}_\parallel$) and perpendicular ($\boldsymbol{\varepsilon}_\perp$) components of dielectric permittivity as well as parallel ($\boldsymbol{\sigma}_\parallel$) and perpendicular ($\boldsymbol{\sigma}_\perp$) components of conductivity using the method reported earlier [99]. $\boldsymbol{\varepsilon}_\parallel$ is also measured by application of electric field to homeotropic cells filled with pure PCH5 as well as CdS nanowire nanocomposites of PCH5. The values of threshold voltage of NLC samples are calculated from measured capacitance data as a function of voltage using the C-V curve method [99]. All the measurements were recorded through a PC with the help of LABVIEW program. Ionic current measurements were performed at room temperature using DC polarization method [99] wherein a dc field was applied across sample cells using source-meter (Keithley 2400) and output dc current was recorded using multi-meter (Keysight 34461A). To study the relaxation dynamics of the CdS nanowire incorporated in NLC, dielectric spectroscopy measurements are performed for samples filled in homeotropic cells in the frequency range of 100Hz-10 MHz.

3.3 RESULTS AND DISCUSSION

The DSC thermographs of heating and cooling cycles of samples of pure PCH5 as well as CdS nanowire nanocomposites of PCH5 at a scan rate of 5 ℃/min are as shown in Figure 3-3. The variation of T_{IN} in nanocomposite samples of CdS nanowire in LC is very small (< 1° C) as compared to that of pure NLC even for higher concentrations (0.5 wt%) of CdS nanowire in LC. For very low concentration of CdS nanowire in PCH5, the relative interaction strength of anisotropic interaction due to nanowire- LC molecules is very small resulting in slightly lower values of T_{IN} in nanocomposite samples of CdS nanowire in LC than the pure NLC due to dilution effect [66]. However, with increase in concentration of CdS nanowire in NLC, the interaction strength increases, due to the strong anisotropy of nanowires and hence the T_{IN} increases in the nanocomposites of CdS nanowire in PCH5 slightly as compared to that of pure NLC. In these samples, dilution effect due to addition of nanowires is compensated by the anisotropic nature of nanowires. With further increase in concentration of nanowires above a critical concentration result in aggregation, again makes the dilution effect to prevail which decreases the I-N transition temperature considerably. The optical textures of pure PCH5 as well as nanocomposites of CdS nanowires in PCH5 filled in planar aligned sample cells kept between crossed polarizers of POM is shown in Figure 3-4. The optical textures of nanocomposite samples with CdS nanowire for concentrations $\leq$ 0.1 wt% in NLC indicates no aggregation of CdS nanowires in the LC cells. The aggregation of nanowires can be clearly seen in LC cells filled with concentration $\geq 0.2\, wt\%$ of CdS nanowire in PCH5 leading to worm like defect texture in these samples (Figure 3-4 e-f).

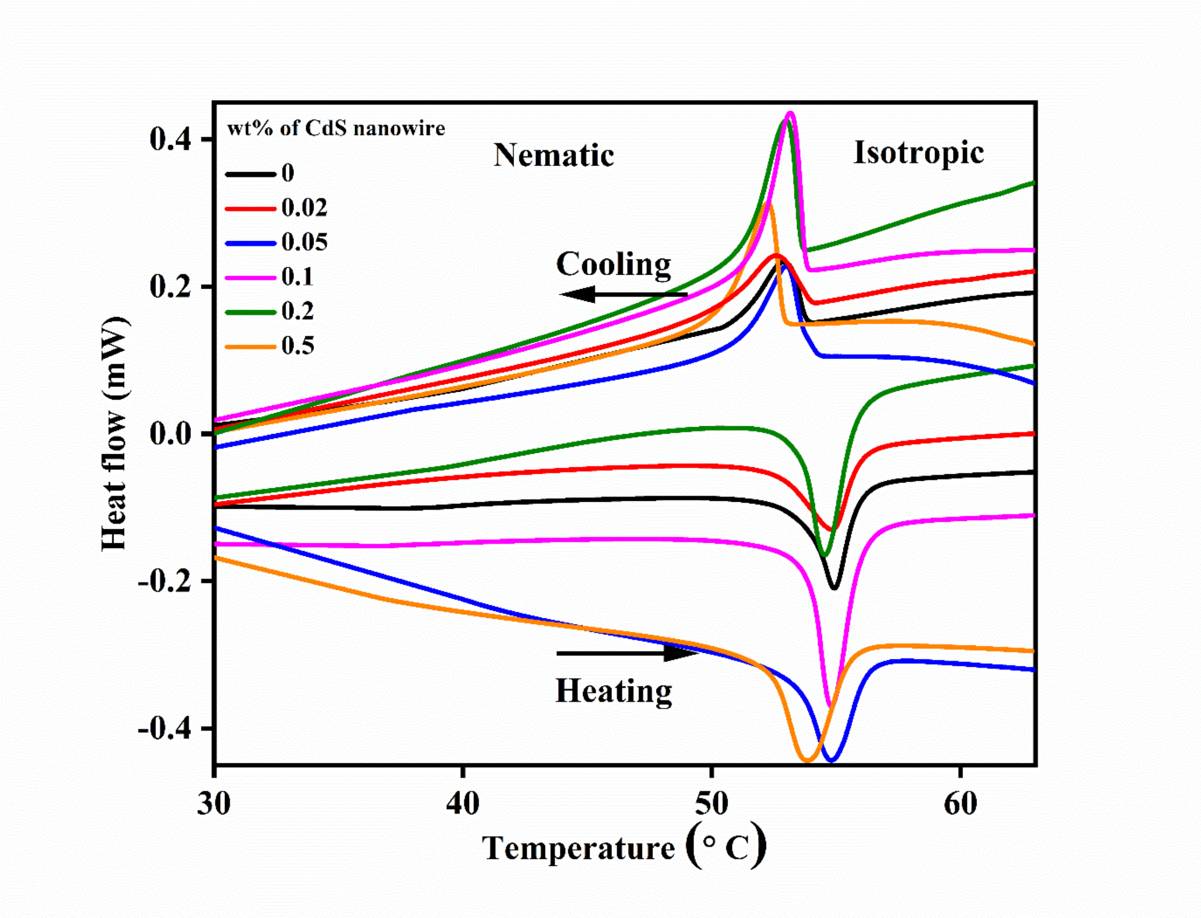

Figure 3-3 DSC thermographs of CdS nanowire nanocomposites of PCH5 samples

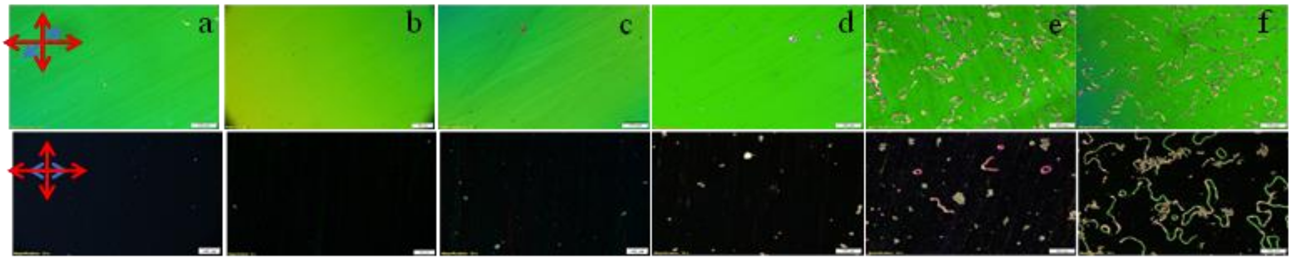

Figure 3-4 Polarizing optical microscope images of CdS nanowire nanocomposites of PCH5 samples where a-f corresponds to concentrations of 0,0.02,0.05,0.1,0.2,0.5 wt% of CdS nanowire in pure PCH5, respectively (scale bar : 100μm)

The value of birefringence (Δn) as a function of temperature is estimated using the transmitted intensity data as a function of temperature for pure PCH5 as well as nanocomposites of CdS nanowires in PCH5 is shown in Figure 3-5.

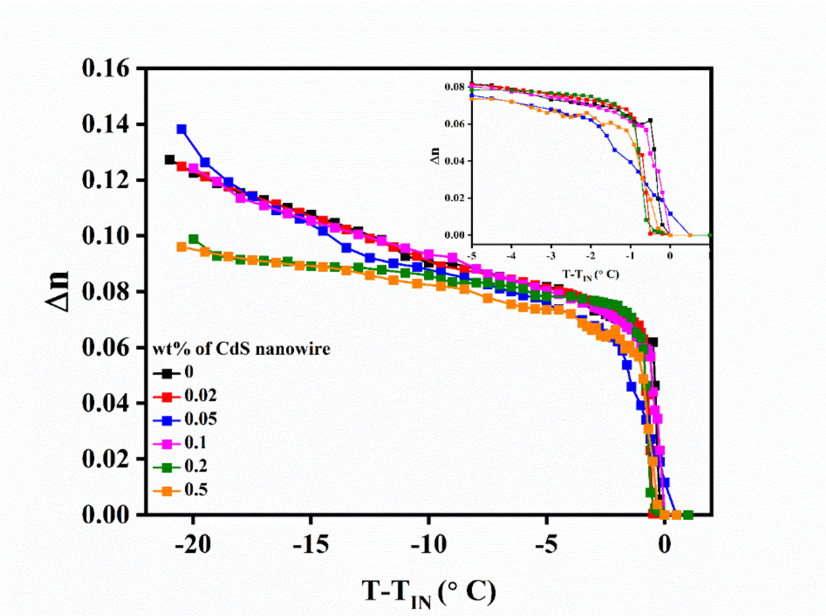

Figure 3-5 Variation of birefringence (Δn) as a function of temperature of CdS nanowire nanocomposites of PCH5 samples; inset shows the variation of birefringence in vicinity of I-N phase transition temperature from $T-T_{IN}$ = 0˚C to $T-T_{IN}$ = -5˚C

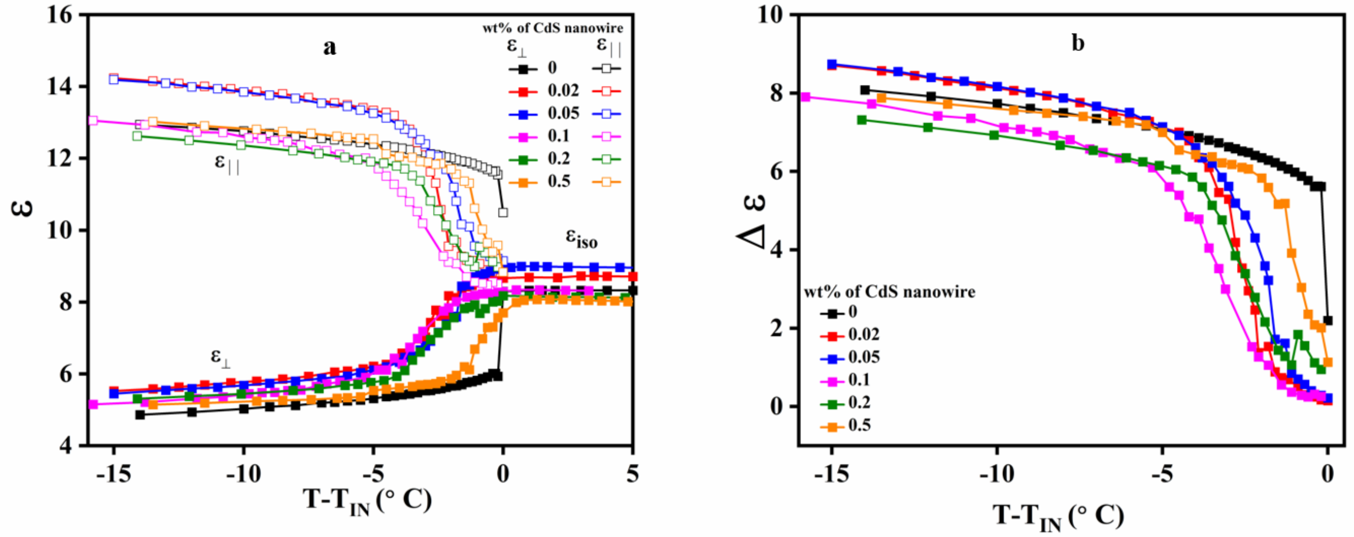

Figure 3-6 (a)Variation of parallel ($\varepsilon_{\parallel}$) and perpendicular ($\varepsilon_{\perp}$) components of dielectric permittivity; (b) Variation of dielectric anisotropy (Δε); as a function of temperature of CdS nanowire nanocomposites of PCH5 samples

For the given source wavelength (λ), the value of birefringence is calculated as,

$$\Delta n = \frac{\lambda}{2\pi d} \Delta\phi$$

where, d is the thickness of LC cell and the phase difference ($\Delta\phi$) is calculated from transmitted intensity (I_{tr}) as,

$$\Delta\phi = 2m\pi \pm \cos^{-1}\left(1 - 2\frac{I_{tr}-I_{min}}{I_0-I_{min}}\right) \qquad m=0,1,2,\ldots$$

where, I_0 is the maximum intensity of incident light.

The observed value of Δn as a function of T-T_{IN} for pure PCH5 is in good agreement with that of literature [100,101] The temperature variation of Δn for various CdS nanocomposites of PCH5 is also plotted in the Figure 3-5. The value of Δn as a function of temperature for concentration of $0.02, 0.05$ and 0.1 $wt\%$ of CdS nanowires in PCH5 remain to be similar as that of the pure NLC. The decrease in the value of Δn as a function of T-T_{IN} is ~2% and ~10% for CdS nanowire concentration of 0.2 $wt\%$ and 0.5 $wt\%$ respectively, as compared to pure NLC at T-T_{IN}= -10 ℃. As temperature lowers down below T-T_{IN}= -10 ℃, the aggregation of CdS nanowires in PCH5 causes the value of Δn to decrease appreciably as compared to that of the pure NLC. The value of Δn decreases by ~ 31% at T-T_{IN} = -15 ℃ for the concentration of 0.2 wt% and 0.5 wt% of CdS nanowire in PCH5.

Variation of parallel ($\varepsilon_{\|}$) and perpendicular ($\varepsilon_{\perp}$) components of dielectric permittivity as a function of T-T_{IN} for pure PCH5 as well as various CdS nanocomposites of PCH5 is shown in Figure 3-6a. Dielectric anisotropy($\Delta\varepsilon$ = $\varepsilon_{\|}$ - $\varepsilon_{\perp}$) derived from parallel and perpendicular components of dielectric permittivity as a function of T-T_{IN} at applied frequency of 4kHz is shown in Figure 3-6b. The measured values of $\Delta\varepsilon$, $\varepsilon_{\|}$ and $\varepsilon_{\perp}$ for pure NLC are in good agreement with earlier reported data[101]. The variation of $\Delta\varepsilon$ as a function of T-T_{IN} clearly indicates the evolution of I-N phase transition from weakly first order for pure NLC to continuous second order for CdS nanocomposites of PCH5.

The value of dielectric permittivity in the isotropic phase (ε_{iso}) of pure PCH5 remains constant up to T_{IN} and then show a sudden jump at T_{IN} showing weakly first order discontinuous behaviour of I-N phase transition. The addition of CdS nanowires in relatively small concentration of 0.02 wt% in NLC causes $\varepsilon_{iso}$to increase by ~ 4.5% in comparison to the value of $\varepsilon_{iso}$of pure NLC. Maximum increase of ~7.7% in the value of ε_{iso} is observed for the nanocomposite sample containing concentration of $0.05\,wt\%$ of CdS nanowire in PCH5 as compared to that of pure NLC. Further increase in the concentration of CdS nanowire to $0.1\ wt\%$ and above causes $\varepsilon_{iso}$to decrease. For the nanocomposite sample containing $0.5\ wt\%$ of CdS nanowires in pure NLC, ε_{iso} decreases by ~3.7% as compared to pure PCH5. Around T_{IN}, the values of $\varepsilon_{\parallel}$ and $\varepsilon_{\perp}$ for nanocomposites of CdS nanowires in PCH5 changes smoothly over a wide range of temperature. As we can observe from Figure 3-6a, for CdS nanocomposite samples of PCH5, the value of $\varepsilon_{\perp}$increases and the value of $\varepsilon_{\parallel}$ decreases as compared to that of pure PCH5 in the vicinity of phase transition. The values of various parameters such as $\varepsilon_{iso}, \varepsilon_{\parallel}, \varepsilon_{\perp}$, $\Delta\varepsilon$ are tabulated in Table 3-1.

Table 3-1 Values of dielectric permittivity at different temperatures for varying concentration (wt%) of CdS nanowire in PCH5

$T-T_{IN}$ (°C) →	**+3**	**-1**			**-5**			**-10**			**-14**		
wt% ↓	$\boldsymbol{\varepsilon_{iso}}$	$\boldsymbol{\varepsilon_{\perp}}$	$\boldsymbol{\varepsilon_{\parallel}}$	$\boldsymbol{\Delta\varepsilon}$	$\boldsymbol{\varepsilon_{\perp}}$	$\boldsymbol{\varepsilon_{\parallel}}$	$\boldsymbol{\Delta\varepsilon}$	$\boldsymbol{\varepsilon_{\perp}}$	$\boldsymbol{\varepsilon_{\parallel}}$	$\boldsymbol{\Delta\varepsilon}$	$\boldsymbol{\varepsilon_{\perp}}$	$\boldsymbol{\varepsilon_{\parallel}}$	$\boldsymbol{\Delta\varepsilon}$
0	8.32	5.82	11.8	5.98	5.32	12.39	7.07	5.02	12.76	7.74	4.86	12.94	8.08
0.02	8.73	8.55	9.05	0.5	6.22	13.33	7.11	5.75	13.86	8.11	5.52	14.22	8.7
0.05	8.98	8.74	9.45	0.71	6.11	13.25	7.14	5.68	13.84	8.16	5.45	14.19	8.74
0.1	8.32	8.19	8.55	0.36	6.1	11.75	5.65	5.44	12.56	7.12	5.21	13.04	7.83
0.2	8.15	7.84	9.06	1.22	5.76	11.91	6.15	5.44	12.36	6.92	5.3	12.62	7.32
0.5	8.04	6.7	10.6	3.9	5.54	12.53	6.99	5.24	12.8	7.56	5.15	13.03	7.88

The observed value of $\Delta\varepsilon$ in the nanocomposites of PCH5 drastically reduces to 0.5 in the 0.02wt% CdS nanowire nanocomposite of PCH5 compared to that of pure PCH5 at $T-T_{IN}=-1°\mathrm{C}$. With increase in concentration of CdS nanowire, the value of $\Delta\varepsilon$ reaches to 1.22 at $T-T_{IN}=-1°\mathrm{C}$ for nanocomposite sample containing 0.2 wt% of CdS nanowire in PCH5 which indicates the emergence of weakly first order nature of I-N phase transition. The weakly first order behaviour of I-N phase transition becomes prominent as CdS nanowire concentration increases to $0.5\ wt\%$ in PCH5 with $\Delta\varepsilon$ = 3.9 at $T-T_{IN}=-1°\mathrm{C}$. The highest value of $\Delta\varepsilon$ is observed for $0.05\ wt\%$ CdS nanowire in PCH5 is ~6.9% higher than that of the pure PCH5.

The lowest value of $\Delta\varepsilon$ is observed for 0.2 $wt\%$ CdS nanowire concentration in PCH5 is ~9.5% lower as compared to that of pure PCH5 at room temperature.

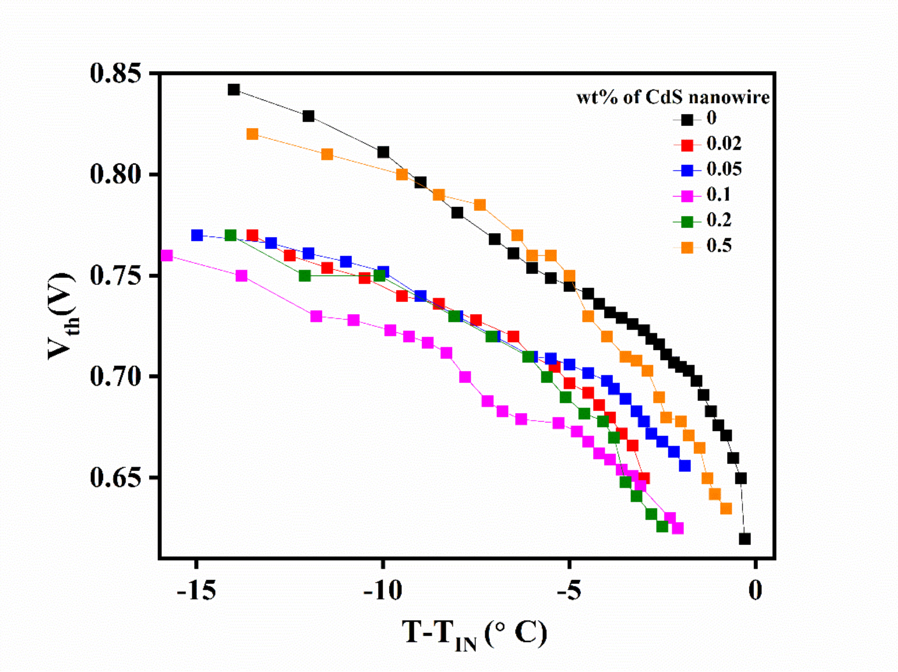

Figure 3-7 Threshold voltage (V_{th}) as a function of temperature for CdS nanowire nanocomposites of PCH5 samples

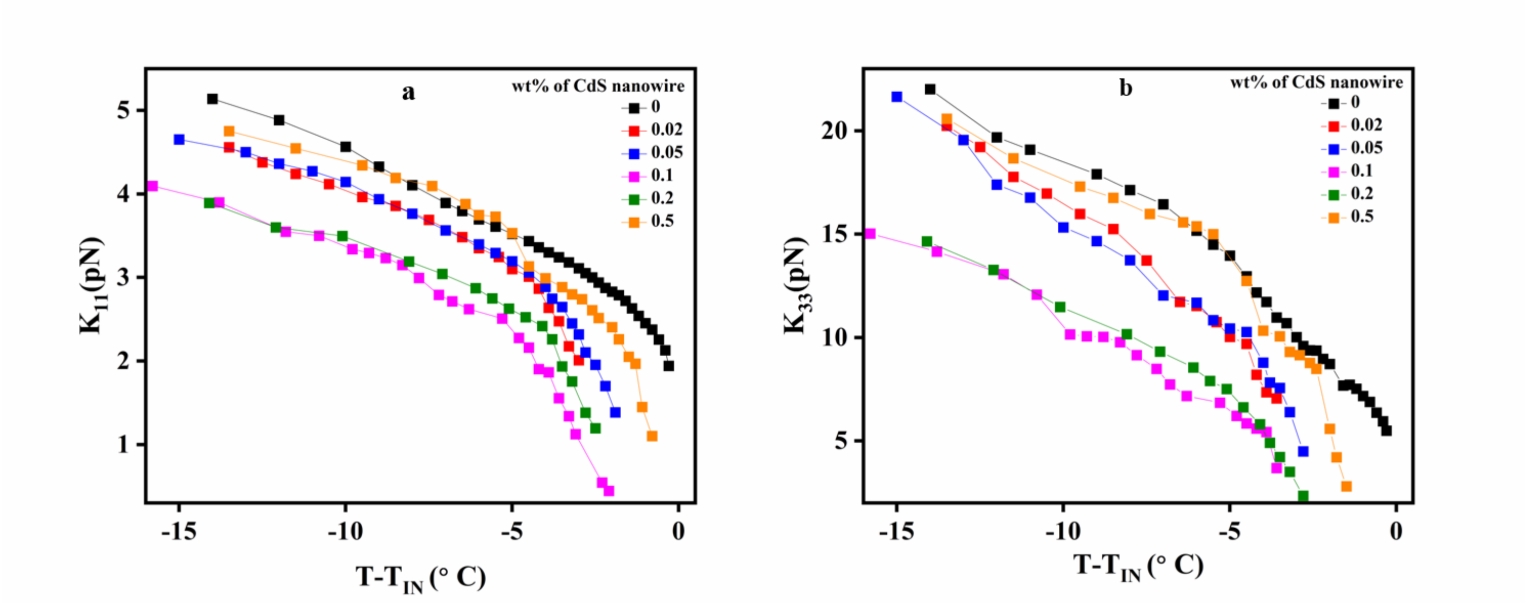

Figure 3-8 (a) Variation of splay elastic constant (K_{11}) as a function of temperature for CdS nanowire nanocomposites of PCH5 samples (b) Variation of bend elastic constant (K_{33}) as a function of temperature for CdS nanowire nanocomposites of PCH5 samples

The Freedericksz transition is the reorientation of nematic director of NLC along the applied electric field. In planar aligned cells, the initiation of Freedericksz transition happens at threshold voltage (V_{th}). Based on the dielectric measurements as a function of applied voltage, the variation of V_{th} as function of $T-T_{IN}$ for pure and nanocomposites of CdS nanowire in PCH5 are estimated and is shown in Figure 3-7. The temperature variation of V_{th} for pure NLC is in good agreement with earlier reported data [102]. Due to the continuous nature of I-N phase transition, it is difficult to find the value of V_{th} near T_{IN} for nanocomposites of CdS nanowire in PCH5.

The addition of CdS nanowire in smaller amounts of 0.02wt% in PCH5 causes V_{th} to decrease by ~ 8.6% at $T-T_{IN} = -14$ ℃. The decrease in V_{th} continues till the concentration of CdS nanowire increases to 0.1 wt% in NLC. For 0.1 wt% CdS in PCH5, V_{th} is reduced by ~10.8% compared to that of pure PCH5 at $T-T_{IN} = -14$ ℃. Initial decrease in the threshold voltage with increasing CdS nanowires may be due to alignment of CdS nanowires along the NLC host director and are helping to switch the molecules in the direction of field even at lower strengths of applied field. Aggregation of CdS nanowires makes the threshold voltage to rise again because of the bundling of nanowires which would require field of higher strength to switch. The value of V_{th} in nanocomposites of ≥ 0.2 wt% of CdS nanowires in PCH5 is higher compared to that of lower concentration nanocomposites due to bundling of CdS nanowires which can be seen as wormlike defect structures in POM images (Figure 3-4e-f). In the planar cell geometry, the threshold voltage is highly sensitive to the splay elastic constant (K_{11}), while the contribution of the bend elastic constant (K_{33}) is only effective at high voltages. Thus, value of K_{11} can be estimated using the measured values of threshold voltage and dielectric anisotropy using the formula: $K_{11} = (\varepsilon_0 \Delta\varepsilon \;/\; \pi^2)\, V_{th}^2$. The values of K_{33} of NLC samples are calculated from measured capacitance data as a function of voltage at voltages higher than the V_{th} using the C-V curve method [103]. Figure 3-8(a) and Figure 3-8(b) shows the variation of K_{11} and K_{33} respectively as a function of $T-T_{IN}$ for nanocomposite samples of CdS nanowire in PCH5. The variation of K_{11} and K_{33} as a function of $T-T_{IN}$ shows the similar trend as that of the threshold voltage.

The short-range orientational order present in the isotropic phase of CdS nanocomposites of PCH5 causes the removal of discontinuity of order parameter on both sides of T_{IN}. The decrease in the value of order parameter at T_{IN} due to addition of CdS nanowire in pure NLC at concentration ≤ 0.2 wt% makes it difficult to calculate the values of K_{11} and K_{33} near T_{IN}.

Below T-T_{IN} = - 2 °C, the value of $\Delta\varepsilon$ for CdS nanocomposites of PCH5 starts increasing but is still lower as compared to that of pure NLC. Hence, the decrease in the values of K_{11} and K_{33} of the CdS nanowire nanocomposites of PCH5 is observed as compared to pure NLC.

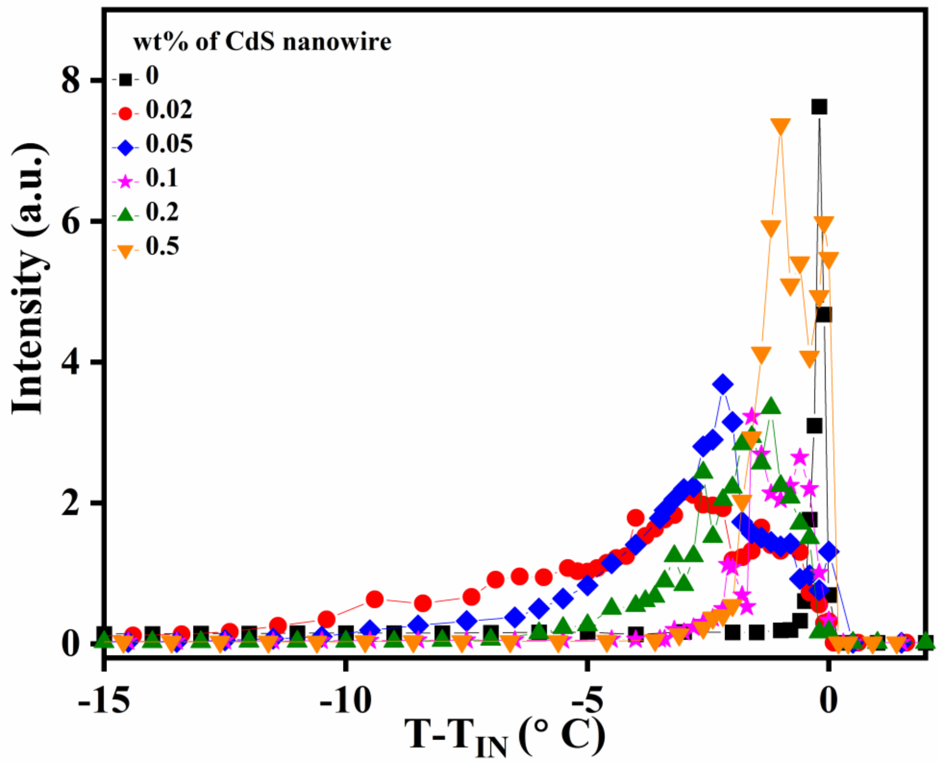

Figure 3-9 Variation of scattered intensity as a function of temperature for CdS nanowire nanocomposites of PCH5 samples from homeotropic cells under crossed polarizers

The highly ordered nematic domains in the vicinity of CdS nanowires may have been preserved even in the isotropic phase of bulk sample due to strong dipolar interactions between CdS nanowire and NLC molecules as well as amongst the NLC molecules in the molecular chains so formed. This may be the reason that the change in components of dielectric permittivity as the CdS nanocomposite sample of PCH5 is cooled from isotropic to nematic phase shows continuous change. This short-range nematic order in the isotropic phase of CdS nanocomposites of PCH5 in contrast to the highly disordered nature of molecules in isotropic phase of pure NLC helps to remove the discontinuity at the phase transition. To find the existence of the short-range nematic ordering in the nanocomposites of CdS nanowire in PCH5, the measurement of scattered light intensity as a function of temperature is also studied in the homeotropically aligned cells. The intensity variation as a function of $T-T_{IN}$ for pure PCH5 as well as CdS nanocomposite samples of PCH5 in homeotropically aligned cells is plotted in Figure 3-9. In the homeotropic alignment, the long axis of NLC molecules on an average is aligned parallel to the applied laser beam. Hence, there should not be any scattering of light when the laser beam passes through the NLC cell except for the very sharp intense peak at the N-I phase transition temperature. However, sample cells consisting of CdS nanocomposites of PCH5 shows contrasting phenomenon. In all the CdS nanocomposite samples of PCH5, a strong enhancement in scattering intensity is seen at the temperatures corresponding to the I-N transition. As soon as the CdS nanowire is introduced in the pure NLC at lower concentration of 0.02 wt%, the nematic domains so created made the applied laser beam to scatter till about $T-T_{IN} = -10$ ℃. This can be observed from the width of the peak in Figure 3-9. The curvature elastic constant K is reduced drastically in nanocomposites of CdS nanowire in PCH5, hence a broad peak in the scattered intensity can be observed, as the scattering intensity is $\propto 1/(K_{22} q^2)$. The width of the secondary peak observed decreases as the CdS nanowire concentration in pure NLC increases. Figure 3-6b also indicates that the second order nature of phase transition is shifted back to weakly first order as the aggregation of nanowires starts to happen in the nanocomposite samples of PCH5 for concentration of CdS nanowire ≥ 0.2 wt%. Because of the aggregation of nanowires some of the CdS nanowire bundles are formed as evident from Figure 3-4e-f which in turn reduces the number as well as length of the molecular chains so formed along the length of nanowire. The decrease in the short-range order present in the higher concentration of CdS nanocomposite sample of PCH5 introduces back the disorder in the isotropic phase of bulk sample responsible for the discontinuity at the I-N phase transition.

We have also carried out conductivity measurements on the CdS nanocomposites of PCH5 to study the effect of CdS nanowires on the ionic conductivity of NLC host matrix. The parallel ($\sigma_{\parallel}$) and perpendicular ($\sigma_{\perp}$) components of bulk ac conductivity at an applied frequency of 4kHz for pure PCH5 as well as CdS nanocomposite samples of PCH5 are shown in Figure 3-10(a). The separation of perpendicular and parallel components of conductivity at T_{IN} is clearly observed for the pure NLC. The bulk conductivity in isotropic phase (σ_{iso}) as well as $\sigma_{\parallel}$ and $\sigma_{\perp}$ are found to be increasing with the increase in concentration of CdS nanowires in PCH5.

As compared to pure NLC, the value of conductivity increases by ~60% with incorporation of 0.02 wt% of CdS nanowire in PCH5. The value of σ_{iso} for pure NLC is observed to be 1.32 μS/m which increases to 8.32 μS/m in case of 0.5 wt% concentration of nanocomposite of CdS nanowire in PCH5. The value of CdS nanowire in PCH5.

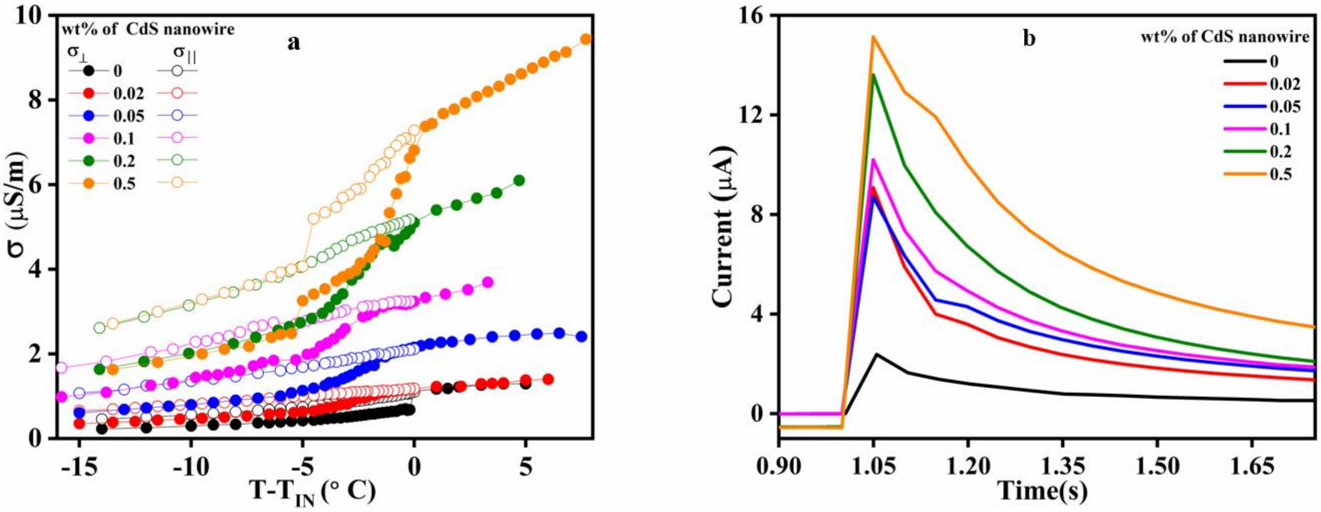

Figure 3-10 (a) Parallel ($\sigma_{\parallel}$) and perpendicular ($\sigma_{\perp}$) components of bulk ac conductivity at applied frequency of 4kHz (b) Ionic current measured by DC polarization measurements at room temperature; for CdS nanowire nanocomposites of PCH5 samples

At $T-T_{IN}$= -14˚C, values of $\sigma_{\parallel}$ and $\sigma_{\perp}$ changes are observed to be 0.45 μS/m and 0.23 μS/m respectively for pure PCH5 and 2.66 μS/m and 1.55 μS/m respectively for 0.5 wt% CdS nanowire in PCH5. The change in the values of conductivity at different temperatures for various concentrations of CdS nanowire in PCH5 is depicted in Table 3-2. The constant increase in the ionic conductivity might be due to the formation of conducting paths by longer nanowires and so formed molecular chains which allow the ions to move from one end to the other end of the NLC cells smoothly. CdS nanowires act as added impurities to the ionic impurities already present in the pure NLC and hence lead to a further increase in the ionic conductivity at higher concentrations of CdS nanowires. The increase in the ionic current at room temperature as measured by DC polarization measurement [35] is shown in the Figure 3-10(b). The value of maximum ionic current of PCH5 increases from 2.37μA to 9.08μA with the addition of 0.02 wt% CdS nanowires in PCH5. Further increase in concentration of CdS nanowire in PCH5 lead to larger values of current. The value of ionic current reaches a value of 15.1μA for concentration of 0.5 wt% of CdS nanowire in pure NLC.

Table 3-2 Values of bulk conductivity at various temperatures for varying concentration (wt%) of CdS nanowire in PCH5

T-T$_{IN}$ (˚C)	**+3**	**-1**			**-5**			**-10**			**-14**		
wt%	σ_{iso}	$\sigma_{\perp}$	$\sigma_{\parallel}$	$\Delta\sigma$	$\sigma_{\perp}$	$\sigma_{\parallel}$	$\Delta\sigma$	$\sigma_{\perp}$	$\sigma_{\parallel}$	$\Delta\sigma$	$\sigma_{\perp}$	$\sigma_{\parallel}$	$\Delta\sigma$
	μS/m												
0	1.26	0.64	1.00	0.36	0.42	0.74	0.32	0.30	0.56	0.26	0.23	0.45	0.22
0.02	1.30	1.12	1.14	0.02	0.64	1.01	0.37	0.48	0.82	0.35	0.38	0.69	0.31
0.05	2.38	2.03	2.04	0.01	1.13	1.69	0.56	0.80	1.36	0.55	0.61	1.07	0.47
0.1	3.62	3.19	3.24	0.05	1.99	2.79	0.80	1.44	2.29	0.85	1.09	1.82	0.73
0.2	5.74	4.70	5.00	0.30	2.73	4.05	1.32	2.01	3.14	1.13	1.63	2.61	0.98
0.5	8.12	5.33	6.76	1.43	3.25	4.07	0.82	2.00	3.29	1.29	1.55	2.66	1.11

To summarize, measurements of dielectric permittivity for CdS nanowire nanocomposites of NLC filled in planar cells show that weakly first order I-N phase transition of pure NLC evolves as continuous I-N phase transition with the incorporation of CdS nanowires ($< 0.2\ wt\%$) in NLC host. However, the conductivity of the CdS nanowire nanocomposites of NLC is observed to increase as compared to pure NLC. The dipole-dipole interactions between CdS nanowires and NLC molecules might play an important role in the observed results. Hence, dielectric spectroscopy measurements of pure and CdS nanowire nanocomposites of NLC filled in homeotropic cells is performed to investigate the relaxation dynamics of the pure and nanocomposite samples. In homeotropic configuration, the applied electric field is in the direction parallel to the long axis of the NLC molecules. The induced dipole moment due to applied electric field is expected to alter the effective dipole moment of the LC sample.

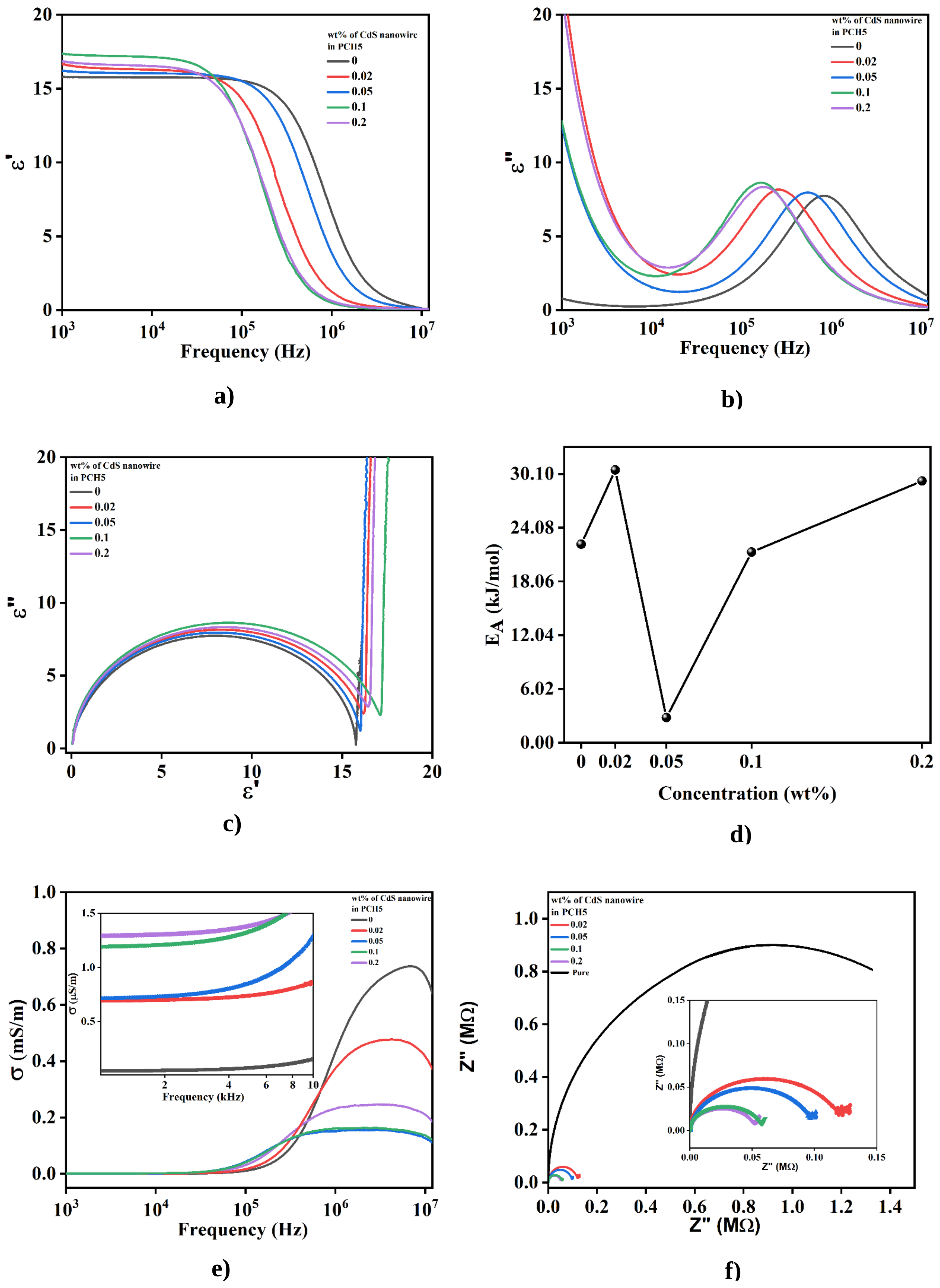
a)
b)
c)
d)
e)
f)

Figure 3-11 Variation of (a) real (ε') (b)imaginary (ε'') part of complex dielectric permittivity; (c) activation energy (E_A); (d) Cole-Cole Plot; (e) bulk ac conductivity (σ); (f) Nyquist plot; for pure PCH5 and nanocomposites of CdS nanowire in PCH5

As aggregation of nanowires in NLC matrix is observed for concentration of CdS nanowire in NLC $\geq 0.2wt\%$, we have performed dielectric spectroscopy measurements for CdS nanowire concentration $\leq 0.2wt\%$ in NLC. The variation of real (ε') and imaginary (ε'') parts of dielectric permittivity as a function of frequency for various concentrations of CdS nanowires in PCH5 at T = 35 ℃ is shown in Fig 3-11 (a, b), respectively. The value of ε' is observed to increase with increase in the concentration of CdS nanowires $\leq 0.1\ wt\%$ in PCH5 which may be due to increase in the total dipole moment of the nanocomposites on incorporation of CdS nanowires in PCH5. However, for concentration of CdS nanowire $\geq 0.2wt\%$ in PCH5, aggregation of CdS nanowires in the NLC matrix is observed and the value of ε' decreases but is still higher than that of pure NLC. The variation of ε''vs frequency is shown in Fig 3-11b. The peak in the MHz region of ε''vs frequency plot is the relaxation frequency (f_r) corresponding to the flip-flop motion of the NLC molecules. The value of f_r deceases with the addition of CdS nanowire in NLC as compared to that of the pure NLC. The Cole-Cole plot (ε'' vs ε') for pure and nanocomposites of CdS nanowire in PCH5 are shown in Fig 3-11c. The plots fitted with Havriliak - Negami Equation shows the Debye type relaxation behaviour in all the samples. The variation of dielectric strength ($\delta\varepsilon = \varepsilon_s - \varepsilon_\infty$) calculated from Cole-Cole plots is enhanced in all nanocomposites of CdS nanowires in PCH5 as compared to pure PCH5. This may be attributed to the observed increase in the value of ε' as shown in Fig 3-11a. The plot of f_r vs 1/T shows Arrhenius type behaviour. The activation energy (E_A) calculated from slope of f_r vs 1/T plot as a function of concentration of CdS nanowire in PCH5 is shown in Fig 3-11d. Variation of bulk conductivity (σ) with varying frequency is shown in Fig 3-11e. Low frequency region (Hz- kHz) of the curve is expected to show ionic relaxations processes in a dielectric medium. The value of σ is clearly observed to be increasing with incorporation of CdS nanowire in PCH5 as compared to pure PCH5 in low frequency region. Considering the combined effects of capacitive as well as resistive components of the LC cell, total impedance of the sample is measured. The variation of imaginary part (Z'') vs real part (Z') of the impedance is called the Nyquist plot. The Nyquist plots for pure and CdS nanowire nanocomposites of PCH5 are as shown in Fig 3-11 f. The diameter of the semicircle in Nyquist plot gives the resistance of the system which is observed to be reduced significantly with the incorporation of CdS nanowires in NLC implying increase in the overall conductivity of the nanocomposite samples as compared to pure NLC. The increase in the conductivity of the nanocomposite samples of PCH5 with the incorporation of CdS nanowires is observed from the measurements of conductivity in planar as well as homeotropic configurations. Hence, we may infer that long length of CdS nanowire provides a path for the conduction of ionic impurities by some possible mechanisms viz., charge transfer, $\pi - \pi$ interactions or hoping mechanism.

3.4 CONCLUSION

In this chapter, we have investigated the effect of incorporation of oleic acid functionalized CdS nanowires in wide temperature range NLC, PCH5. The key observations are as follows:

- The weakly first order I-N phase transition of NLC, PCH5 evolves into a continuous second order phase transition on incorporation of CdS nanowires in PCH5.
- The increase in the dielectric permittivity values in isotropic phase of low concentration CdS nanowire nanocomposite samples of NLC enclosed in planar aligned cells reveal that incorporated CdS nanowires in NLC lead to formation of small nematic domains of LC molecules even in isotropic phase of these nanocomposites.
- The scattered intensity measurements carried out on these nanocomposites enclosed in homeotropic cells further confirm that these short range ordered nematic domains created around these CdS nanowires in isotropic phase go on slowly increasing resulting in a second order I-N phase transition.
- In nanocomposites of NLC with CdS nanowire (<0.2 wt%), the alignment of CdS nanowires along the NLC host director leads to reduction of threshold voltage. The decrease in order parameter due to addition of large aspect ratio CdS nanowires leads to the decrease in splay and bend elastic constant. The favourable paths created due to long lengths of CdS nanowires makes the ion transport easy causing the bulk conductivity of these nanocomposites to increase.
- Further, the measurements of dielectric permittivity and conductivity as a function of frequency for samples filled in homeotropic cells complements the observed results of planar aligned cells. This also explains that the relaxation due to flip-flop motion of NLC molecule around short axis of rotation indeed slows down due to incorporation of CdS nanowire in PCH5.

CHAPTER 4

ZINC OLEATE NANOROD INDUCED VERTICAL ALIGNMENT OF LIQUID CRYSTAL

In previous chapter, we have shown that the behaviour of I-N phase transition of NLC is altered on incorporation of CdS nanowire functionalized with oleic acid. Incorporation of functionalized CdS nanowires leads to increase in overall conductivity of the nanocomposite sample as compared to pure NLC. To study the effect of another 1D nanomaterial on phase transition and properties of LC, zinc oxide nanorod functionalized with oleic acid (ZOR) is synthesized. Positive dielectric anisotropy liquid crystal 4′-Octyl-4-biphenylcarbonitrile (8CB) exhibiting nematic as well as smectic A phase is taken as host LC. The studies on investigation of incorporation of ZOR on I-N as well as N-SmA phase transition are presented in this chapter. An interesting result observed is that incorporation of ZOR ($\geq 0.3\, wt\%$) in LC matrix induces vertical alignment even in the samples filled in planar cells. The nanocomposite samples filled in unaligned cells also show homeotropic alignment of host liquid crystal molecules for concentration of ZOR $\geq 0.3\, wt\%$ in LC. Hence, systematic investigation of the textural, dielectric and conductivity properties of nanocomposites filled in planar cells is performed with increasing concentration of nanorods. At nanorod concentration $\leq\ 0.2\, wt\%$ in 8CB, the order parameter of nanocomposite samples is found to be increasing and ionic conductivity is found to be decreasing as compared to pure LC. Beyond $0.3\, wt\%$ concentration of nanorods in 8CB, vertical alignment of host LC is observed even in planar aligned cell. The vertical alignment of LC molecules in ZOR nanocomposites is confirmed through ATR-FTIR absorption spectra studies. The measurement of various dielectric properties of ZOR nanocomposites of 8CB as a function of frequency in homeotropic cells is also presented to understand the dipolar interactions and relaxation processes of the nanocomposite system. The dielectric strength of the ZOR nanocomposite samples is observed to be decreasing as compared to pure LC whereas magnitude of activation energy increases with the addition of ZOR in the LC. Conductivity of the nanocomposite samples is observed to be decreasing as compared to pure LC which suggests the adsorption of ionic impurities on the surface of zinc oleate nanorods.

Key findings of the study are published in

- Zinc Oleate Nanorod-Induced Vertical Alignment of Nematic Liquid Crystal, **Shweta Mishra**, Manjuladevi V, Raj Kumar Gupta, ACS Omega, 7, 50, 46466–46474, 2022, https://doi.org/10.1021/acsomega.2c05196

4.1 INTRODUCTION

Vertical alignment (VA) mode has been adopted for a variety of displays to improve the display performance persistently. This technique fetched revolutionary changes in the field of liquid crystal displays (LCDs). Various alignment modes, viz., planar, twisted nematic (TN) [72,104], vertical alignment (VA)[105], in-plane switching (IPS)[106], fringe-field switching (FFS)[107] are used in LC cells employed for LCDs. In the LC cells, twist, vertical, and splay alignments of the LC molecules are formed in the off-state of the applied field depending on the geometry of the LC cells. Generally, layers of polyimides or silanes with different chemical structures are used to produce such alignments. The main-chain type polyimides are used in the IPS mode cell to form a homogeneous alignment [108–110] and silanes or side-chain type polyimides are used in the VA-mode cell to form a homeotropic alignment [52,106,111]. The preparation of these alignment layers usually requires large quantities of solvent, high temperature operation for the thermal imidization reaction and a rubbing process. Rubbing process has some serious disadvantages like debris creation, electrostatic discharge, and partial particles which can introduce local defects, streaks and result in low-quality LCDs [112]. In comparison to FFS and IPS modes, the VA mode does not include any rubbing process for device fabrication and offers a very high contrast at normal incidence, mainly attributed to the initial vertical alignment of LCs [105]. The LC cells prepared without using alignment layers are suitable for fabricating flexible LC displays which require a low temperature process [75]. Dispersion of nanoparticles shows promising and easier approach for vertical alignment instead of using processes like self-assembled monolayers, photoalignment or evaporated oxide[113–115]. Several groups have reported vertical alignment of LCs using different nanoparticles (NPs) such as fullerenes [116], gold NPs [117,118], Nickel NPs [119], quantum dots[120,121] and polyhedral oligomeric silsesquioxane (POSS) NPs [113,116,122,123] . These VALC devices without any alignment layer displayed an ideal dark state under crossed polarizers. The realization of true dark state without application of external field helps to produce high contrast ratio in LCDs. Apart from displays, VALC devices find applications in sensors as well [124,125]. Nakamura et. al. proposed that vertical alignment can be induced by using fullerene particles without using alignment layers [126]. Jeng et al. reported vertical alignment of the LCs without an alignment layer by addition of nanoparticles of POSS into negative dielectric anisotropy LCs [116,123,127]. The electro-optical properties of these LC cells were found to be similar to a conventional homeotropic LC cell with alignment layers. The major problem for the application of POSS is the poor compatibility with LC media and weak interaction with LC molecules [128]. Pristine POSS NPs highly aggregate themselves in the LC media and create the macroscopic micron size domains resulting in severe light scatterings [122,129]. Addition of 1D nanomaterials to LC hosts in small quantity has shown betterment of the display parameters such as electro-optic switching time, contrast ratio and threshold voltage as observed by various research groups [51,78,94,130]. Addition of various types of CNT is widely studied and proven to show great potential as a doping material in LC for device applications[62,97,131] . But vertical alignment with the addition of 1D nanomaterials is yet to be explored. Here, we present the alignment properties of host LC molecules with positive dielectric anisotropy by addition of zinc oxide nanorods capped with oleic acid (ZOR). The vertically aligned domains of LC molecules are observed in unaligned LC cells with addition of low amount (0.3-0.5 wt%) of ZOR. Systematic investigation of effect of concentration of ZOR on dielectric and conductivity properties of host LC and its nanocomposites filled in planar cells is performed. The homeotropic alignment of LC molecules is observed despite of the presence of homogeneous alignment layer. The results are compared with the measurement carried out on nanocomposites filled in conventional homeotropic cell. Further, dielectric spectroscopy of pure and ZOR nanocomposites of 8CB is performed. the dielectric spectroscopy is an important tool to study the characteristic properties of composites of nanomaterial and liquid crystal (LC) [19,62,132,133]. Broadband dielectric spectroscopy is a technique that measures dielectric and conductivity properties of samples over a wide range of frequency with the application of low amplitude electric field [17]. The dielectric spectroscopy data obtained from LC samples can be used to understand the relaxation behaviour, ion mobility as well as diffusion process [62]. This study also helps to understand the dipolar interactions, order parameter and polarization behaviour of the nanocomposite system which may be helpful for the understanding of the molecular dynamics of LC matrix with the addition of nanoparticles.

4.2 EXPERIMENTAL

4.2.1 Synthesis of zinc oxide nanorods capped with oleic acid

Zinc oxide nanorods capped with oleic acid (ZOR) are synthesized using reflux method [134]. Zinc acetate dihydrate ($Zn(OAc)_2$), trioctylamine and oleic acid are purchased from Sigma-Aldrich and used as received. In a typical synthesis procedure, 4 mmol of $Zn(OAc)_2$ is added to 12 mmol of oleic acid followed by addition of 7.5 mL of trioctylamine under constant stirring. The reaction is carried out at 280 ˚C for 2 hours. The colour of the solution gradually changes to yellow and becomes little cloudy indicating the formation of nanorods. After the completion of reaction, solution is cooled down to room temperature and washed using ethanol several times till all the unreacted solvent is removed. The final product is dried in air at 80˚C and preserved for further studies.

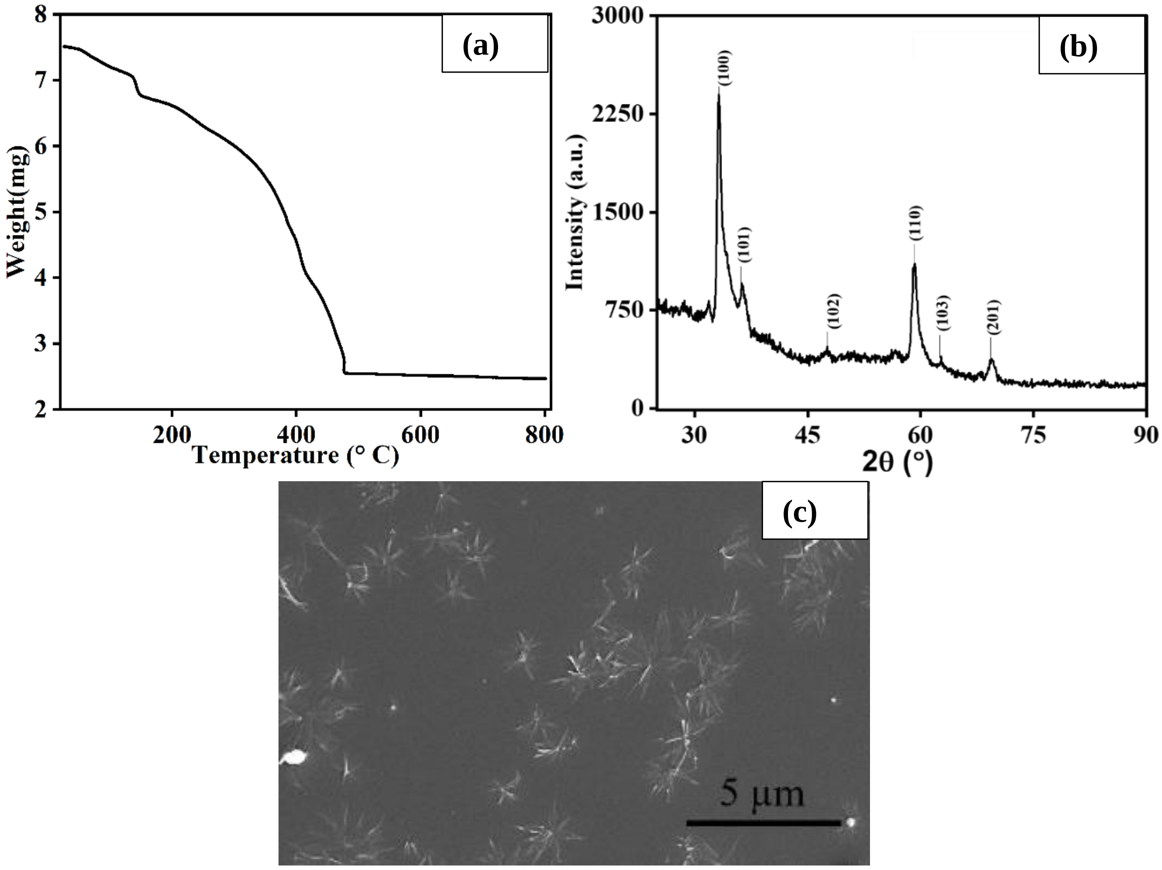

Figure 4-1 (a) TGA curve during heating cycle under N_2 flow (b)Powder XRD pattern (c)FE-SEM image of synthesized ZOR

The thermogravimetric analysis (TGA; Perkin Elmer TGA4000) of prepared sample is shown in Fig 4-1a. The actual weight loss is observed from $250℃ - 480\ ℃$ which shows the formation of zinc oxide nanorods capped with oleic acid [135]. The powder X-ray diffraction (XRD) pattern of synthesized ZOR was obtained using Rigaku Smartlab Studio II. The field emission scanning electron microscope (FE-SEM) image of ZOR is captured using FEI Apreo LoVac instrument. Fig 4-1 (b) shows the XRD pattern of as synthesized ZOR. Morphological structure of synthesized ZOR is shown in Fig 4-1(c). The nanorods obtained are bunched together to form a flower like structure. As observed from FESEM image, the nanorods are 50-60 nm wide and 1-1.2 micron in length.

4.2.2 Preparation of LC sample cells

For this experimental study, we have taken 4′-Octyl-4-biphenylcarbonitrile (8CB) as liquid crystalline host material procured from Sigma-Aldrich. The phase sequence of LC host 8CB is as follows: I (40.5℃) N (32.5℃) Sm-A (21.5℃) Cr.

The solution of 0.25 mg/mL of ZOR in chloroform is prepared and is ultrasonicated for about two hours to get a homogeneous dispersion. Calculated quantity of this solution is added into host LC to obtain various nanocomposites of concentrations (C_{ZOR}), viz., 0.05, 0.1, 0.2, 0.3, 0.4, 0.5, 1, 2 wt% of ZOR in 8CB. Sufficient time is allowed for the solvent to evaporate from the nanocomposites. For the electro-optic and dielectric measurements, we have used planar aligned cells of thickness ∼7.5 μm. Dielectric spectroscopy measurements are performed on pure and ZOR nanocomposites filled in homeotropic cells of thickness ∼7.5 μm.

4.2.3 Characterization Techniques

Thickness of the sample cells is measured using an interferometric fibre-optics spectrometer (Ocean-optics USB4000-XR1-ES). To study the alignment characteristics, cells using ITO plates with no alignment layers (unaligned cells) are also prepared. Optical texture of the LC filled sample cells is observed under polarizing optical microscope (POM; Olympus BX53M) at room temperature. The sample cell is placed inside the hot stage (Micro-optik MDTC600) with temperature control of 0.1℃ having a small hole in the middle to allow light to pass through. This assembly was then kept on the rotating stage of the POM between crossed polarizers. A laser beam of wavelength 633 nm passes through the sample placed between crossed polarizers. The planar cell is kept between crossed polarizers with a rubbing direction at an angle of 45° to either of the polarizers. The transmitted intensity (I_{tr}) as a function of temperature is recorded and used to estimate the birefringence (Δn) of the samples. As added nanoparticles do fluoresce, fluorescence confocal microscopy (ZEISS LSM880) with laser of wavelength ($\lambda = 370\,nm$) is performed to investigate the bulk and interfacial properties of ZOR in host LC. Dielectric permittivity (ε) measurements as a function of voltage are performed at an applied frequency of 4 kHz. Dielectric permittivity at applied voltage less than threshold voltage ($\varepsilon_{low(p)}$) and larger than threshold voltage ($\varepsilon_{high(p)}$) is measured using planar cells filled with pure and ZOR nanocomposites of 8CB. Threshold voltage (V_{th}) is measured with the help of capacitance-voltage (C-V) curve for nanocomposite samples filled in planar cell. Simultaneous measurements of components of conductivity, $\sigma_{high(p)}$ and $\sigma_{low(p)}$ are also performed using the method reported earlier [52]. Measurement of dielectric permittivity is also performed by application of electric field to homeotropic cells (ε_h) filled with pure as well as ZOR doped 8CB. All the measurements were recorded through a PC with the help of LABVIEW program. To understand the role of ZOR in the vertical alignment of 8CB, Fourier transform infrared (FTIR) absorption spectra of films of pure and ZOR doped 8CB in attenuated total reflection (ATR) mode are obtained using Perkin Elmer Spectrophotometer equipped with GladiATR. The ATR substrate is made up of diamond crystal with incident angle of 45°. The sample filled planar cell is broken laterally to acquire the ATR-FTIR spectra of aligned sample films. Similar samples were used to acquire the thin film XRD pattern to investigate the change in the smectic bilayer structure (SmA$_d$) of pure 8CB with the addition of ZOR. FTIR and XRD measurements are performed at room temperature where host LC exhibits smectic phase. Broadband dielectric spectroscopy of the samples is performed with the help of impedance analyser (Keysight E4990A) in the frequency range of 100Hz to 10MHz. Various parameters such as capacitance (Cp), loss factor (tan δ) and conductivity (σ) are measured in the given frequency range. Complex dielectric permittivity (ε^*) is calculated as

$$\varepsilon^* = \varepsilon' + i\varepsilon'' = \frac{C_p}{C_0} + i\varepsilon' tan\delta$$

where, ε' is real and ε'' is imaginary part of dielectric permittivity. C_0 is the capacitance of the empty cell before filling the sample.

4.3 RESULTS AND DISCUSSION

The optical textures of pure and ZOR nanocomposites of 8CB observed under cross polarizers of POM are as shown in Fig4-2. The optical textures are recorded for pure and ZOR nanocomposites of 8CB filled in planar, homeotropic as well as unaligned cells. Homogeneous and uniform alignment of molecules of pure LC is observed in planar and homeotropic cells, whereas characteristic schlieren texture of nematic phase can be observed in unaligned cell. The addition of ZOR for concentration upto 0.2 wt% (taken as critical concentration, C_{ZOR}^*) of 8CB also shows uniform alignment. When C_{ZOR} increases to 0.3 wt% in 8CB, we can notice the presence of homeotropically aligned domains in planar cell. With further increase in C_{ZOR}, vertically aligned domains increase.

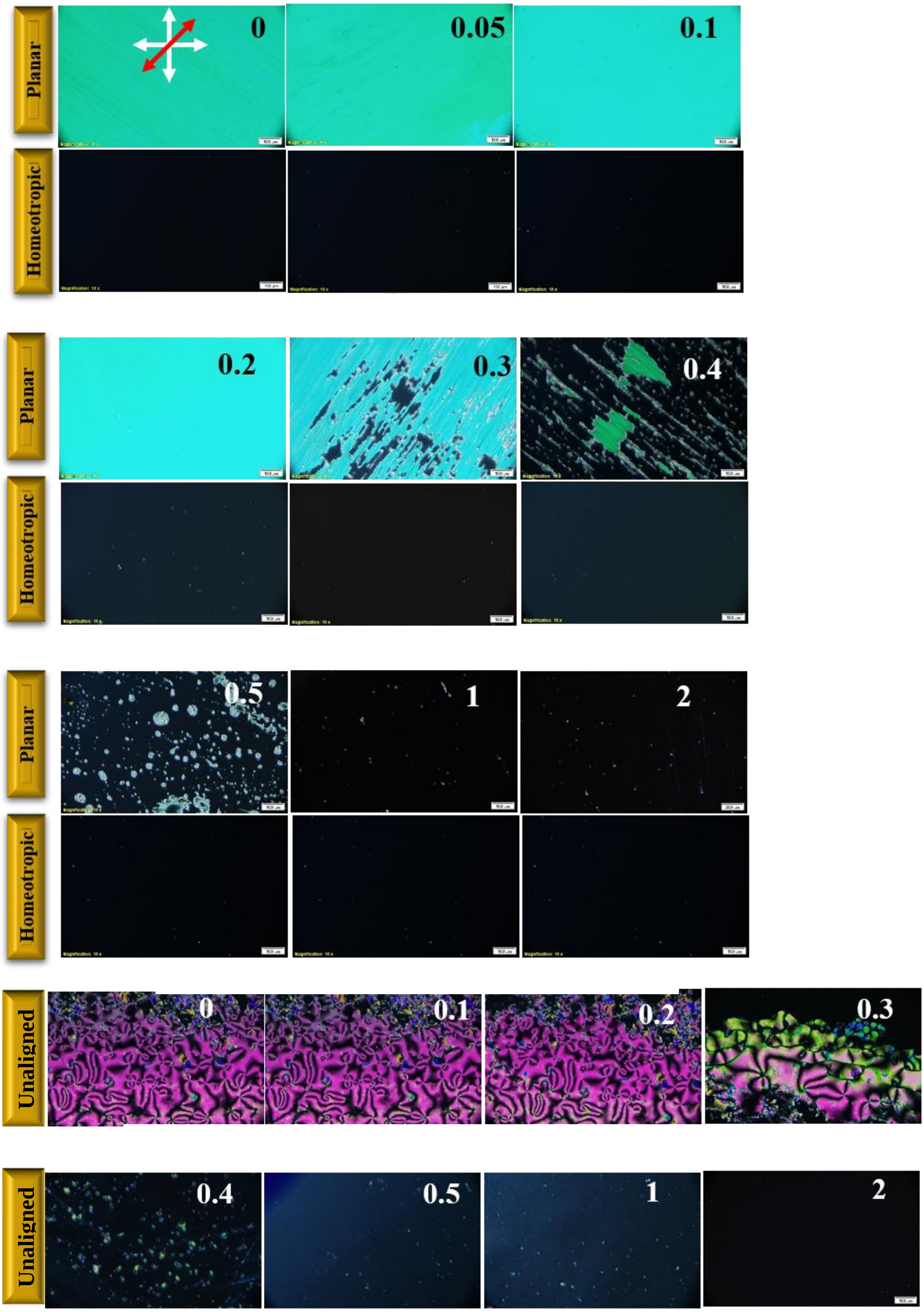

Figure 4-2 Optical textures of pure and ZOR nanocomposites of 8CB (T=35°C) in planar cells (row 1); homeotropic cells (row 2); and in unaligned cells observed under POM (numbers show C_{ZOR} in 8CB)

Complete dark texture of the planar as well as uncoated cells similar to that of the homeotropic cells, filled with ZOR nanocomposites of 8CB can be observed for $C_{ZOR} \geq 0.5$ wt% on rotation of microscope stage under crossed polarizers. This shows that, the presence of ZOR in 8CB helps the host LC molecules to align vertically owing to the interaction between ZOR and LC molecules. However, no aggregation of ZOR is observed in nanocomposite samples for the samples under investigation. Fluorescence confocal microscopy (FCM) images of pure and ZOR nanocomposites of 8CB are shown in Fig 4-3. The FCM images (left panel) are split into RGB components, and the blue component (indicating fluorescence of ZOR) is considered for drawing a line profile along the arrows as shown in the FCM images (right panel). Pure 8CB does not show any fluorescence (Fig 3e) and hence its analysis is not presented. However, fluorescence in ZOR nanocomposites of 8CB clearly indicates ZOR uniformly dispersed in the bulk of LC. As it can also be observed from the line profile, the higher value of fluorescence intensity is appearing in the bulk region of the sample cells filled with nanocomposites having dispersed ZOR (Fig 4-3(b-d)). To further comprehend the inference, a sample cell is prepared with the ZOR directly coated on the ITO substrate. This cell is then filled with pure 8CB, and FCM images are recorded. The line profile for this sample (right panel, Fig 4-3a) shows significant overlap in the interfacial region.

The alignment of LC molecules in nanocomposites depends on the shape of nanoparticle, chemical modification of the surface of particles, the miscibility of particles in the host and the properties of the confining substrates [136,137]. Several groups have shown that functionalized spherical nanoparticles or quantum dots (4-5 nm) accumulate at the surface of the substrate due to the low miscibility with the nematic hosts altering the boundary conditions which results in the modification of initial alignment layer [121,138,139]. However, the 1D shape anisotropy as similar to that of LC molecules and large aspect ratio (∼50:1000 nm) of ZOR helps LC molecules to form domains around dispersed nanorods. Hence, presence of ZOR is observed to be in the bulk instead of accumulating at the surface.

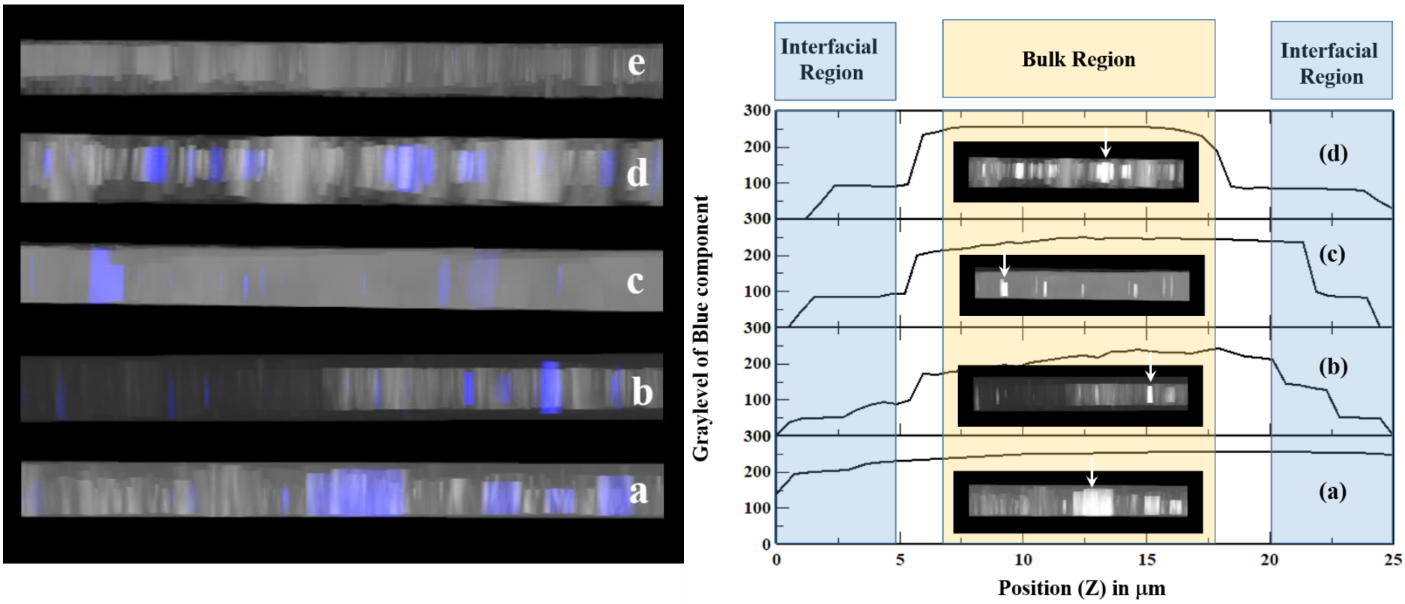

Figure 4-3 (left panel) Fluorescence confocal microscopy images and (right panel) Analysis of FCM images of (a) sample cell prepared by ZOR coated ITO substrate and then filled with 8CB (b)0.05 (c) 0.3 (d)2 wt% ZOR nanocomposites of 8CB (T=35℃) in planar cells (e) FCM image of pure 8CB showing no fluorescence.

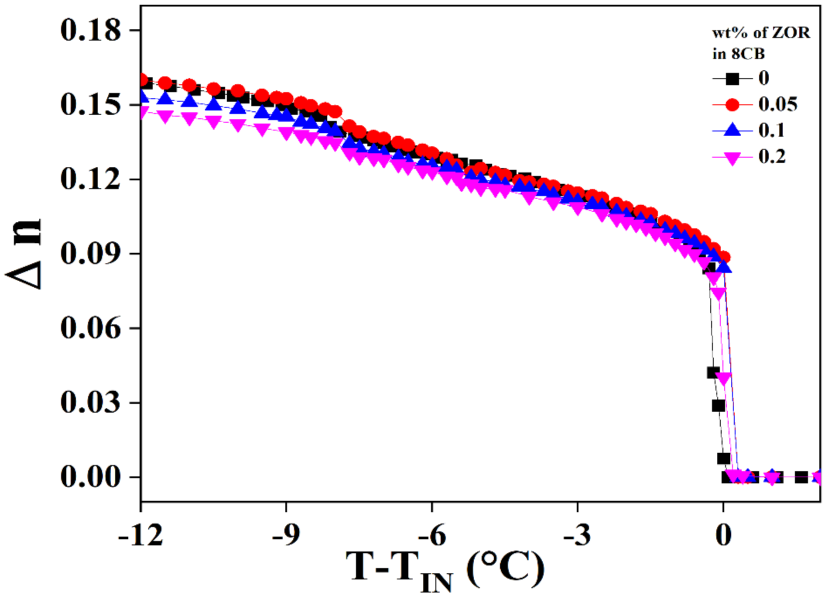

Figure 4-4 Birefringence (Δn) of pure and ZOR nanocomposites of 8CB ($C_{ZOR} \leq 0.2$) as a function of temperature

Based on the observation of optical textures, birefringence of pure and ZOR nanocomposites of 8CB is performed for $C_{ZOR} < C^*_{ZOR}$. The temperature variation of birefringence (Δn) for samples filled in planar cells is as shown in Fig 4-4. The change in the value of Δn is observed to be negligible as compared to the pure LC with the addition of ZOR. The decrease in the value of Δn as a function of temperature is observed at C^*_{ZOR}, as compared to pure 8CB.

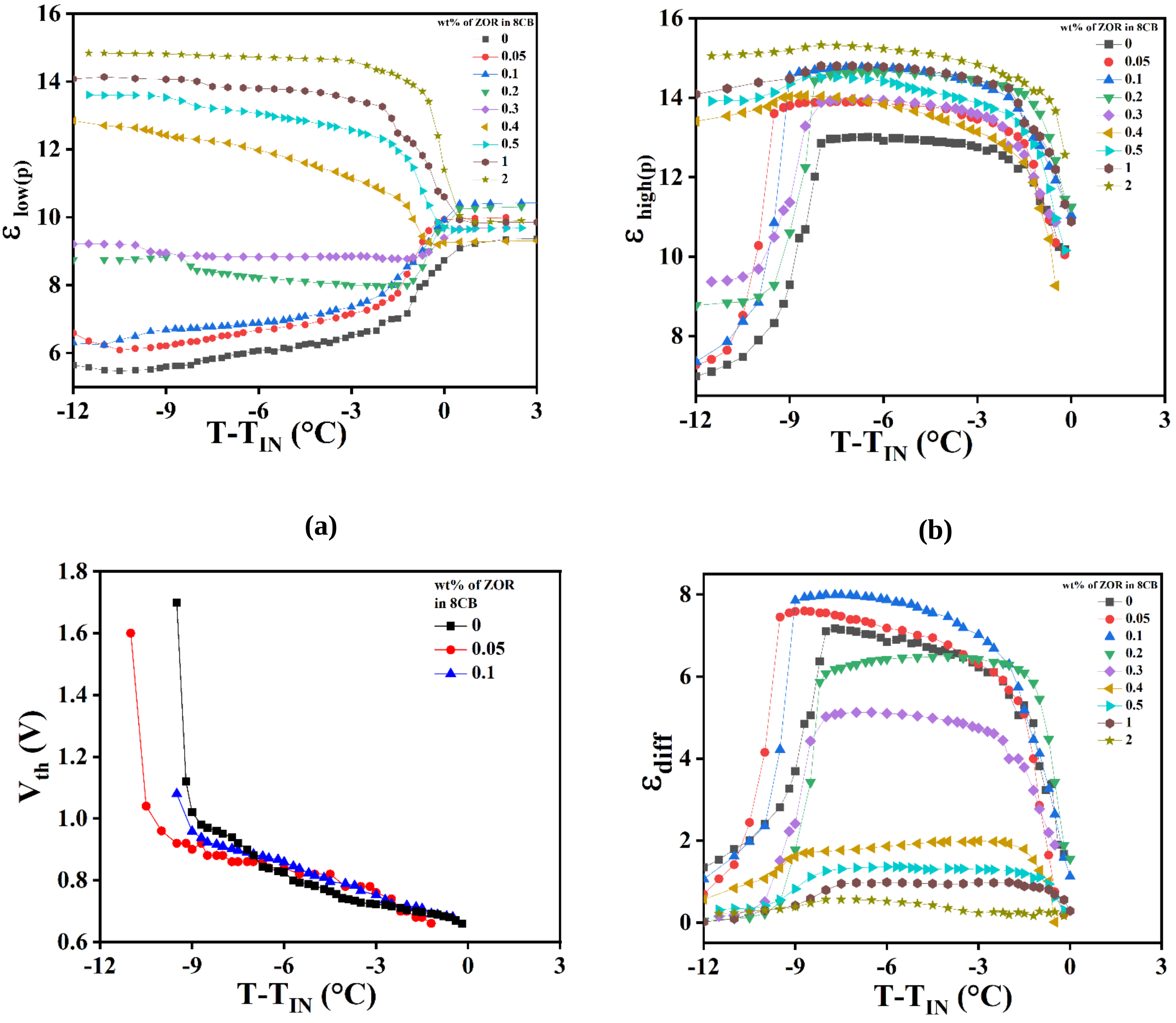

(a)

(b)

(c)

(d)

Figure 4-5 Variation of (a, b) components of dielectric permittivity as a function of temperature; (c) threshold voltage (V_{th}) for $C_{ZOR} \leq 0.2$; (d) $\varepsilon_{diff} = \varepsilon_{high(p)} - \varepsilon_{low(p)}$; for pure and ZOR nanocomposites of 8CB filled in planar cells as a function of temperature

Variation of dielectric permittivity as a function of temperature for pure and ZOR nanocomposites of 8CB filled in planar cells is presented in Fig 4-5. Here, the component of dielectric permittivity measured at V (0.5 V) < threshold voltage (V_{th}), is abbreviated as $\varepsilon_{low(p)}$,whereas the one measured at V (5V) > V_{th}, is abbreviated as $\varepsilon_{high(p)}$. In the isotropic phase, the value of dielectric permittivity, ε_{iso} increases with increase in concentration of ZOR in 8CB may be due to presence of short-range nematic order in isotropic phase of nanocomposite samples. At $C_{ZOR} \geq C^*_{ZOR}$, the value of ε_{iso} starts decreasing but is still higher than that of the pure LC. The value of $\varepsilon_{low(p)}$ increases with increase in the C_{ZOR} in 8CB as shown in Fig 4-5a. At C^*_{ZOR}, sudden increase in the value $\varepsilon_{low(p)}$ can be observed as shown in Fig 4-5b. This is due to added ZOR is helping the LC molecules in the vicinity of ZOR to orient vertically by overcoming the anchoring energy. The inference is further supported by FTIR and XRD measurements discussed later. The variation of V_{th} as a function of temperature in pure and nanocomposite samples < C^*_{ZOR} is shown in Fig 4-5c. The value of V_{th} in nematic phase which is proportional to the order parameter of nematic phase increases with decreasing temperature. However, V_{th} diverges as we approach the N-SmA transition temperature due to the formation of short range ordered cybotactic groups in the nematic phase [80]. Variation of V_{th} as a function of temperature in nanocomposite samples clearly indicates the nematic phase range has increased for C_{ZOR}= 0.05 wt% which is consistent with the results shown in Fig 4-5a. With further increase in C_{ZOR} = 0.1 wt%, the temperature range for nematic phase reduces but is similar to that of the pure LC. The measurement of V_{th} for $C_{ZOR} \geq 0.2$ wt% is not possible due to the tendency of vertical alignment of LC molecules with the aid of ZOR in nanocomposite samples as observed in Fig 4-5a. At C_{ZOR} = 0.3 wt%, the value of $\varepsilon_{low(p)}$ as a function of temperature almost flattens due to co-existence of vertically aligned as well as planar aligned domains as evident from optical textures as well. The measurement of V_{th} for concentration of ZOR $\geq C^*_{ZOR}$ is not possible, because of the tendency of LC molecules to vertically align in the presence of ZOR. For $C_{ZOR} \geq 0.4\, wt\%$, the curvature of $\varepsilon_{low(p)}$ as a function of temperature changes its sign due to dominance of vertically aligned domains which is clearly evident from the optical textures. Here, the value of $\varepsilon_{low(p)}$ changes similar to the variation of parallel component of dielectric permittivity. Kumar et. al. proposed that adsorption of ZnO nanoparticles on the substrate surface helps to reduce the surface energy of the substrate which subsequently produces the homeotropic alignment [140]. Choudhary et. al. reported that the enhanced local ordering of NLC molecules on the surface of a nanoparticles contributes largely to inducing homeotropic alignment of bulk LC material within the confined geometry of the sample cell [141]. The values of $\varepsilon_{high(p)}$ are observed to be increasing at any given temperature for all ZOR nanocomposites as compared to pure LC as shown in Fig 5a. The increase in the value of $\varepsilon_{high(p)}$ is attributed to the increase in the net dipole moment of the ZOR nanocomposites of 8CB, hence the order parameter, as compared to the pure LC. Singh et. al. reported that the enhancement in the net dipole moment of the nanocomposite system shows the parallel correlation between the dipole moments of LC molecules and nanorods [70]. A sudden decrease in the value of $\varepsilon_{high(p)}$ observed at N-SmA transition temperature is due to negligible effect of applied electric field on orientation of LC molecules due to emergence of smectic layering. The difference ($\varepsilon_{diff} = \varepsilon_{high(p)} - \varepsilon_{low(p)}$) for pure and ZOR nanocomposites of 8CB is shown in Fig 4-5d. The initial addition of ZOR ($C_{ZOR} < C^*_{ZOR}$), the values of ε_{diff} increases as compared to that of pure LC. The nematic temperature range is also observed to increase by 1.5 ℃ for C_{ZOR}= 0.05 wt% as compared to the pure 8CB. The value of ε_{diff} as well as nematic temperature range goes on decreasing with increase in $C_{ZOR} \geq C^*_{ZOR}$. The value of ε_{diff} is almost zero for C_{ZOR} = 2 wt% which confirms that alignment of 2wt% nanocomposite of 8CB is nearly homeotropic in the planar aligned cell. The value of ε_h measured for samples filled in homeotropic cells are compared with the values of $\varepsilon_{high(p)}$ measured using planar aligned cells. The value of $\varepsilon_{high(p)}$ measured for nanocomposite sample with the lowest concentration C_{ZOR}= 0.05 wt%, is ~ 5% lower than that of the value of ε_h due to the surface anchoring of LC molecules in the nanocomposite sample filled in planar cell. With increase in C_{ZOR}, the value of $\varepsilon_{high(p)}$ approaches the value of ε_h and is in agreement (~0.5% lower) for C_{ZOR} = 2 wt% which suggests that the nearly homeotropic configuration is achieved even in planar aligned cells.

The components of bulk ac conductivity at 0.5V ($\sigma_{low\ (p)}$) and 5V ($\sigma_{high\ (p)}$) are also measured for pure and ZOR nanocomposites of 8CB and temperature variation of ln (σ) is shown in Fig 4-6(a, b). The interesting fact observed here is that we obtain two regimes, one where bulk conductivity decreases ($C_{ZOR} \leq C^*_{ZOR}$) and the other where bulk conductivity is higher than that of the pure 8CB ($C_{ZOR} > C^*_{ZOR}$). Former one may be considered as ion capturing regime where the ionic impurities in the bulk 8CB are adsorbed by the added ZOR [142]. In the latter case, the formation of vertically aligned domains is facilitating the mobility of ions along with addition of external ions which causes the increase in conductivity in nanocomposite samples as compared to the pure LC. Maximum decrease of 57% in the ionic conductivity of the nanocomposite system for $C_{ZOR} < C^*_{ZOR}$ is also observed due to adsorption of ionic impurities by ZOR. The variation of σ as a function of C_{ZOR} in 8CB in Fig 4-6c which shows that the value of σ becomes almost constant after attaining a maximum at $C_{ZOR} = 0.5\ wt\%$.

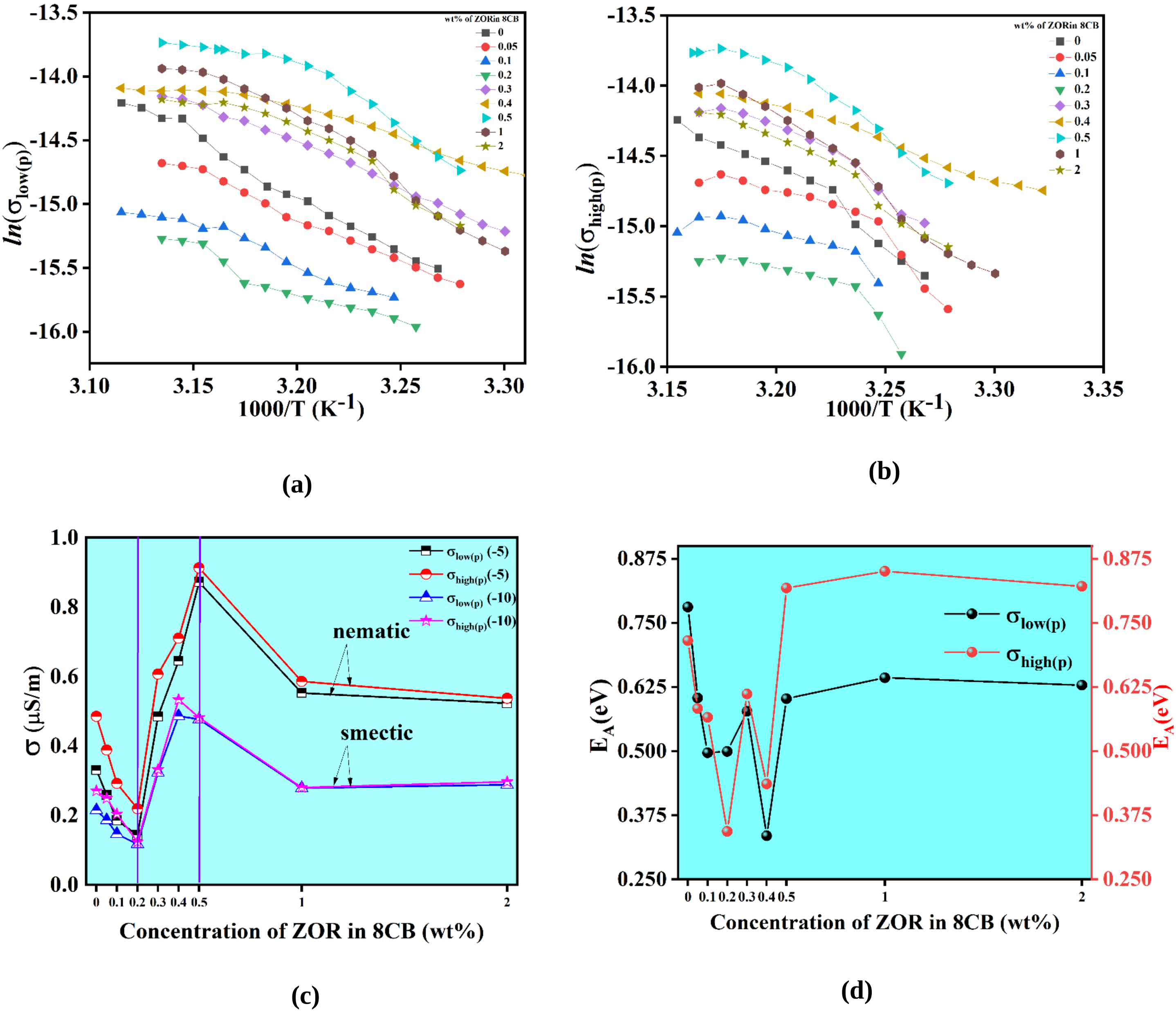

(a)

(b)

(c)

(d)

Figure 4-6 Variation of (a, b) components of bulk ac conductivity as a function of temperature; (c) bulk ac conductivity as a function of C_{ZOR} (numbers in the bracket denote $T-T_{IN}$ (°C)); (d) thermal activation energy as a function of C_{ZOR}

The analysis of temperature dependence of bulk conductivity shows that it can be satisfactorily described by the Arrhenius relationship, $\sigma = \exp\left(-\frac{E_A}{k_\beta T}\right)$, where E_A is the thermal activation energy. The variation of activation energy with increasing concentration of ZOR in 8CB is shown in Fig 4-6d for both components of bulk ac conductivity. The behaviour of bulk conductivity of ZOR nanocomposites of 8CB can be explained using simple model of thermal activation [58,143]. As observed from Fig 4-6d, the thermal activation energy becomes almost constant for $C_{ZOR} \geq 0.5\ wt\%$,i.e., when the host LC molecules are almost vertically aligned in the presence of ZOR.

To understand the role of ZOR in the vertical alignment of 8CB molecules, FTIR spectra of the pure and ZOR nanocomposites of 8CB are recorded. The ATR-FTIR spectra recorded in the range 400-4000 cm^{-1} of pure and ZOR nanocomposites of 8CB are shown in Fig 4-7(a,b). The IR band at 1792 cm^{-1} which is assigned to bridging C=O band is observed in all the ZOR nanocomposites, and not observed for pure 8CB (Fig 4-7a). The characteristic bands of 8CB are identified [144] and the integrated absorption for some of the bands as a function of concentration of ZOR in 8CB are shown in Fig. 4-7c. It can be noted from the variation that the integrated absorption increases due to incorporation of ZOR. The absorption of a given band depends on the interaction of the corresponding transition dipole moment and the IR field. In a planar cell filled with pure LC, molecules lie nearly flat to the surface. Therefore, the volume density of the transition dipole moments is expected to be least in this geometry. This gives rise to least absorption for any bands where the molecules are constrained in planar geometry. Similarly, in the homeotropic geometry, the volume density of the transition dipole moment of a given band is expected to be large which give rise to highest value for the absorption band. These behaviours are clearly seen from the Fig 4-7c. Due to incorporation of the ZOR, the planar alignment of the molecules gets perturbed, and a fraction of molecules show tendency to align vertically. Due to this perturbed alignment with increase in C_{ZOR}, an increasing trend in the absorption values is observed. The samples with $C_{ZOR} \geq 0.5$, show a complete homeotropic alignment. The intermediate concentration ranges 0.2 – 0.4 wt% of ZOR may indicate the transition wherein both the planar and homeotropic alignment coexisted.

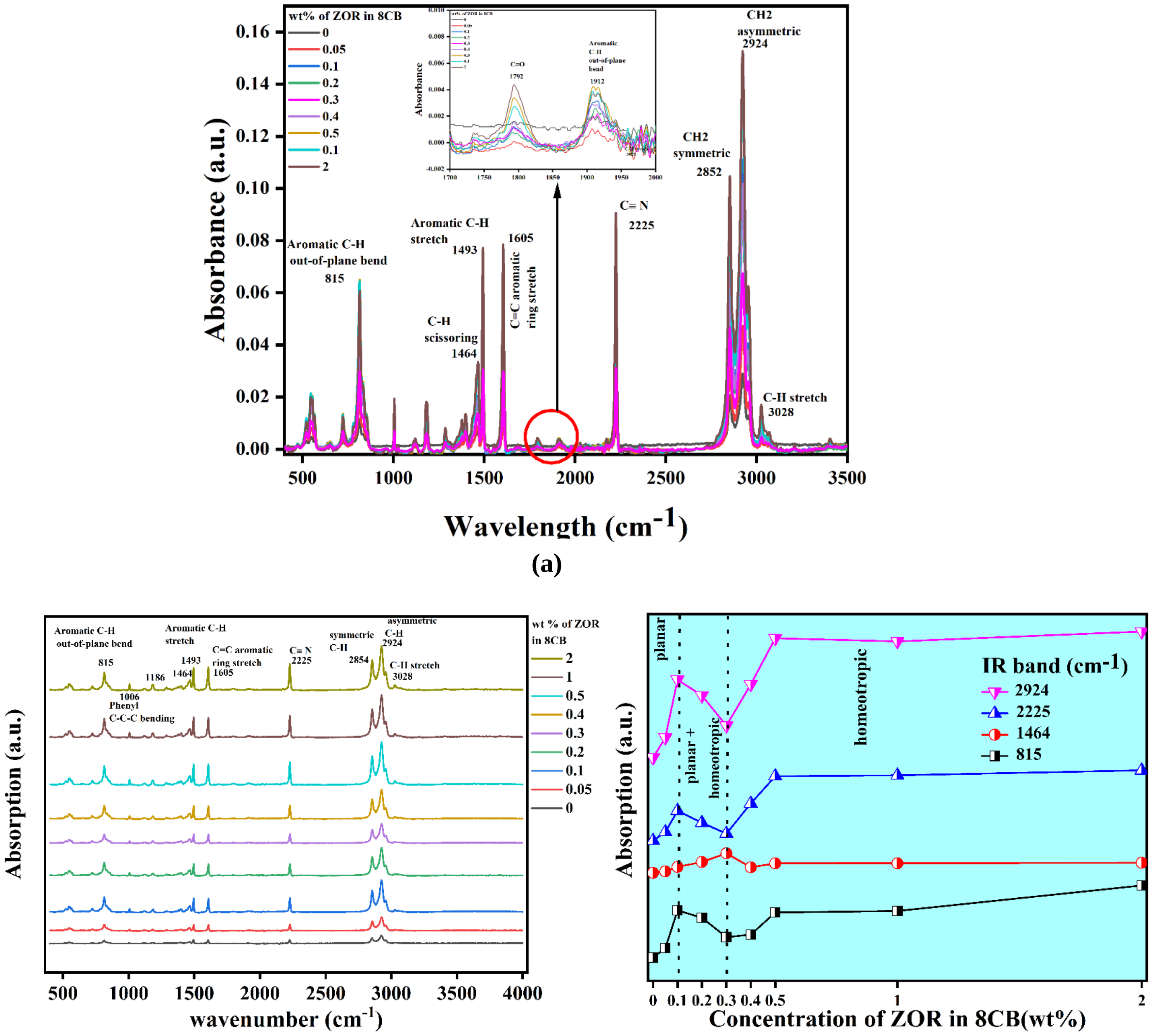

(a)

(b)

(c)

Figure 4-7 (a) Absorption spectra of pure and ZOR nanocomposites of 8CB recorded using ATR-FTIR (inset shows the bridging C=O band at 1792cm^{-1} that is absent in pure 8CB but can be observed in ZOR nanocomposites) (b)ATR-FTIR absorption spectra; (c) Variation of absorption intensity of IR bands as a function of C_{ZOR}; of pure and ZOR nanocomposites of 8CB

Further, the XRD patterns of pure and ZOR nanocomposites of 8CB are recorded. The peak in the low angle region (< 6 °) as shown in Fig4-8 arises due to scattering by the liquid crystal molecules. The layer spacing (d) corresponding to $2\theta \sim 3.09°$ is 24.86 Å, typical of the partial bilayer structure of pure 8CB in SmA phase can be clearly observed [145,146]. With increase in concentration of ZOR this peak gets broadened. However, the emergence of new peak at $2\theta \sim$ 5.5°, is observed for ZOR nanocomposites of 8CB for $C_{ZOR} \geq C_{ZOR}^*$ corresponding to the layer spacing of 13.92 - 13.6 Å which clearly indicates that there is change in partial bilayer layer spacing of ZOR nanocomposites of 8CB due to the co-existence of homeotropic and planar domains.

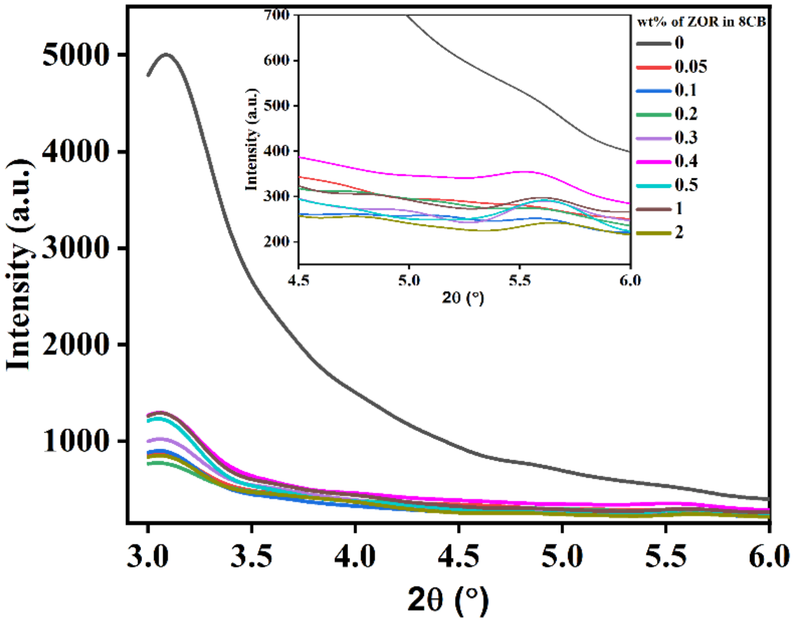

Figure 4-8 XRD pattern of pure and ZOR nanocomposites of 8CB

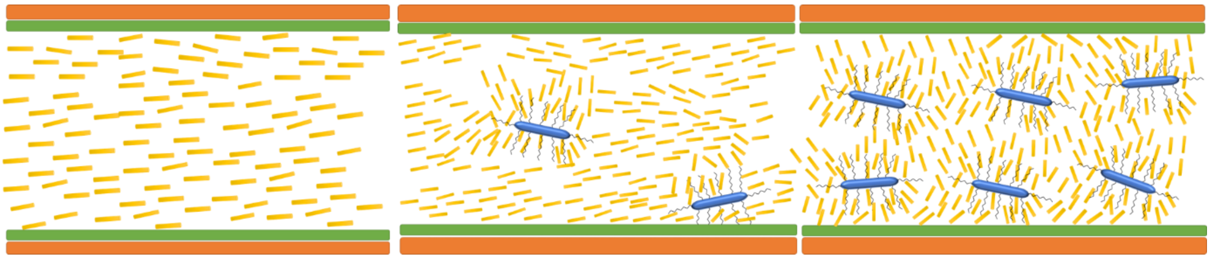

Pure 8CB

8CB+ZOR (0.02-0.04 wt%)

8CB+ZOR (≥ 0.5wt%)

Figure 4-9 Schematic representation of vertical alignment of 8CB due to incorporation of ZOR

A model is proposed based on the observed results as shown in Fig 4-9 showing the role of ZOR in the vertical alignment of host 8CB molecules. The molecular length of oleic acid functional group (~ 19.2Å) is comparable to that of the host 8CB molecule (~ 22 Å). Also, the molecules of 8CB can have pretilt angles upto 22° with respect to the substrate surface as reported earlier [147]. When the concentration of ZOR is low in the nanocomposite samples, the nanorods are preferentially near the substrate surface where anchoring energy of the substrate holds the host LC molecules to exhibit the planar configuration (schlieren texture in case of uncoated cells). With further increase in the concentration of ZOR, the nanorods in the bulk of the system causes the host LC molecules to align vertically achieving homeotropic configuration. The van-der Waal's interaction between oleic acid functional group and 8CB molecule might help the host LC molecules to overcome the anchoring energy of the substrate surface to align in the homeotropic configuration.

As discussed above, textural and dielectric properties of ZOR incorporated 8CB reveals the induced vertical alignment ($C_{ZOR} \geq 0.3\,wt\%$) of LC molecules even in planar cells. The conductivity of the ZOR nanocomposites, however, are found to decrease for $C_{ZOR} < 0.3\,wt\%$ as compared to pure LC. Hence, a study of conductivity and relaxation properties of ZOR nanocomposites of 8CB is performed using dielectric spectroscopy on samples filled in homeotropic cells for 0.1 wt% $\leq C_{ZOR} \leq 0.5\,wt\%$. Fig 4-10 (a) shows the variation of real (ε') and imaginary (ε'') parts of dielectric permittivity as a function of frequency for pure and ZOR nanocomposites of 8CB. The value of ε' is observed to decrease with increasing concentration of ZOR in 8CB which implies that the parallel correlation in dipoles of LC molecules is decreasing with the addition of ZOR. According to Maier-Meier theory,

$$\Delta\varepsilon' = \frac{NhF}{\varepsilon_0}\left[\Delta\alpha - \frac{F}{2kT}\,\mu^2\,(1 - 3cos^2\theta)\right]S$$

where, $\Delta\varepsilon'$ is directly proportional to macroscopic parameters S (order parameter) and N (number of LC molecules per unit volume). With increasing C_{ZOR}, N is expected to decrease due to large size of ZOR which in turn may lead to reduction of $\Delta\varepsilon'$. The magnitude of dielectric loss (ε'') at low frequency region (10^2-10^4 Hz) is observed to be decreasing ($C_{ZOR} \leq 0.4$) with the addition of ZOR.

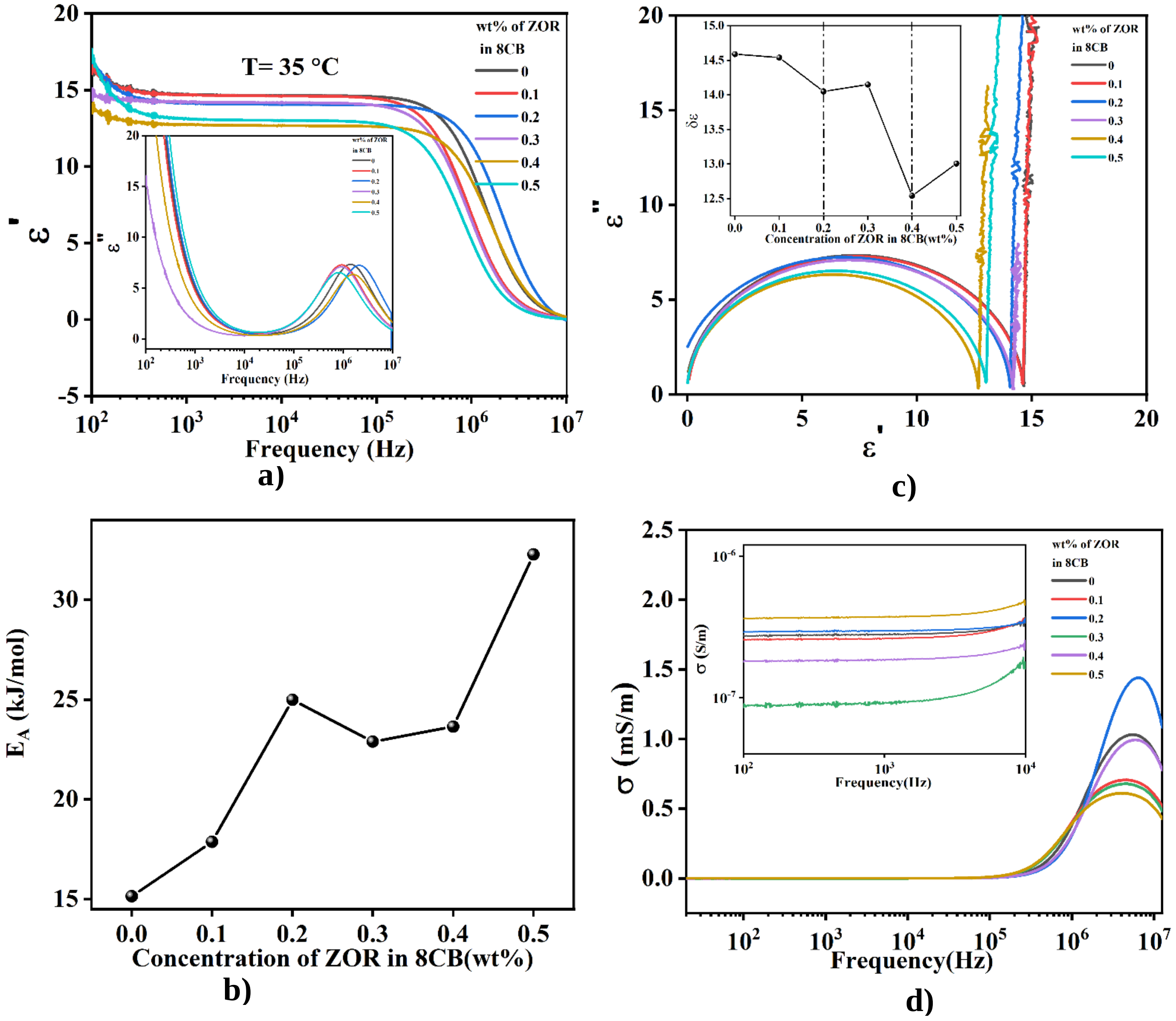

Figure 4-10 Variation of (a) real (ε') part and imaginary (ε'') part, of dielectric permittivity as a function of frequency (b) Cole-Cole Plot (inset: dielectric strength ($\delta\varepsilon$)) (c) Activation Energy (E_A) (d) bulk ac conductivity (σ); of pure and ZOR nanocomposites of 8CB filled in homeotropic cells at T=35℃

The graphs of ε'' vs ε' (Cole-Cole plot) for pure and ZOR nanocomposites of 8CB are shown in Fig 4-10b. The plots fitted with Havriliak - Negami equation shows the Debye type relaxation behaviour in all the samples. The variation of dielectric strength ($\delta\varepsilon = \varepsilon_s - \varepsilon_\infty$) as a function of C_{ZOR} in 8CB is shown in inset of Fig 4-10b. The dielectric strength calculated from Cole-Cole plots is observed to be decreasing with the addition of ZOR in 8CB as compared to pure LC. Mishra et al. [148] have observed decrease in the value of δε in a system of NLC doped with gold nanoparticles. They have suggested that the observed reduction of δε is due to the possible reduction of dipole moment due to the disorder induced by the dopant in host LC. Hence, decrease in the value of δε of ZOR nanocomposites as compared to pure LC may be attributed to the observed decrease in the value of ε' (Fig 4-10 a). As already discussed, the addition of ZOR in 8CB is observed to induce vertical alignment of LC molecules in planar cells for $C_{ZOR} > 0.4$ wt% and shows the mixed alignment state due to defect structure for $0.2 \leq C_{ZOR} \leq 0.4$. The fluctuation in the value of relaxation frequency (f_r) as a function of concentration for $0.2 \leq C_{ZOR} \leq 0.4$ might be due to the local defect structures created by addition of ZOR in 8CB. The bulky size of ZOR, interaction of functional group (oleic acid) of ZOR with surface anchored silane molecules as well as with LC molecules may affect the overall alignment of the nanocomposite sample. In the homeotropic alignment, the relaxation observed in MHz range is due to flip flop motion of LC molecules along the short axis. Slopes of the ln (f_r) vs inverse of the temperature plots have been obtained by the method of least square fit. Magnitude of activation energy calculated from the temperature variation of f_r shown in Fig 4-10c is observed to be increasing with the increasing C_{ZOR} in 8CB. The activation energy relates to the reorientation of the molecule around an axis perpendicular to the director. Increase in the value of E_A for nanocomposite samples as compared to pure LC suggests that ions would have higher activation barrier for mobility which in turn reduces the ionic conductivity in nanocomposites [149]. Variation in bulk ac conductivity (σ) of pure and ZOR nanocomposites of 8CB as a function of frequency is shown in Fig 4-10d. Inset shows the variation of σ in low frequency range (10^2- 10^4 Hz) where ionic contribution prevails. The value of σ is observed to be decreasing for $C_{ZOR} < 0.5\ wt\%$ as compared to pure LC in low frequency range. The adsorption of ions on the surface of ZOR may be the reason for decrease in the value of σ for ZOR nanocomposites of 8CB. Increase in the activation energy indicates the reduction in ion mobility in ZOR nanocomposites as compared to pure LC. For $C_{ZOR} \geq 0.5\ wt\%$ homeotropic alignment is favoured in planar and unaligned cells. Hence, for $C_{ZOR} = 0.5\ wt\%$ filled in homeotropic cell, a reduction in the value of f_r can be clearly observed (Fig 4-10a) and also increase in the ionic conductivity is observed due to formation of conduction pathways.

4.4 CONCLUSION

In this chapter, the effect of incorporation of oleic acid functionalized zinc oxide nanorods on various properties of liquid crystal are investigated. Systematic investigation reveals that ZOR induces vertical alignment of LC molecules above a critical concentration. Various properties are studies with respect to the concentration of ZOR in LC, 8CB and the findings are as follows:

- Zinc oxide nanorods capped with oleic acid (ZOR) are synthesized using reflux method. Crystalline phase and morphological structures of synthesized ZOR is confirmed using powder XRD and FE-SEM measurements.
- Homeotropic alignment of host LC molecules is observed for ZOR concentration above critical concentration of 0.2 wt% in 8CB. The vertical alignment can be achieved in unaligned ITO cells as well, which signifies that interaction of ZOR with host LC is responsible for vertical alignment of LC molecules.
- Maximum decrease of 57% in the ionic conductivity of the nanocomposite system for $C_{ZOR} < C_{ZOR}^{*}$ is observed due to adsorption of ionic impurities by ZOR.
- Further, dielectric spectroscopy studies on ZOR nanocomposites of 8CB is performed for 0.1 wt% $\leq \mathrm{C}_{ZOR} \leq 0.5\, wt\%$ to understand the relaxation dynamics of LC molecules in homeotropic alignment due to addition of ZOR. Magnitude of activation energy calculated from temperature variation of relaxation frequency is observed to be increasing implying reduction in the ion mobility in ZOR nanocomposites as compared to pure LC. Ionic conductivity is also observed to be reduced in the nanocomposites ($\mathrm{C}_{ZOR} \leq 0.4\, wt\%$) as compared to pure LC.

CHAPTER 5

EFFECT OF SHAPE OF ZINC OXIDE NANOPARTICLE ON ELECTRO-OPTIC AND DIELECTRIC PROPERTIES OF NEMATIC LIQUID CRYSTAL

Effect of incorporation of oleic acid functionalized CdS nanowires in PCH5 and oleic acid functionalized ZnO nanorods in 8CB on properties of host LC are presented in Chapter3 and Chapter4, respectively. To carry out a comparative study between the effect of functionalized and unfunctionalized nanomaterials, we synthesized zinc oxide (ZnO) nanoparticles of different shapes, i.e., nanospheres, nanorods and nanowires. The synthesized ZnO nanospheres, nanorods, and nanowires are incorporated in NLC matrix to further explore effect of shape of nanoparticle on behaviour of phase transition as well as other properties of NLC. Properties of liquid crystal incorporated with various shapes of a nanomaterial are expected to show multifaceted behaviour as properties of nanomaterial are remarkably dependent on its size and shape. Nanocomposites of 0.01 wt% ZnO nano- sphere, rods, and wires in NLC, PCH5 are prepared. The addition of ZnO nanoparticles to NLC leads to increase in the order parameter and reduction in threshold voltage, response time as well as ionic conductivity as compared to the pure NLC host. Dielectric permittivity measurements indicate nanoparticle induces short range order in isotropic phase. Dielectric measurements also show increase in order parameter in nanocomposites with 1D nanoparticles whereas negligible change is observed in nanocomposites with spherical nanoparticles in NLC in deep nematic range. The ATR-FTIR measurements support the enhancement in parallel correlation of dipole moments in ZnO nanocomposites as compared to pure NLC.

Key findings of the study are published in

- Effect of shape of ZnO nanoparticle on electro-optic and dielectric properties of nematic liquid crystal, **Shweta Mishra**, Manjuladevi V, Raj Kumar Gupta, J Mol Liq; 386:122482, 2023. https://doi.org/10.1016/j.molliq.2023.122482

5.1 INTRODUCTION

Nanomaterial assisted improvement in the characteristics of liquid crystals (LCs) have attracted a great deal of interest from researchers worldwide. Larger surface to volume ratio and quantum confinement effects makes nanomaterials to exhibit promising electrical, electronic, and optical properties[27]. Advances in preparation of nanomaterials have launched a new stage in the development of liquid crystal composites in terms of nanomaterial induced alignment, low threshold voltage, faster electro-optical response, enhanced dielectric behaviour, increased luminescence intensity, etc [60,150]. Researchers in the LC field have explored various nanomaterials including metallic, metal oxide, semiconducting, polymeric, ferroelectric nanoparticles (NPs), quantum dots (0D), rods, wires (1D) (QDs/QRs/QWs) to observe such promising improvements. Metal NPs (Au, Ag, Pd, Pt) can alter the elastic coefficient and rotational viscosity of the composite and lead to reduction in response time and threshold volage [72,151–154]. However, increase in the driving voltage (V_d) by doping these metal NPs may provide high electronic power consumption which needs to be avoided. Ferromagnetic and ferroelectric nanoparticle suspensions show increase in the dielectric anisotropy of the LC [48,155]. Addition of various metal oxide NPs (MgO, ZnO, TiO_2, Fe_3O_4 etc.) to liquid crystalline hosts is extensively studied which manifests the enhancement in device applications[134,149,156–158]. Besides these NPs, incorporation of carbon-based nanomaterials such as single- and multiwalled carbon nanotubes (S/M-WCNTs), graphene flakes, graphene QDs (GQDs), fullerenes, carbon dot have also been immensely investigated which shows exciting features in LC materials [58,60,62]. Similar organic structure and overlapping orbitals as π–π stacking of electrons could provide a pathway for the strong interaction between the LCs and carbon nanomaterials. Studies revealed that CNTs can influence nematic ordering, hence altering the electrical properties of the host LC[64,159]. Moreover, an increase in LC alignments, an improvement in the electro-optic response for displays, a change in the nematic to isotropic transition temperature, and an alteration of the ion concentration are also observed in the LC-CNT composites[46,56]. Classical Onsager theory[11] depicts that nematic phase is exhibited by rod-shaped molecules. Shape anisotropy is an important factor, and it might be expected that rod-like NPs, should cause an improvement of the nematic order. Since different NPs influence the properties of liquid crystals in different ways, the research community working with such systems is multidisciplinary.

The extreme size-dependent characteristics of nanomaterials provide an easy pathway to tailor their properties. In the composite systems of nanomaterials and LCs, both size and shape of

NPs play a very significant role. Several researchers have investigated the effect of doping of various nanoparticles differing in size and shape independently. Spherical NPs are observed to decrease the order parameter while elongated particles fit into liquid crystalline ordering and promote long-range molecular interactions[46]. Also, at higher concentrations of NPs in LC host, phenomenon of aggregation or phase separation may occur unlike in nanocomposites with low concentrations of NPs [46,136,138]. However, there are very few reports on collective studies of the effect of shape anisotropy of a given nanomaterial on physical properties of NLC[35,55,160]. In this article, we are reporting the effect of shape of the nanomaterial on the electro-optic and dielectric properties of LC. Zinc oxide (ZnO), a wide band-gap semiconducting material is selected for preparation of nanocomposites. ZnO is one of the potential candidates in the field of optoelectronics due to its high excitonic binding energy (60 meV), which depends on the dielectric constant of the materials. ZnO nanostructures are proven to be highly potential candidates in various fields such as sensors, transistors, photovoltaics, and drug delivery as well. In particular, we have synthesized nanospheres, nanorods, and nanowires of ZnO and incorporated them in a room temperature nematic liquid crystal. The evolution of birefringence and dielectric permittivity which gives insight into the order parameter of the system and dipolar interactions between LC molecules and ZnO nanoparticles is investigated. Further, the investigation of variation of various properties such as dielectric anisotropy, switching time, threshold voltage and ionic conductivity of LC-ZnO nanocomposites are reported. As, we have observed in earlier chapters that functionalized zinc oxide nanorods have the tendency to induce vertical alignment of LC molecules (concentration$\geq$ $0.2\ wt\%$) and functionalized CdS nanowires show continuous phase transition in the concentration range of $0.02\ - 0.05\ wt\%$. Hence, in this study nanocomposite samples of concentration 0.01, 0.02 and 0.05 wt% of ZnO NPs in NLC are prepared. However, no significant change in the properties of nanocomposite samples with increase in the concentration is observed. Hence, further investigations are carried out by optimizing the concentration of ZnO NPs in NLC = 0.01 wt% and the effect of shape of NPs on physical properties of NLC are measured followed by the discussion of results.

5.2 EXPERIMENTAL

For this experimental study, we have taken 4-(trans-4’pentylcyclohexyl)-benzonitrile (PCH5) as nematic liquid crystalline host material procured from Sigma-Aldrich. The NLC host PCH5 exhibits the phase transition sequence: Isotropic (55.3˚C) Nematic (30˚C) Crystal.

5.2.1 Synthesis of zinc oxide nanoparticles of different shape

NLC nanocomposites were prepared using zinc oxide nanoparticles (ZnO NPs) of various shapes synthesized in the laboratory. Here, ZnO NPs are synthesized by thermal decomposition of zinc acetate dihydrate (Sigma-Aldrich). Calculated quantity of the precursor was placed in an alumina crucible which is covered by an alumina lid. This assembly is transferred into the furnace. The crucible was heated to 300 ℃ and held for a period of 3 h, producing ZnO NPs in the powder form. The obtained NPs are stored for further analysis. The change in the reaction temperature and time yield various shapes of nanoparticles. The summary of the reaction temperature, heating time and the shape of the nanoparticle in the final product obtained is listed in Table 5-1. As synthesized NPs are dissolved in chloroform and ultrasonicated for about two hours to get a homogeneous dispersion. Calculated quantity of these solutions is added into host NLC to obtain 0.01 wt % nanocomposites. Sufficient time is allowed for the solvent to evaporate from the nanocomposite samples.

Table 5-1 Synthesis details of zinc oxide nanoparticles of various shapes

Temperature (℃)	**Heating Time (hrs)**	**Shape of nanoparticle**
600	12	Nanospheres
600	3	Nanowires
300	3	Nanorods

For the electro-optic and dielectric measurements, we have used planar aligned cells of thickness ~7 μm and area ~ 0.8 cm^2.

5.2.2 Characterization techniques

The crystalline phase of as synthesized NPs is estimated using X-ray diffraction (XRD) measurements using Rigaku Smartlab Studio X-ray diffractometer. The morphology of the synthesized particles is investigated using field emission scanning electron microscope (FE-SEM; FEI Apreo LoVac). UV-Vis absorption spectra of the nanomaterials are recorded using Thermo Scientific Evolution 201 in the wavelength range of $200 - 700\ nm$.

Differential scanning calorimetry (DSC) of pure and ZnO nanocomposites of PCH5 is performed using PerkinElmer DSC4000 at a heating/ cooling rate of $5℃/min$ in N_2 environment. Thickness of the sample cells is measured using an interferometric fibre-optics spectrometer (Ocean-optics USB4000-XR1-ES). To study the dispersion characteristics of NPs in the LC host matrix, fluorescence confocal microscopy (FCM) of pure and ZnO nanocomposites of PCH5 is performed using Zeiss LSM880. Optical texture of the LC filled sample cells is observed under polarizing optical microscope (POM; Olympus BX53M) at temperature, T= 40℃. The sample cell is placed inside the hot stage (Micro-optik MDTC600) having a small hole in the middle to allow light to pass through with temperature control of 0.1 ℃. This assembly was then kept on the rotating stage of the POM between crossed polarizers. A laser beam of wavelength ~ 633 nm passes through the sample placed between crossed polarizers. The sample cell is adjusted with a rubbing direction at an angle of 45° to either of the polarizers. The transmitted intensity as a function of temperature is recorded and used to estimate the birefringence of the nematic samples. Further, switching time measurement of the pure as well nanocomposites of NLC is performed by applying square wave of frequency 60 Hz using digital storage oscilloscope (DSO; Keysight EDUX1002G) at various applied voltage at different temperatures. To study the dipolar interactions of the ZnO NPs with LC molecules, Fourier transform infrared spectroscopy (FTIR) was performed using Perkin Elmer spectrophotometer equipped with ATR accessory (GladiATR) having diamond crystal with angle of incidence of 45°.

Measurements of dielectric permittivity (ε) as well as bulk ac conductivity (σ) as a function of voltage are performed at an applied frequency of 4 kHz. Sample cells with homogeneous alignment are filled with pure and nanocomposites of PCH5 are subjected to varying electric field to obtain parallel ($\varepsilon_{\|}$) and perpendicular ($\varepsilon_{\perp}$) components of dielectric permittivity as well as parallel ($\sigma_{\|}$) and perpendicular ($\sigma_{\perp}$) components of conductivity using the method reported earlier[52]. The variation of capacitance as a function of voltage is also used to determine threshold voltage (V_{th}). All the measurements were recorded through a PC with the help of LABVIEW program.

5.3 RESULTS AND DISCUSSION

The XRD spectra of as synthesized ZnO NPs are shown in Fig5-1(i). Synthesized ZnO NPs are observed to exhibit wurtzite crystal structure as confirmed using JCPDS card no. 36-1451. The unit cell of wurtzite crystal structure of synthesized ZnO NPs is shown in Fig 5-1(ii)d. The morphological characterization of ZnO NPs performed using FESEM is shown in Fig 5-1 (ii). The surface topography shows the formation of quasi-spherical NPs (ZS) having length: width ($l\!:w \sim 50\!:50$ nm), nanorods (ZR) of ($l\!:w \sim 50$ nm$:1\mu$m) and nanowires of ($l\!:w \sim 50$nm$:10\mu$m).

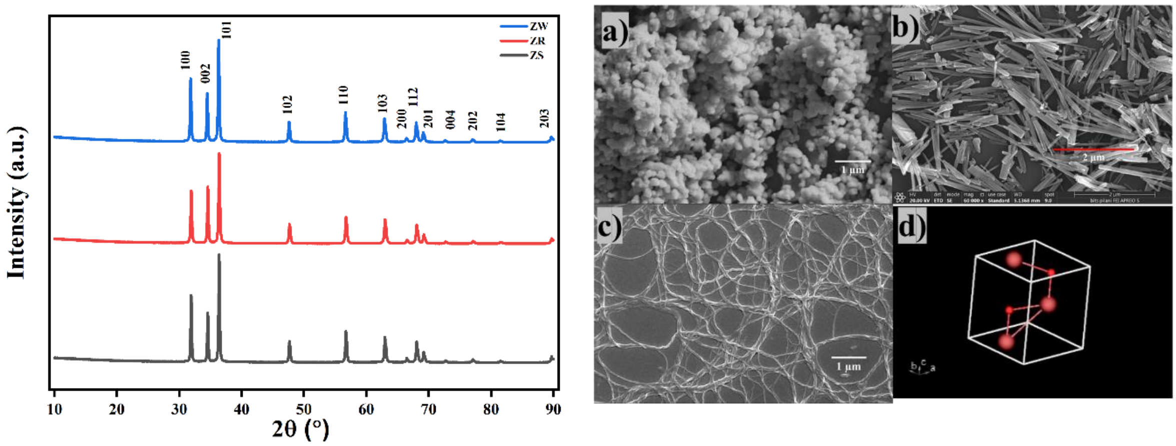

(i)

(ii)

Figure 5-1 (i) XRD pattern of synthesized ZnO nanoparticles (ii) FESEM images of a) ZnO nanospheres (ZS) synthesized at 600°C-12 hrs b) ZnO nanorods (ZR) synthesized at 300°C-3 hrs c) ZnO nanowires (ZW) synthesized at 600°C -3 hrs d) Wurtzite unit cell crystal structure of ZnO

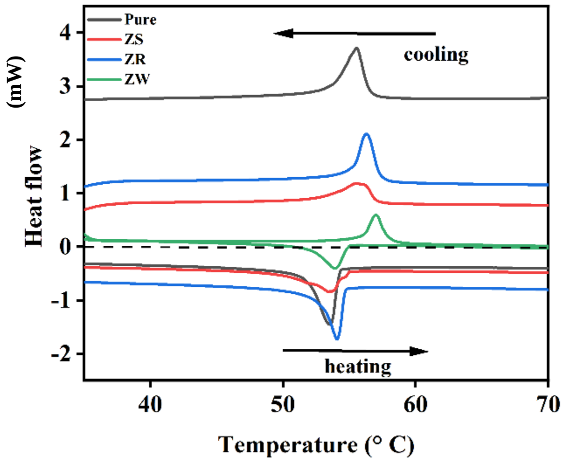

	Heating (°C)	Cooling (°C)
PCH5		

Figure 5-2 DSC thermograms of pure and 0.01 wt% ZnO nanocomposites of PCH5

Table 5-2 Phase transition temperature of ZnO nanocomposites of PCH5 obtained from DSC thermographs.

UV-Vis absorption spectra of ZnO nanomaterials shows the absorption peak at $380\ nm$. The nanomaterial characterization confirms the highly crystalline, stable ZnO nanostructures (spheres, rods, and wires) with wide band gap of $\sim 3.3\ eV$. The DSC thermograms of pure and ZnO nanocomposites of PCH5 are shown in Fig 5-2 and corresponding isotropic-nematic (I-N) phase transition temperatures in heating and cooling cycles are listed in Table 5-2 alongside Fig 5-2. The addition of nanospheres does not affect the I-N transition temperature whereas addition of 1D nanoparticles tends to increase the I-N transition temperature as compared to that of the pure NLC. Increase in the ordering of molecules due to addition of 1D nanoparticles having similar shape anisotropy as that of the NLC molecules may be one of the reasons for increase in the I-N phase transition temperature.

Figure 5-3 Optical textures of pure and 0.01 wt% ZnO nanocomposites of PCH5 observed between crossed polarizers under POM showing homogeneous alignment and no aggregation of nanoparticles in NLC.

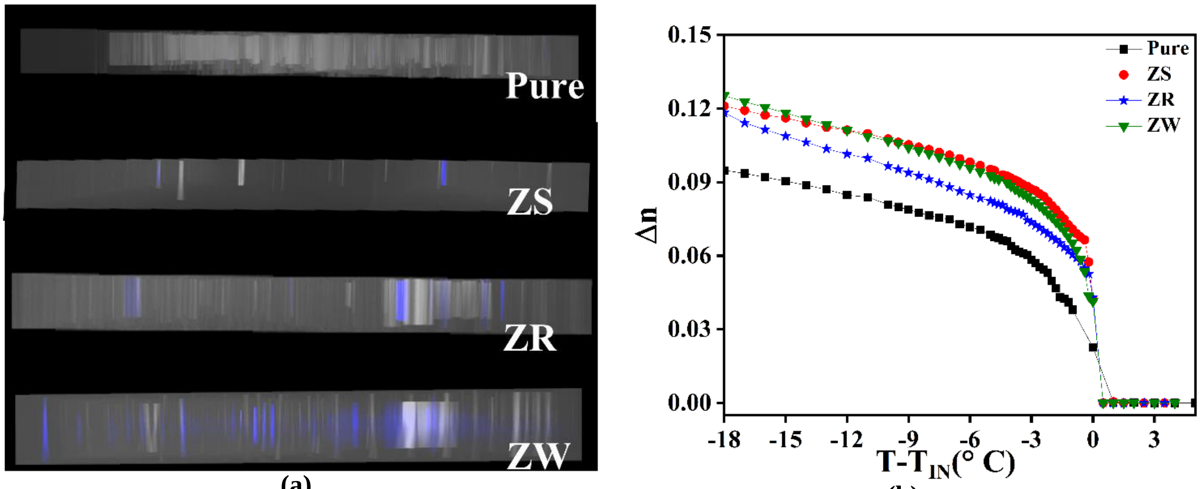

(a)

(b)

Figure 5-4 (a)FCM images (b) Variation of birefringence with temperature; of pure and 0.01 wt% ZnO nanocomposites of PCH5

The optical textures of sample cells kept between crossed polarizers of POM are observed as shown in Fig 5-3. Uniform alignment of samples in planar cells is observed indicating the homogeneous dispersion of NPs in host NLC. No aggregation in nanocomposite samples is observed at NP concentration of 0.01 wt% in NLC. The FCM images of pure and ZnO nanocomposites of LC are shown in Fig 5-4a. As ZnO NPs show fluorescence in UV region, FCM images are taken using laser of excitation wavelength ($\lambda = 370\ nm$). As we can observe, the nanoparticles are dispersed in the NLC matrix without aggregation or accumulation at the substrate surfaces. Variation of birefringence (Δn) of host NLC with addition of ZnO NPs as a function of temperature is shown in Fig 5-4b. As we can observe, the value of (Δn) at any given temperature increases by ~ 20% with addition of nanoparticles at given concentration. The ATR-FTIR absorption spectra of pure and ZnO nanocomposites of PCH5 are recorded and shown in Fig 5-5a. Various IR absorption bands are identified and corresponding vibrational modes are marked [161] listed in Table5-3. The values of integrated absorption of some selected IR peaks are plotted for various ZnO nanocomposites of PCH5 as shown in Fig 5-5b. With the addition of ZnO NPs in NLC host, integrated absorption for all peaks is observed to increase 4-fold as compared to that of pure NLC. This shows that the parallel correlation of dipole moments has been enhanced due to addition of 0.01 wt% ZnO nanoparticles in PCH5.

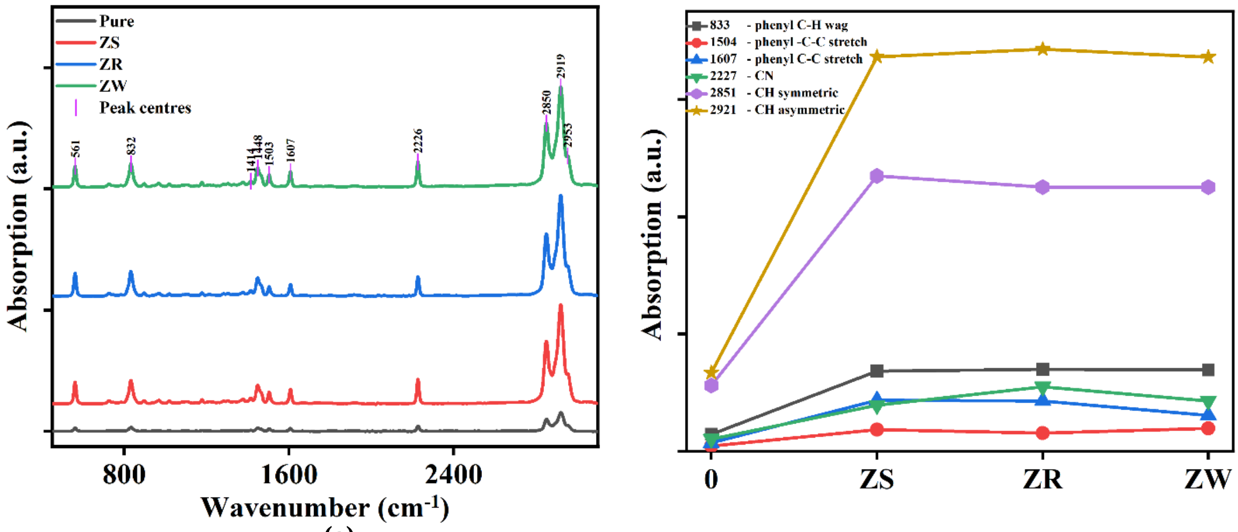

(a)

(b)

Figure 5-5 (a)ATR-FTIR absorption spectra; (b) integrated absorption of selected absorption peaks; of pure and 0.01 wt% ZnO nanocomposites of PCH5 in planar aligned cells

Table 5-3 Selected IR absorption bands and corresponding vibrational modes of NLC (PCH5)

IR Absorption Band (cm^{-1})	**Vibrational Mode**
832	Phenyl -CH wagging
1448	-CH deformation
1503	Phenyl C-C stretch
1607	Phenyl C-C stretch
2226	-C≡N
2850	-CH symmetric stretch
2953	-CH asymmetric stretch

The variation of dielectric permittivity (($\varepsilon_{\parallel}$) and ($\varepsilon_{\perp}$)) and dielectric anisotropy ($\Delta\varepsilon = \varepsilon_{\parallel} - \varepsilon_{\perp}$) with the incorporation of ZnO NPs in PCH5 is shown Fig 5-6(a) and Fig 5-6(b), respectively. The temperature variation of ε can be described using three regions. Region 1 describes the variation of ε in isotropic phase ($T - T_{IN} \gtrsim 0$°C), Region 2 describes the evolution of ε near I-N phase transition (-4℃ $\lesssim T - T_{IN} \lesssim 0$℃), and Region 3 describes the evolution of ε in deep nematic phase ($T - T_{IN} \lesssim -4$℃), for pure and ZnO nanocomposites of PCH5. In region1, value of ε is observed to be increasing in ZnO nanocomposites as compared to pure NLC. The values of $\varepsilon_{\perp}$ increases for all nanocomposite samples as compared to pure NLC in region2 and region 3. But evolution of $\varepsilon_{\parallel}$ shows different behaviour in various ZnO nanocomposites under investigation as compared to pure NLC in region 2 and 3. For ZS nanocomposites, the values of $\varepsilon_{\parallel}$ is observed to be decreasing as compared to pure NLC in region 2 which further becomes almost equal to that of pure NLC in region 3. Collectively, the value of $\Delta\varepsilon$ for ZS nanocomposites is observed to decrease as compared to pure PCH5 in region 2 and then becomes almost equal in region 3. For ZR nanocomposites, the values of $\varepsilon_{\parallel}$ are observed to be increasing of PCH5 in region 2 as well as in region3 as compared to pure PCH5. However, the value of $\Delta\varepsilon$ for ZR nanocomposites is observed to decrease in region 2 as compared to pure PCH5 which increases significantly in region 3 (~ 23% at $T - T_{IN} = -15$°C) as compared to pure PCH5. In case of ZW nanocomposites, value of ε in isotropic phase, values of $\varepsilon_{\perp}$ and $\varepsilon_{\parallel}$ and the value of $\Delta\varepsilon$ in all three regions is observed to be increasing as compared to that of pure NLC. The evolution of ε gives insight into the dominant way of dipole-dipole arrangement in the given system. Sridevi et.al. suggested that increase in the $\Delta\varepsilon$ could be either due to an increased nematic orientational order or a reduced antiparallel correlation between the neighbouring molecules[77]. According to Maier and Meier theory, the anisotropy is directly proportional to order parameter (S) of the system ($\Delta\varepsilon \propto S$) as

$$\Delta\varepsilon = \frac{NhF}{\varepsilon_0}\left[\Delta\alpha - \frac{F}{2kT}\,\mu^2\,(1 - 3cos^2\beta)\right]S$$

where, N is the number density, h is the cavity field factor, F is feedback factor, $\Delta\alpha$ is the polarizability anisotropy, μ is the resultant dipole moment and β is the angle between long axis and dipole moment of LC molecules. Garbovskiy et. al.[46] also reported that 1D nanoparticles help increase the order parameter of the composite system of NP in LC. Gorkunov et.al.[66] and Osipov et.al.[162] have reported that the addition of isotropic particles mainly leads to dilution of system. However, better alignment can be achieved by incorporation of strongly anisotropic nanoparticles in the LC matrix.

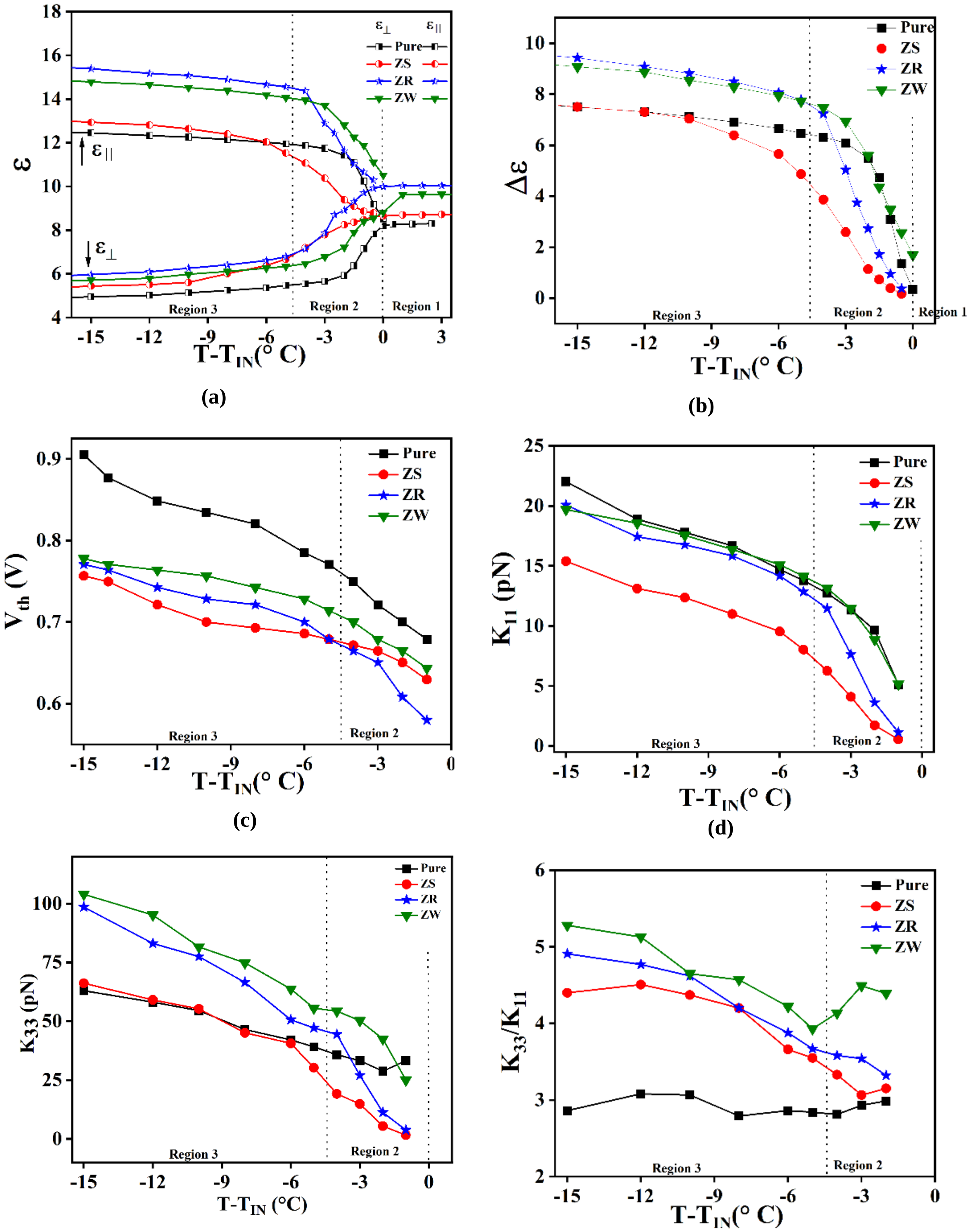

(a) (b) (c) (d) (e) (f)

Figure 5-6 Variation of (a) parallel ($\varepsilon_{\parallel}$) and perpendicular ($\varepsilon_{\perp}$) components of dielectric permittivity; (b) dielectric anisotropy ($\Delta\varepsilon$); (c) Threshold Voltage (V_{th}); (d) splay elastic constant (K_{11}); (e) bend elastic constant (K_{33}); (f) K_{33}/K_{11}; as a function of temperature of pure and 0.01 wt% ZnO nanocomposites of PCH5 at $f = 4$kHz

From the variation of birefringence as a function of temperature, the order parameter ($\Delta \mathrm{n} \propto S$) is observed to be increasing in all nanocomposite samples as compared to pure NLC. Whereas in the frequency range of $\sim kHz$, the evolution of order parameter from isotropic to deep nematic temperature range has different behaviours. The relaxation dynamics of the ZnO nanoparticles in nematic matrix may also be one of the important factors that governs the evolution of order parameter over a range of frequencies. The self-assembly of nanoparticles to form chain like structures is observed due to nematic ordering in nanocomposites of NLC[163]. To minimize the elastic distortions in the LC, spherical particles tends to be distributed into cylindrically symmetric chain/strands along nematic director[11]. Anisotropic cylindrically symmetric nematic environment favours a cylindrically symmetric arrangement of nanospheres. The chain length and rigidity of such chains affect the I-N phase transition as well as the nematic order parameter[67]. Optical textures show uniform alignment indicating uniform nematic director field. Hence, at length scales probed by visible light, arrangement of nanoparticles should be small structures due to their low concentration and homogeneous distribution. Moderate chain length and moderately stiff chains are expected to decrease the order parameter in the I-N phase transition region causing the weakly first order transition to transform to nearly continuous transition[67]. Basu et. al. showed that presence of small amount of nanospheres induces local random disorders in nematic media. But the strong applied field allows the system to improve nematic ordering which compensates for the disorder effect[163]. On the contrary, here, similar shape anisotropy of the ZR and ZW with that of the LC molecules and their presence in the bulk helps to increase the overall order of the nanocomposite system. Further, presence of nanosphere arrays may increase the mean viscosity and allow the system to relax slower. Thus, we may infer that the nanocomposite samples containing ZR and ZW in PCH5 manifests better alignment and increased order parameter as compared to ZS nanocomposite of PCH5. The value of threshold voltage (V_{th}) is estimated from dielectric measurements using variation of capacitance as a function of voltage[52] at different temperatures is shown in Fig 5-6c. The addition of ZnO NPs decreases the V_{th} of the nanocomposite samples as compared to pure NLC. The value of V_{th} reduces by 16%, 14% and 13% at $T - T_{IN} = -15°\mathrm{C}$, is observed with the addition of 0.01 wt% ZS, ZR and ZW, respectively in nanocomposites as compared to NLC host. In the planar cell geometry, the threshold voltage is highly sensitive to the splay elastic constant K_{11}, while the contribution of the bend elastic constant K_{33} is only effective at high voltages. The change in the value of

V_{th} depends on change in the ratio of splay elastic constant (K_{11}) and dielectric anisotropy ($\Delta\varepsilon$) by equation,

$$V_{th} = \pi\sqrt{\frac{K_{11}}{\varepsilon_0 \Delta\varepsilon}}$$

where, ε_0 is the permittivity of free space. So, increase in the value of $\Delta\varepsilon$ or decrease in the value of K_{11} or the combined effect of both leads to decrease in the value of V_{th}. The variation of K_{11}, K_{33} and ratio K_{33}/K_{11} is shown in Fig 5-6 (d, e, f), respectively. The value of bend elastic constant (K_{33}) is estimated using the method given by Uchida et. al[103]. The variation in elastic constants as a function of temperature can also be described using the regions stated earlier. The value of K_{11} is observed to be decreasing in all ZnO nanocomposites in region 2 as well as region 3 as compared pure PCH5. The value of K_{11} is reduced by ~ 32% with addition of ZS in PCH5 and by ~ 9% with addition of ZR and ZW in PCH5 in region 3. The evolution of K_{33}, however, shows interesting behaviour in ZnO nanocomposites as compared to pure PCH5. In ZS nanocomposites, K_{33} is observed to decrease in region2 and further becomes similar to that of pure PCH5 in region 3. For ZR nanocomposites of PCH5, value of K_{33} is observed to decrease in region 2 and increase significantly in region 3 as compared to pure NLC. Whereas the value of K_{33} in ZW nanocomposites is enhanced in region 2 as well as region 3 as compared to pure NLC. The ratio (K_{33}/K_{11}) is observed to be increasing with the incorporation of ZnO nanoparticles in PCH5 as compared to pure PCH5, significantly in region 3. The variation of elastic constant as a function of temperature depends mainly on the characteristics of the short range order present in the sample in the given temperature range[164,165]. According to Maier-Saupe theory, the elastic constants are proportional to the square of the scalar order parameter (S^2) i.e., a higher order parameter should lead to an increase in elastic constants[166] or vice-versa. However, the observed decrease in K_{11} may be because the addition of spherical nanoparticles effectively causes dilution of the NLC matrix. The decrease in the value of K_{11} is the main reason for decrease of V_{th} in ZS nanocomposites of PCH5 as $\Delta\varepsilon$ is negligibly altered as compared to pure PCH5 at $T - T_{IN} = -15°\text{C}$. However, combined effect of decrease of K_{11} and increase of $\Delta\varepsilon$ may lead to decrease in the value of V_{th} in ZR and ZW nanocomposites of PCH5. The value of K_{33} shows a large temperature dependence near the nematic to isotropic phase transition[164]. This strong temperature dependence of K_{33} can be explained because structural changes in short range order are more strongly weighted in K_{33}. Another explanation of the strong temperature dependence of K_{33}

near the nematic to isotropic phase transition is the fluctuation of the order parameter, S. Such fluctuations give rise to some uncertainty in the preferred direction. Therefore, elastic constants having connection to the preferred direction are expected to show an abnormal temperature dependence near the nematic to isotropic phase transition. Amongst the measured elastic constants, only K_{33} is connected to the preferred z-direction. Short range order may be induced due to incorporation of nanoparticles in the nanocomposite samples as observed from Fig 6a where ε in isotropic phase is observed to be increasing in nanocomposite samples as compared to pure NLC. Nanoparticle induced local disorders in the nanocomposite samples reduces the order parameter near I-N phase transition. But with decrease in the temperature, nematic ordering increases and favours the orientation of 1D nanoparticles along the global nematic director. However, in nanocomposites containing spherical nanoparticles, nematic potential may equal but does not overcome the local distortion as temperature decreases causing the order parameter to be similar as compared to pure NLC at lower temperatures. Therefore, the use of nanoparticles can benefit systems requiring lower driving voltages, however, cannot be implemented in devices requiring a high refresh rate.

The response time measurements of the pure and ZnO NP incorporated PCH5 is performed, and the results are shown in Fig 5-7. In the planar configuration, the transmitted intensity through the cell decreases after the voltage is turned on and the time required to drop from 90% to 10% of maximum value is defined as rise time, (τ_r). After turning off the voltage, the transmitted intensity increases, and time required rise from 10% to 90% of its maximum value is decay time (τ_d). The variation of rise time (τ_r), decay time (τ_d) and total response time ($\tau = \tau_d + \tau_r$) with varying voltage (V_{pp} ~ 5-10 V) at $T - T_{IN} = -15°\mathrm{C}$ are shown in Fig 5-7(a, c, e), respectively. The variation of τ_r, τ_d and τ as a function of varying temperature are shown in Fig 5-7(b, d, f), respectively. The rise time of the nanocomposites are observed to be negligibly changing as compared to pure NLC with varying voltages. However, significant variation in τ_d has been observed. Addition of isotropic ZS in PCH5 negligibly affects τ_d, whereas addition of 1D, ZR and ZW shows ~ 15 % reduction in τ_d as compared to pure NLC. Overall, the value of τ slightly increases (~ 3%) with addition of ZS but substantially reduces by ~15 % with addition of ZR and ZW in PCH5 as compared to the pure PCH5.

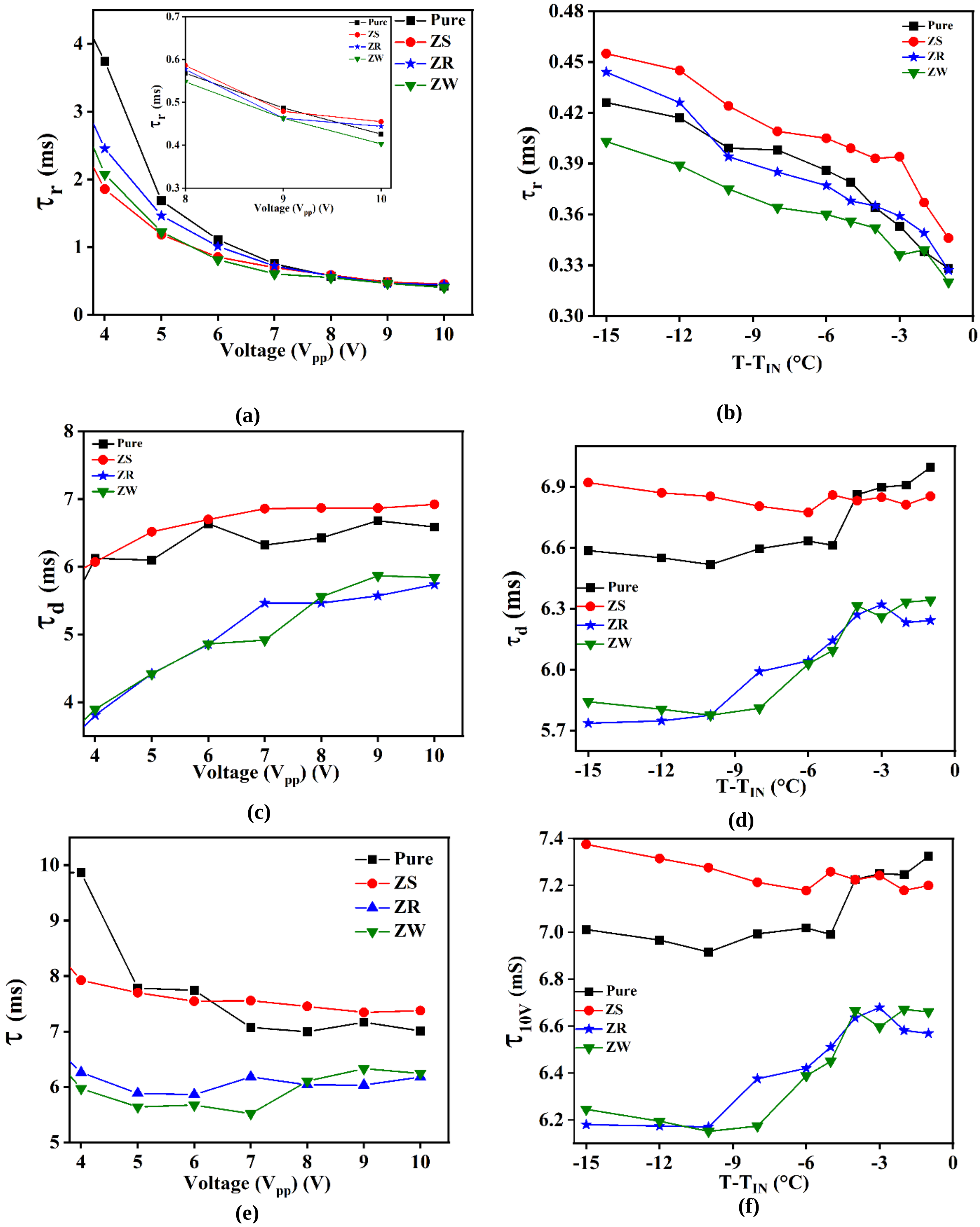

(a) (b) (c) (d) (e) (f)

Figure 5-7 Variation of rise time (a, d); decay time (b, e); total response time (c, f) as a function of voltage at $T - T_{IN} = -15$°C (left column) and temperature (right column), respectively, for pure and ZnO nanocomposites of PCH5 at *f* = 60Hz

The response time of the LC in planar alignment for weak anchoring depends on various parameters according to equation[167],

$$\left[\tau_r = \frac{\gamma}{\left(\Delta\varepsilon\frac{E^2}{4\pi}\right) - \left(\frac{K_{11}\pi^2}{d^2}\right)}\right]$$

$$\left[\tau_d = \frac{\gamma d^2}{K\pi^2}\right]$$

where, γ- effective viscosity of the LC medium and K- effective elastic constant ($K = K_{11} - \frac{K_{22}}{2} + \frac{K_{33}}{4}$). The estimated variation of viscoelastic ratio (γ/K) as a function of temperature for pure and ZnO NP incorporated PCH5 is shown in Fig 5-8a. Local disorders induced by addition of ZS may cause hindrance to the reorientation of molecules in the direction of applied field which may be one of the reasons for slight increase in the response time of the ZS nanocomposite of PCH5. The reduction in viscoelastic ratio (γ/K) as shown in Fig 5-8a speeds up the fall times[168] as observed in the ZR and ZW nanocomposites of PCH5. Reduction in the ionic impurities may also be one of the reasons for the faster response time in 1D nanocomposites of PCH5 as compared to pure PCH5.

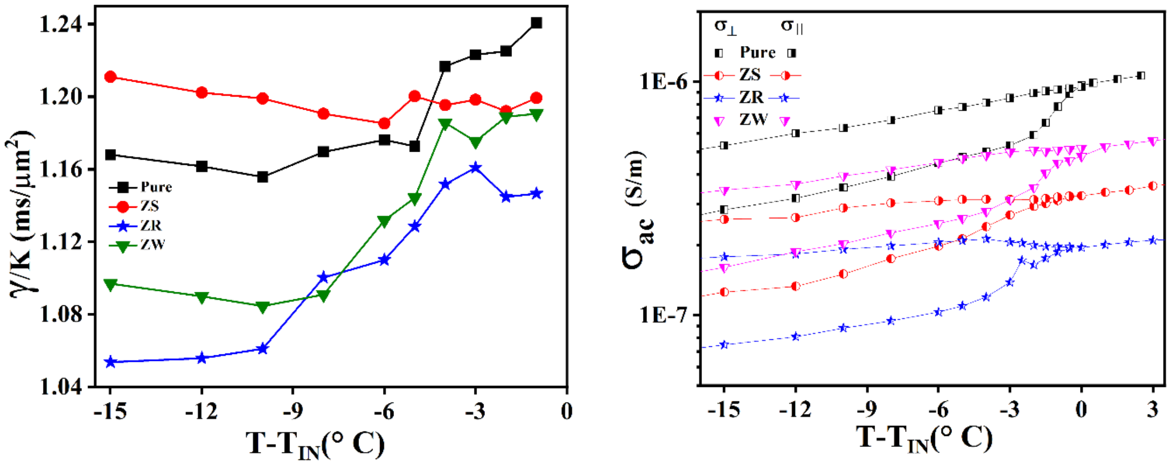

(a) (b)

Figure 5-8 (a)Viscoelastic ratio (γ/K) (b) Bulk ac conductivity (σ_{ac}) of pure and 0.01 wt% ZnO nanocomposites of PCH5 as a function of temperature

Variation of bulk ac conductivity (σ_{ac})with the incorporation of ZnO NP is shown in Fig 5-8b. The addition of 0.01 wt% ZnO NP decreases the σ_{ac} of the nanocomposites as compared to pure NLC. The reduction of 53%, 70% and 36% in the value of σ_{ac} is observed in ZS, ZR and ZW nanocomposites, respectively, as compared to pure NLC. Addition of 0.01 wt% ZnO NP effectively traps the ionic impurities in the nanocomposite systems. Due to higher surface area of 1D NPs as compared to spherical NPs, efficient reduction in σ_{ac} is observed due to ZR nanocomposites as compared to ZS nanocomposites. However, due to longer length of NW which may be making pathway for the ionic conduction makes it less efficient in impurity trapping. It has been observed in LC nanocomposites with nanowires such as CdS[52], CNTs[73,169] etc. that the long lengths of wires can provide pathways for the conduction of impurity ions by various mechanisms such as hopping, charge transfer or $\pi - \pi$ interaction between dopant and LC molecules.

The comparison of values of various physical properties of NLC and its ZnO nanocomposites is presented in Table 5-4. As we can observe from the comparison Table 4, nanocomposites of NLC containing 1D NPs show enhanced characteristics properties as compared to that with spherical NPs in optical as well as low ($\sim kHz$) frequency regions. Hence, 1D NPs can be considered as potential candidates over spherical NPs while preparing nanocomposites of LC for the enhancement of device parameters of display applications with high refresh rate. But as ionic conductivity is also one of the crucial parameters for display applications, composites of NLC with nanorods of ZnO are observed to be better than that with nanowires of ZnO. Overall, nanorods of ZnO are observed to be more efficient in ion trapping due to high surface area hence decreasing the response time as well as the threshold voltage of the nanocomposite system as compared to pure NLC.

Table 5-4 Comparison of values of different physical properties of pure and 0.01 wt% ZnO nanocomposites of PCH5 at $T - T_{IN} = -15^\circ\mathrm{C}$ (marked values show maximum enhancement in the value of particular parameter in ZnO nanocomposites as compared to pure NLC)

	Pure	**ZS**	**ZR**	**ZW**
Δn	0.09	0.12	**0.11**	0.12
$\varepsilon_{\perp}$	4.95	5.44	**5.97**	5.71
$\varepsilon_{\parallel}$	12.44	12.94	14.79	**15.39**
$\Delta\varepsilon$	7.49	7.5	**9.42**	9.07
$V_{th}(V)$	0.9	**0.76**	0.77	0.78
$K_{11}(pN)$	22	15.4	**20.1**	19.7
$K_{33}(pN)$	62.9	66.2	98.6	**104**
K_{33}/K_{11}	2.86	4.4	4.91	**5.28**
$\sigma_{\perp}(\mu S/m)$	0.28	0.13	**0.074**	0.16
$\sigma_{\parallel}(\mu S/m)$	0.53	0.26	**0.18**	0.34
$\tau_r(ms)$	0.43	0.46	0.44	**0.4**
$\tau_d(ms)$	6.6	6.9	**5.7**	5.8
$\tau(ms)$	7.02	7.3	**6.1**	6.2

5.4 CONCLUSION

As discussed in Chapter 1 and Chapter 2, 1D nanostructures affect the physical properties of liquid crystals substantially, hence we have carried out a systematic study to investigate the effect of shape of nanoparticle on properties

- Pronounced increase in birefringence & dielectric anisotropy and reduction in V_{th}, response time as well as viscoelastic ratio is observed in NLC nanocomposites of ZR and ZW as compared to ZS nanocomposites of NLC.
- Incorporation of ZnO NPs in NLC also helps trapping of ionic impurities efficiently.
- The incorporation of ZnO nanoparticles of different shapes in NLC demonstrated that 1D nanoparticles show enhanced effects as compared to spherical nanoparticles for device applications, especially, displays.
- Among the 1D nanostructures, incorporated ZnO nanorods at low concentration (0.01 wt%) in NLC leads to significant improvement in the display device parameters.

CHAPTER 6

EFFECT OF SIZE OF ZINC OXIDE NANORODS ON ELECTRO-OPTIC AND DIELECTRIC PROPERTIES OF NEMATIC LIQUID CRYSTAL

The results of Chapter 5 indicate that unfunctionalized nanorods can be considered as better choice to make composites with NLC for the enhancement in device parameters. Hence, a systematic investigation on effect of different size of nanorods on physical properties of nematic liquid crystal is carried out and results are presented in this chapter. The zinc oxide nanorods (ZR) of similar aspect ratio (4-5) but different size (length: width) abbreviated as., ZR1(10:50), ZR2 and ZR3 are synthesized. Nanocomposites of synthesized nanorods with wide temperature range nematic liquid crystal, PCH5 are prepared. The smaller nanorods (ZR1) are expected to form chain like structures in host NLC matrix leading to softening of order parameter at the isotropic-nematic transition. As the size of the nanorods increases the discontinuity of order parameter at I-N transition is observed to increase. The threshold voltage, electro-optic response time and conductivity of the nanocomposite samples is also observed to decrease with the incorporation of ZR in host NLC.

The manuscript for the work done in this chapter is in preparation

- Effect of size of ZnO nanorods on electro-optic and dielectric properties of nematic liquid crystal, **Shweta Mishra**, Manjuladevi V, Raj Kumar Gupta (in preparation).

6.1 INTRODUCTION

Improvement in the characteristic features of LC for technological advances in device applications is always at a forefront for the researchers in the field. With the advent of nanotechnology and nanomaterials which show some drastically interesting phenomena and huge impact on futuristic technologies; researchers in LC field are also trying to make use of features of nanoparticles to modify physical properties of LCs [26]. Various research groups have tried doping metallic (e.g. Ag, Au) [47], semiconducting (e.g. ZnS, ZnO, PbS, TiSiO4, etc.)[49–52], ferroelectric (e.g. BaTiO3)[48], magnetic (e.g. Fe3O4) nano particles in LC matrix which showed improvement in physical parameters such as switching time, threshold voltage, elastic constant ratio etc. Incorporation of anisotropic nanostructures such as nanorods, nanoplatelets, nanosheets, in LC have also been studied by few research groups [47,54,58,78,170]. Nematic phase exhibited by calamitic liquid crystals is the most useful of all the LC phases known in display device applications because of their long range orientational order, low viscosity, and large elastic constant ratio. NLCs composed of rod-shaped molecules are easy to align and can be switched at low strengths of electric fields as compared to their other shape anisotropic counterparts, discotic and bent core nematic. 1D-NPs such as nanorods, nanowires and nanotubes [50–52,61–65] with similar shape anisotropy as that of NLC host molecules makes them naturally suited as dopant materials in NLC. Composites of 1D-NPs with LC host are expected to exhibit synergetic orientational ordering. However, the mixing behaviour is observed to be quite complex. Addition of a relatively small amount ($\leq 1\, wt\%$) of 1D-NPs to the nematic LC host can alter the orientational order of the host medium [46]. These changes perhaps depend on various factors such as the diameter and aspect ratio of the dispersed 1D-NPs as compared to that of the LC molecules and the interaction between the NPs and LC molecules [49,52,66,69–72]. The interfacial interaction between the NPs and LC molecules may change the surface anchoring conditions[138]. The variation of dielectric and electro-optic properties of NLCs with the dispersion of carbon nanotube (CNT) is extensively studied owing to the fascinating properties exhibited by the CNTs [56,65,73]. But there are very few reports available which shows the effect of various sizes (diameter: length ($d{:}\, l$)) of nanorods on the physical characteristics of host NLC. Here, we are reporting the effect of zinc oxide nanorods of varying size on the physical properties of wide temperature range NLC, PCH5. Zinc oxide (ZnO) is a wide band-gap semiconducting material and generally investigated for its potential applications in the various fields such as sensors, optoelectronics, photovoltaics, and drug delivery. The results of the improvement in various display device properties with the incorporation of ZnO nanorods of three different size of similar aspect ratio in PCH5 are presented here. These studies indicate that the properties of host NLC can be tuned as the function of size as well as concentration of ZnO nanorods.

6.2 EXPERIMENTAL

6.2.1 Materials

4-(trans-4’pentylcyclohexyl)-benzonitrile (PCH5) and Zinc acetate dihydrate ($Zn(ac)_2.2H_2O$) are procured from Sigma-Aldrich. Sodium Hydroxide (NaOH), Methanol, Ethanol and Iso-propanol are procured from Merck.

6.2.2 Synthesis of ZnO nanorods

Zinc oxide nanorods (ZR) of three different sizes are prepared using solvothermal synthesis [171]. First, 0.1 M $Zn(ac)_2.2H_2O$ and 0.5 M NaOH solutions are prepared in methanol separately. Then, two of the solutions are mixed and stirred properly to get a clear transparent solution for 30 min. The clear solution is then transferred to Teflon-lined autoclave of 100mL capacity. The autoclave is maintained at 150℃ for 24 hrs and then allowed to cool down to room temperature naturally. Obtained precipitate is separated by centrifugation and washed with ethanol thrice. The obtained product was dried in air at 60℃ for 2 hrs. Similarly, above mentioned procedure is repeated by taking the solvent as ethanol and iso-propanol to obtain the different sizes of the synthesized nanorods. Samples prepared with methanol, ethanol and iso-propanol are named as ZR1, ZR2 and ZR3, respectively.

6.2.3 Preparation of nanocomposite sample

For this experimental study, we have taken 4-(trans-4’pentylcyclohexyl)-benzonitrile (PCH5) as nematic liquid crystalline host material procured from Sigma-Aldrich. The NLC host PCH5 exhibits the phase transition sequence: Isotropic (55.3˚C) Nematic (30˚C) Crystal.

NLC nanocomposites are prepared using ZR of various sizes synthesized in the laboratory. As synthesized ZR1, ZR2 and ZR3 are dissolved in chloroform and ultrasonicated for about two hours to get homogeneous dispersions. Calculated quantity of these solutions is added into the host NLC to obtain the concentration of ZR (wt%) in host LC (C_{ZR}) to be 0.01, 0.02 and 0.05. The nanocomposite solutions are further sonicated for uniform mixing and then left for 3 days to allow the solvent to evaporate completely.

6.2.4 Characterization techniques

The crystalline phase of as synthesized products is estimated using powder X-ray diffraction (XRD) using Rigaku Smartlab Studio X-ray diffractometer with Cu K_α ($\lambda = 1.5406$ Å) in the range $2\theta = 10° - 90°$ at scanning rate of $4°/min$ at an operating voltage of 40 kV. The morphology of the synthesized particles is investigated using transmission electron microscope (TEM; FEI Tecnai G2 20 S-TWIN) and field emission scanning electron microscope (FE-SEM; FEI Apreo LoVac). The optical band gap of the synthesized samples is obtained using UV-Vis absorption spectra in the wavelength range $200 - 700\ nm$.

For the electro-optic and dielectric measurements, we have used planar aligned cells of thickness ~ 7 μm and area ~ 0.8 cm^2. Thickness of the sample cells is measured using an interferometric fibre-optics spectrometer (Ocean-optics USB4000-XR1-ES). To observe the optical texture of the LC filled sample cells, polarizing optical microscope (POM; Olympus BX53M) is used. To investigate the dispersion properties of the ZR in nematic matrix inside the cell, fluorescence confocal microscopy (LSM880, Zeiss) is performed. The sample cell is placed inside the hot stage (Micro-optik MDTC600) with temperature control of 0.1 ℃ having a small hole in the middle to allow light to pass through. This assembly was then kept on the rotating stage of the POM between crossed polarizers. A laser beam of wavelength 633 nm is allowed to pass through the sample. The planar aligned cell is kept between crossed polarizers with a rubbing direction at an angle of 45° to either of the polarizers. The transmitted intensity (I) as a function of temperature is recorded and used to estimate the birefringence of the nematic samples. Further, electro-optic switching times such as rise time (τ_r), decay time (τ_d) and total response time ($\tau_R = \tau_r + \tau_d$) are measured for the pure as well nanocomposites of NLC by applying square wave of frequency 60 Hz using digital storage oscilloscope (DSO; Keysight EDUX1002G) at various applied voltages. Measurement of dielectric permittivity (ε), dielectric anisotropy ($\Delta\varepsilon$), threshold voltage (V_{th}) and bulk ac conductivity (σ_{ac}) is performed as per method discussed in the Chapter2.

6.3 RESULTS AND DISCUSSION

The typical XRD pattern of ZR powder samples prepared using different solvents is shown in Fig 6-1a. All the peaks as observed from Fig 6-1a matches well with that of bulk ZnO exhibiting hexagonal wurtzite crystal structure. The anisotropic growth of ZnO along c-axis (101) is observed with no peaks of hydroxides, hence confirming uniform formation of ZnO. Morphology of the synthesized samples is investigated using electron microscopy (TEM and

FESEM) and results are shown in Fig 6-1(b). With the decreasing polarity of the solvents, the diameter of synthesized ZR is observed to be increasing. The diameter(nm) to length(nm) ratio for ZR1 is found to be $\sim 10nm: 50\ nm,$ ZR2 is $\sim 50nm: 200nm$ and ZR3 is $\sim 1\mu m: 5\mu m$ as observed from the electron microscopy images. The nanocomposite samples of ZR with host NLC, PCH5, are prepared as described earlier and the effect of size of synthesized ZR on physical properties of PCH5 are investigated.

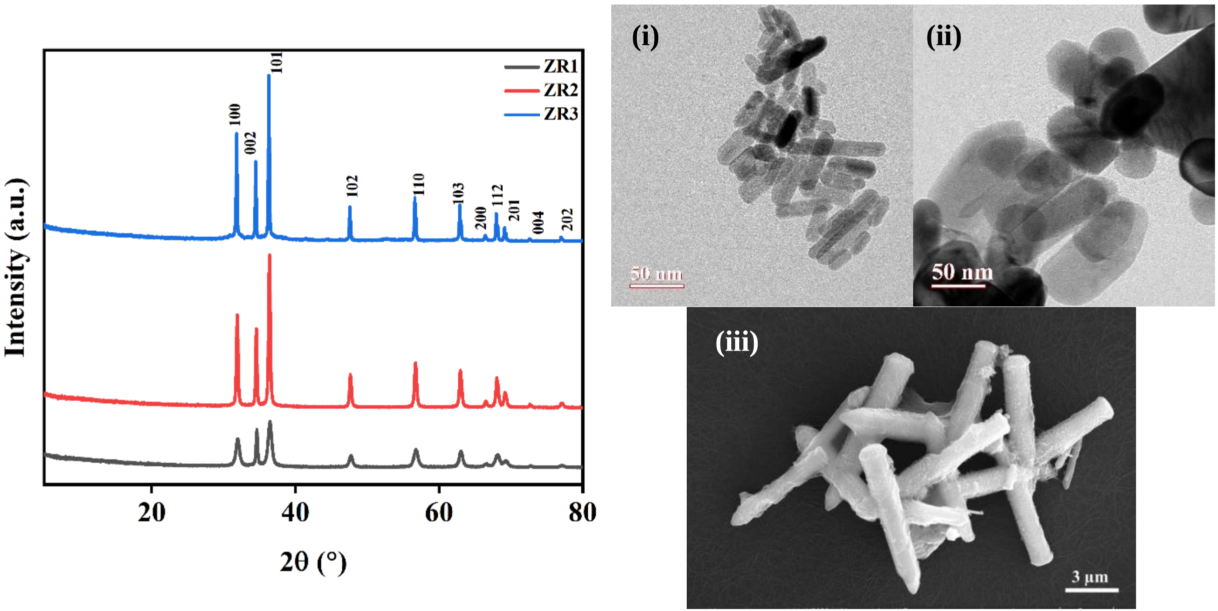

Figure 6-1 (a)X-ray diffraction pattern of synthesized zinc oxide nanorods using methanol (ZR1), ethanol (ZR2) and Iso-propanol (ZR3) as solvent; (b) Transmission electron microscopy images of ZR1(i) & ZR2(ii) and FESEM image of ZR3(iii)

The alignment characteristics of pure PCH5 and ZR nanocomposites of PCH5 filled in planar configuration is observed under crossed polarizers of POM and the optical textures are shown in Fig 6-2. Optical textures show no aggregations for the nanocomposite samples under investigation. Hence, ZR is homogeneously dispersed in host NLC, and uniform alignment without aggregation is observed for nanocomposite samples under investigation. Further, confocal microscopy images of pure and ZR nanocomposites of PCH5 are shown in Fig.6-3. FCM images show that ZR is dispersed in the bulk of the nematic matrix and no aggregation or accumulation near the interfaces is observed. Hence, ZR is expected to be homogeneously dispersed in the bulk of the nematic matrix.

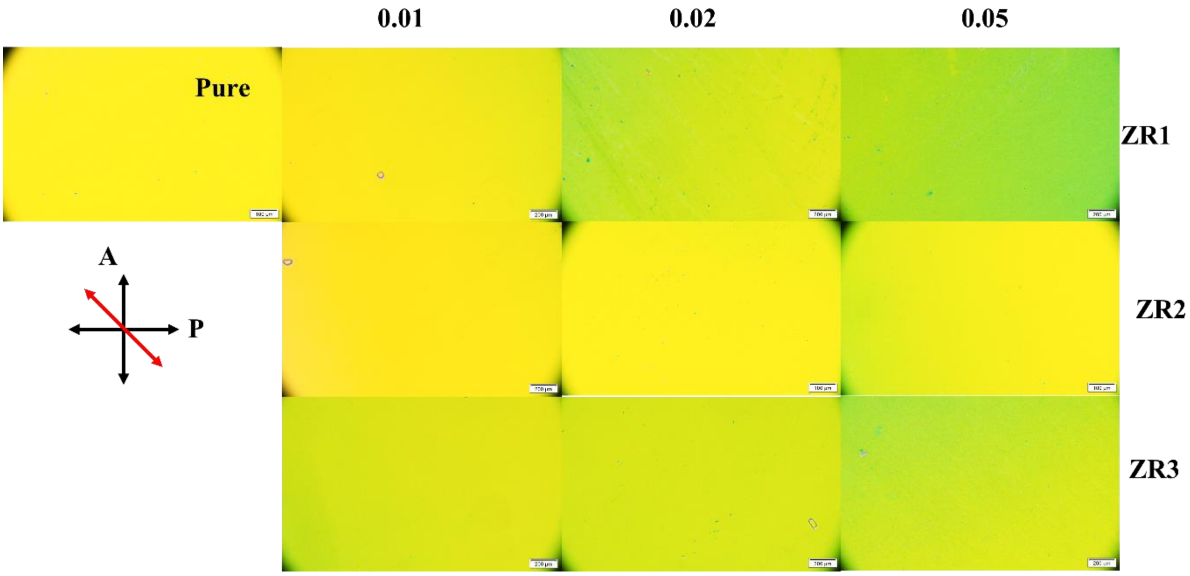

Figure 6-2 Optical textures of pure and ZR nanocomposites of PCH5 filled in planar cell observed between crossed polarizers of POM (numbers indicate the concentration of nanorod in PCH5) at T= 35℃. (A and P denote crossed polarizes; red line denotes rubbing direction of sample filled planar cell = 45° to either polarizer)

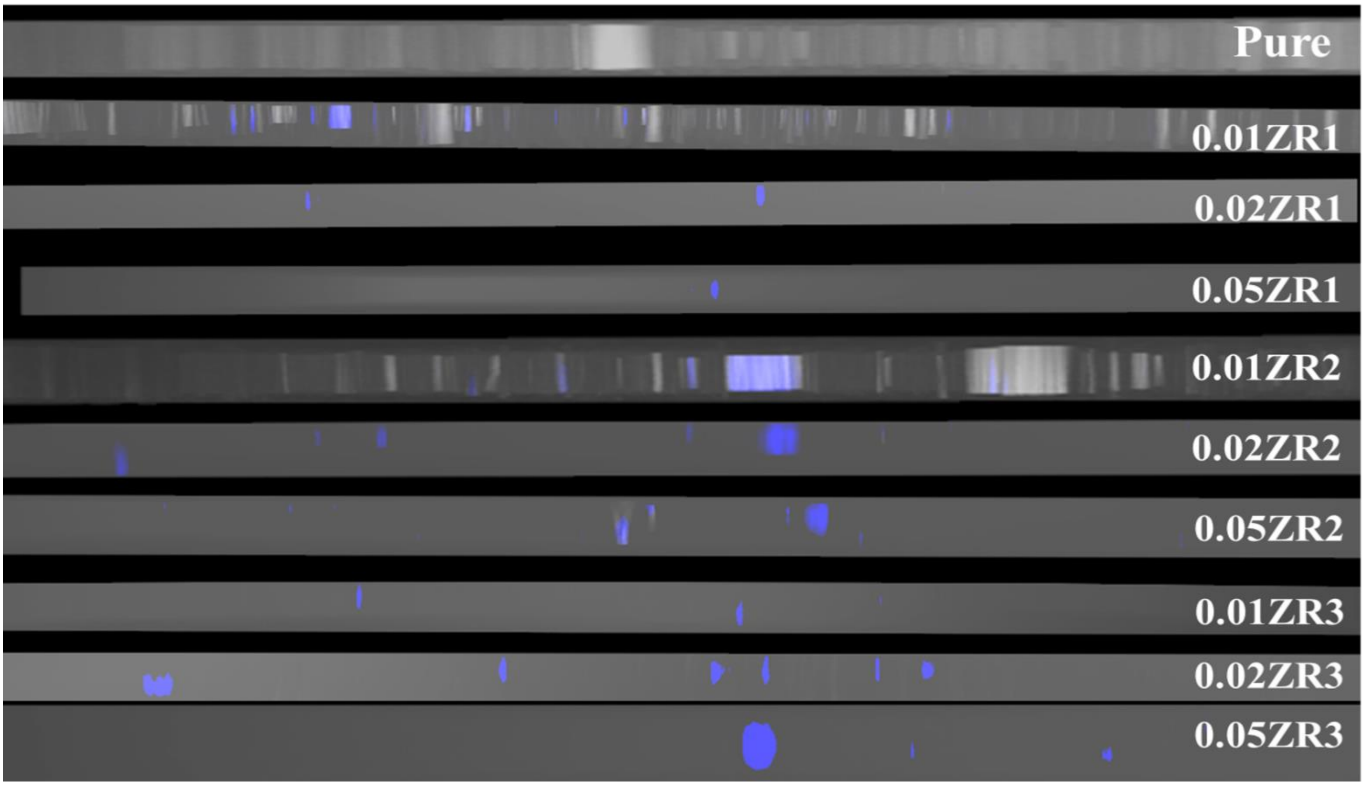

Figure 6-3 Fluorescence confocal microscopy images of pure and ZR nanocomposites of PCH5 at room temperature

The variation of Δn as a function of temperature for various concentration of ZR1, ZR2 and ZR3 is shown in Fig 6-4. With the addition of ZR, the value of Δn is observed to be increasing in all nanocomposite samples as compared to pure PCH5. At T-T$_{IN}$ = -15℃, for nanocomposites containing ZR1 and ZR2, value of Δn increases by 5% and 8%, respectively for lower concentration (0.01 wt%) and then shows negligible difference at higher concentrations (0.02 and 0.05 wt%) as compared to pure NLC. However, the value of Δn increases with increasing concentration of ZR3 in NLC host with maximum increase of 8% at 0.05 wt% ZR3 in PCH5.

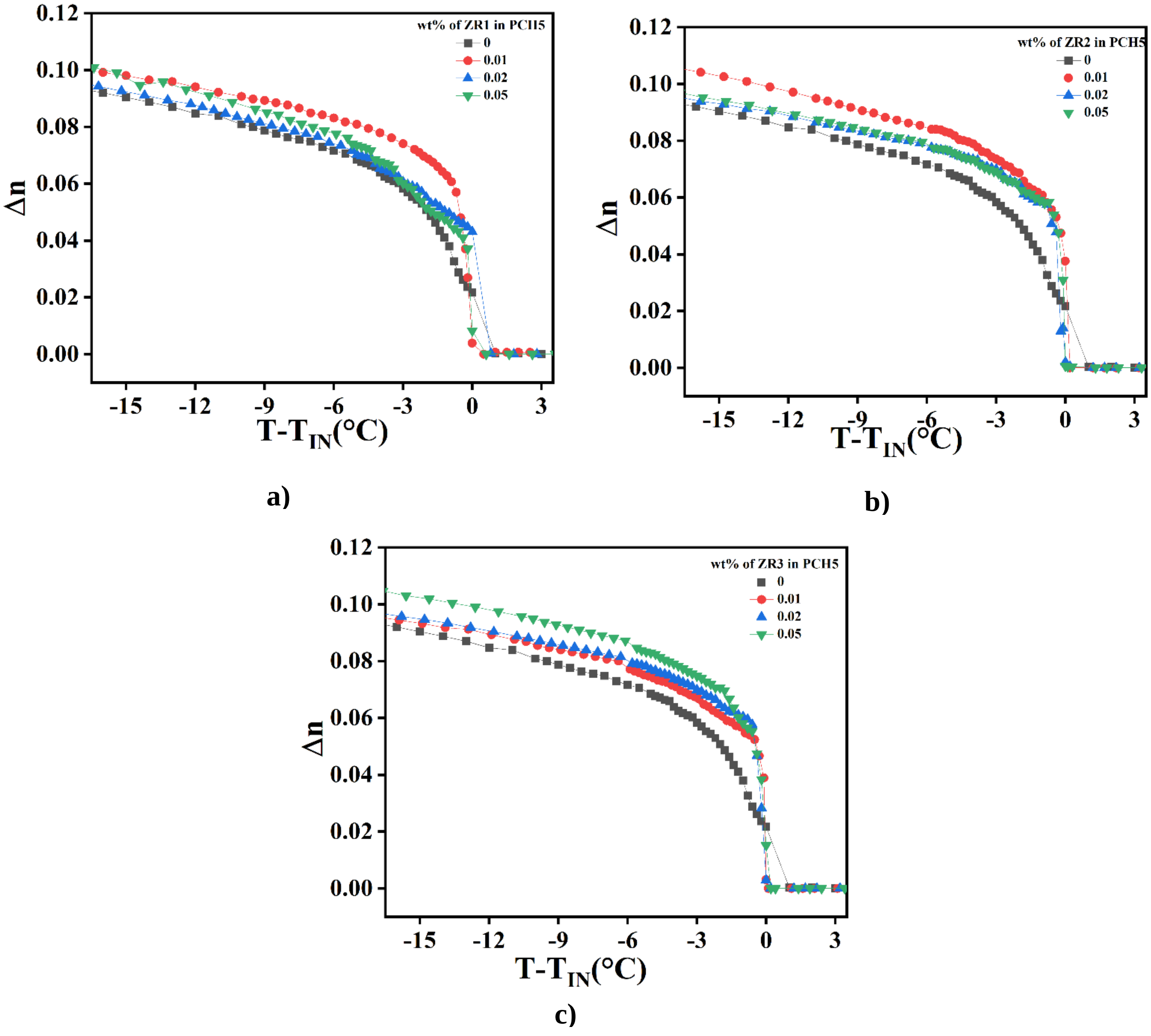

a)

b)

c)

Figure 6-4 Variation of birefringence (Δn) as a function of temperature for pure and (a)ZR1; (b)ZR2; (c) ZR3 nanocomposites of PCH5

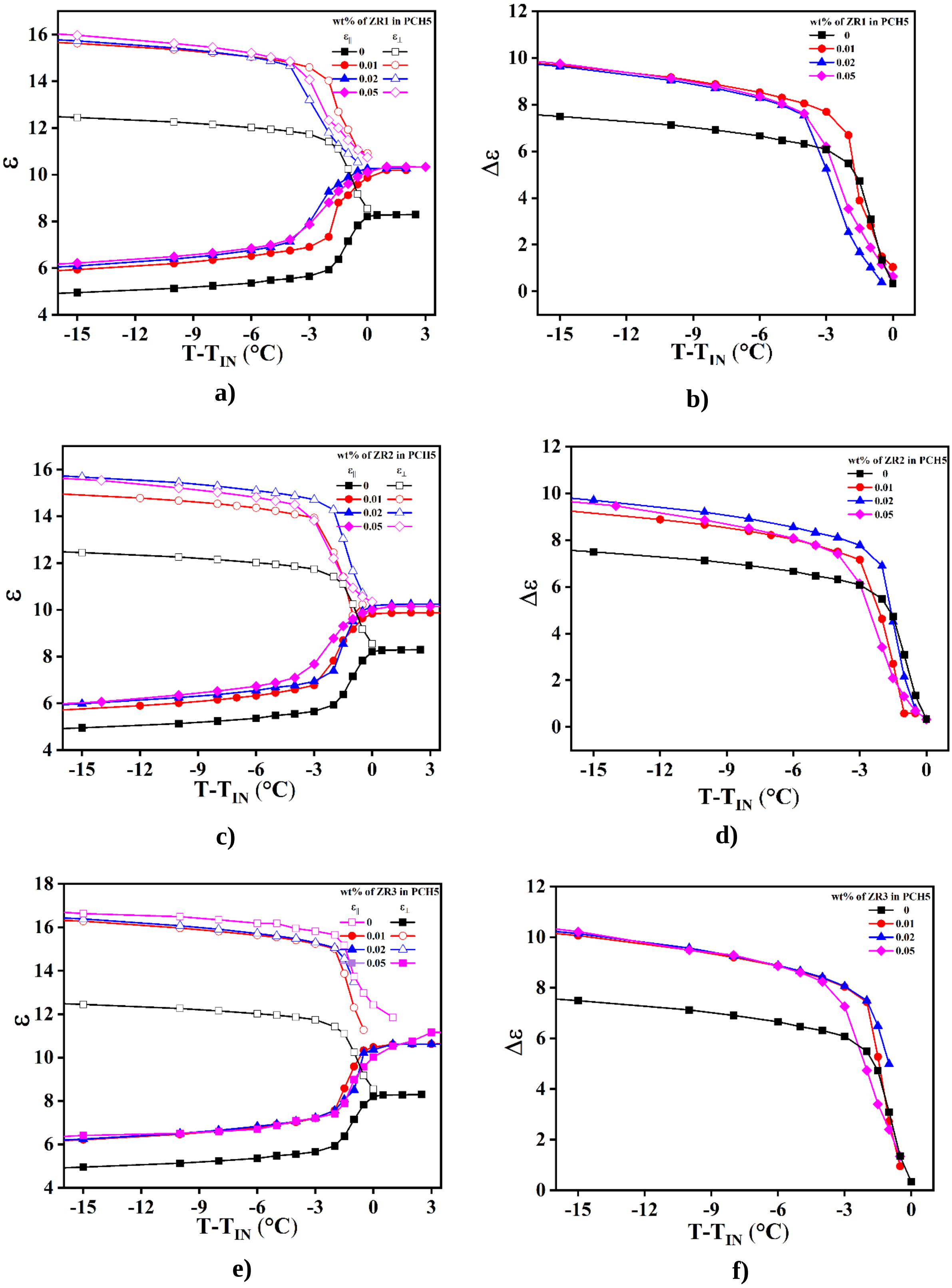

a)

b)

c)

d)

e)

f)

Figure 6-5 Variation of dielectric permittivity as a function of temperature for pure and ZR nanocomposites of PCH5 (variation of parallel ($\varepsilon_{\parallel}$) and perpendicular ($\varepsilon_{\perp}$) components of dielectric permittivity for ZR1 (a), ZR2(c) and ZR3(e) nanocomposites (left column); and respective variation of dielectric anisotropy ($\Delta\varepsilon$) (b,d,f, respectively) (right column))

Variation of parallel ($\varepsilon_{\parallel}$) and perpendicular ($\varepsilon_{\perp}$) components of dielectric permittivity as a function of temperature for various concentration of ZR1, ZR2 and ZR3 in PCH5 are shown in Fig 6-5 (a,c,e). Variation of dielectric anisotropy, $\Delta\varepsilon = \varepsilon_{\parallel} - \varepsilon_{\perp}$ as a function of temperature for various concentration of ZR1, ZR2 and ZR3 in PCH5 are shown in Fig 6-5 (b,d,f). The variation of $\varepsilon_{\perp}$, $\varepsilon_{\parallel}$ and $\Delta\varepsilon$ as a function of concentrations for various sizes of ZR at $T - T_{IN} = -15°\mathrm{C}$ are shown in Fig 6- 6a, Fig 6- 6b and Fig 6- 6c, respectively. The values of both $\varepsilon_{\parallel}$ and $\varepsilon_{\perp}$are observed to increase in all nanocomposite samples as compared to pure NLC. The evolution of $\Delta\varepsilon$ with temperature helps comprehending the order in the system with varying temperature. To understand the results, the temperature axis is divided into three regions, viz, region 1 ($T - T_{IN} > 0°\mathrm{C}$), region 2 (-4 ℃ $< T - T_{IN} < 0°\mathrm{C}$) and region 3 ($-4$ ℃ $> T - T_{IN}$). In region 1, value of ε increases with increasing concentration of ZR in PCH5 for all nanorods. This may be because of the presence of short-range nematic order induced by the presence of nanorods in the isotropic phase of the NLC. However, in region 2, behaviour of $\Delta\varepsilon$ is different for the three sizes of nanorods incorporated in PCH5. For small nanorods (ZR1), the $\Delta\varepsilon$ is observed to vary slowly near I-N phase transition as compared to pure NLC and the value of $\Delta\varepsilon$ is observed to be less than that of pure NLC. The formation of chainlike structures of smaller nanoparticles under the influence of orientational ordering of LC molecules in nematic phase could be one of the possible reasons for the slow evolution of $\Delta\varepsilon$ from isotropic into nematic phase in ZR nanocomposites of PCH5. Egorov et al.[67] and Gorkunov et al.[66,79] have reported that long, and moderately stiff chains of particles may lead to the softening of order parameter at I-N phase transition. The observations reported in our previous work[52,172] also suggests that chain like structure formed by spherical particles or long nanowires incorporated at low concentration in NLC shows nearly continuous isotropic-nematic phase transition. In ZR2 nanocomposites, variation of $\Delta\varepsilon$ is observed to be faster and more discontinuous near I-N phase transition. And, for larger nanorods (ZR3), the value of $\Delta\varepsilon$ seem to increase as compared to pure NLC at lower concentration (C_{ZR3} = 0.01 & 0.02) of nanorods in PCH5. In region3, the value of $\Delta\varepsilon$ is observed to increase for all ZR nanocomposites of PCH5 as compared to pure PCH5. For ZR1 and ZR3 nanocomposites, the value of $\Delta\varepsilon$ increases with the incorporation of nanorods in PCH5 but does not change significantly with further increase in concentration of nanorods. However, for ZR2 nanocomposites, though initial addition of nanorods leads to increase in the value of $\Delta\varepsilon$ as compared to pure NLC, it starts decreasing for C_{ZR2} = 0.05 but is still higher than that of pure NLC.

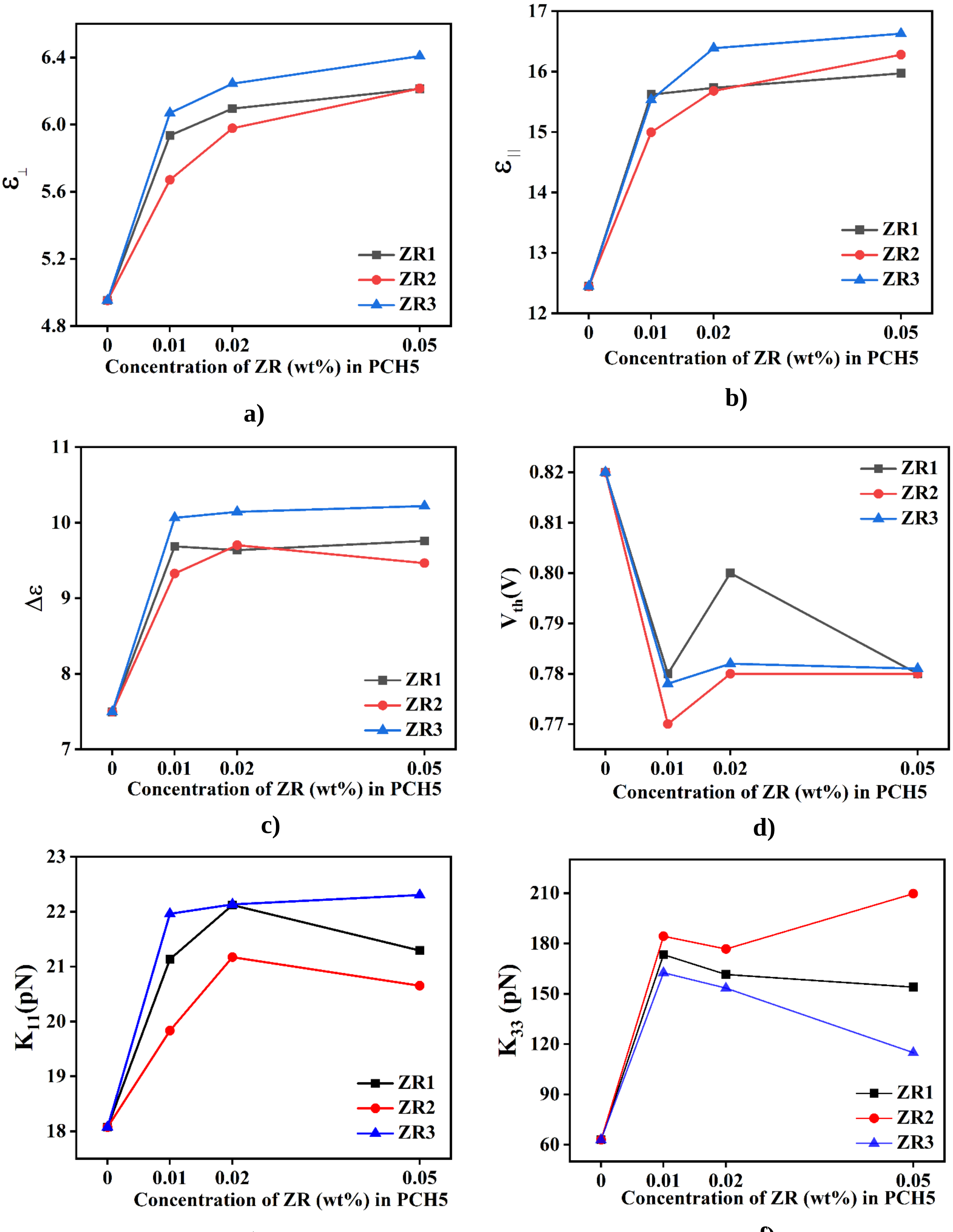

a)

b)

c)

d)

e)

f)

Figure 6-6 Variation of (a) $\varepsilon_\perp$; (b) $\varepsilon_\parallel$; (c) Δε; (d) threshold voltage (V_{th}); (e)splay elastic constant (K_{11}) (f) bend elastic constant (K_{33}); for ZR nanocomposites of PCH5 as a function of concentration of ZR (C_{ZR}) at $T - T_{IN} = -15$℃

The results of variation of $\Delta\varepsilon$ (Fig 6-5 (b, d, f)) measured at 4 kHz complements with that of the variation of Δn as shown in Fig 6-4 for ZR nanocomposites of PCH5. According to Maier-Meier theory[16],

$$\Delta\varepsilon = \frac{NhF}{\varepsilon_0}\left[\Delta\alpha - \frac{F}{2kT}\,\mu^2\,(1 - 3cos^2\beta)\right]S$$

where, $\Delta\varepsilon$ is directly proportional to macroscopic S (order parameter). Hence, increase in the value of $\Delta\varepsilon$ suggests increase of order parameter of nanocomposites with the incorporation of ZR in PCH5. Also, classical Onsager theory predicts that the rod shaped particles may cause the increase of the order in nematic matrix as compared to other shapes such as spheres or discs[11,68]. The variation of $\Delta\varepsilon$ as a function of concentration of ZR in PCH5 at $T - T_{IN} = -15°\mathrm{C}$ is shown in Fig 6-6c. The observed results indicate that incorporation of larger nanorods (ZR3) leads to increase in the order parameter of ZR nanocomposites more as compared to smaller nanorods (ZR1 & ZR2). The variation of threshold voltage (V_{th}) for pure and ZR nanocomposites of PCH5 at $T - T_{IN} = -15°\mathrm{C}$ is shown in Fig 6-6d. Overall, incorporation of ZR in PCH5 helps to decrease the V_{th} at all C_{ZR} under investigation. The maximum decrease is observed for nanocomposite containing C_{ZR}= 0.01 in PCH5. The value of V_{th} slightly increases with further increase in C_{ZR} (0.02 & 0.05) but is still lower than that of the pure NLC. The threshold voltage of the LC in planar configuration varies as

$$V_{th} = \pi\sqrt{\frac{K_{11}}{\varepsilon_0\Delta\varepsilon}}$$

where, K_{11} is splay elastic constant and $\Delta\varepsilon$ is the dielectric anisotropy of the medium. The variation of splay elastic constant (K_{11}) for pure and ZR nanocomposites of PCH5 at $T - T_{IN} = -15°\mathrm{C}$ is shown in Fig 6-6e. The value of K_{11} increases in all ZR nanocomposites of PCH5 as compared to pure PCH5 with a maximum increase in ZR3 nanocomposites. The variation of bend elastic constant (K_{33}) as a function of concentration of ZR in PCH5 at $T - T_{IN} = -15°\mathrm{C}$ is shown in Fig 6-6f. Here, the value of K_{33} is also observed to increase as compared to pure NLC in ZR nanocomposites of PCH5. According to the continuum theory for NLC, the variation of K_{ii} (i= 1, 3 for planar configuration) is directly proportional to S^2 [2,24]. Hence, the observed increase in the value of elastic constants complements the observation that $\Delta\varepsilon$ and hence, order parameter of the nanocomposite system is enhanced with the incorporation of nanorods in the NLC matrix. The variation of ratio of bend to splay elastic constant (K_{33}/ K_{11}) as a function of concentration of ZR in PCH5 at $T - T_{IN} = -15°C$ is shown in Fig 6-7.

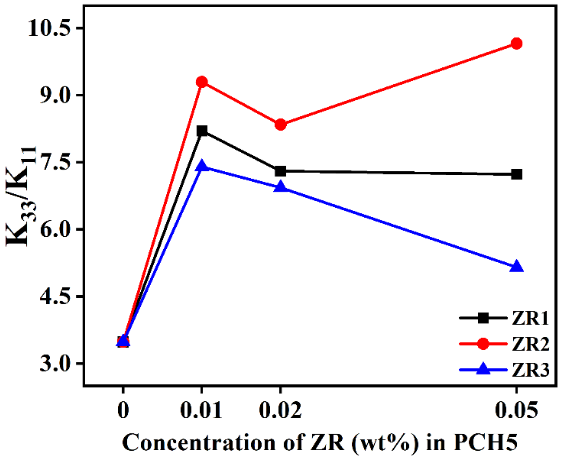

Figure 6-7 Variation of ratio of K_{33}/K_{11} for pure and ZR nanocomposites of PCH5 at $T - T_{IN} = -15°C$

The value of K_{33}/ K_{11} is almost independent of temperature in deep nematic region. These properties are also important for display applications where reduced V_{th} and higher multiplexing devices are required.

Electro-optic response time is also one of the important parameters for device applications. Measurements of rise time (τ_r), decay time (τ_d) and total response time (τ) for the pure and ZR nanocomposites of PCH5 filled in planar cells are performed applying square wave of frequency 60Hz at various voltages and the results are shown in Fig 6-8. Maximum decrease in the total response time of the ZR nanocomposite samples as compared to pure PCH5 by 8.6%, 5.5% and 4.1 % is observed for C_{ZR}= 0.02 of ZR1, ZR2 and ZR3, respectively. Shorter nanorods (ZR1) are observed to be more efficient for the reduction of response time as compared to larger ones (ZR2 & ZR3). Reduction in the value of V_{th}, enhancement in the order parameter and enhancement of K_{33}/K_{11} collectively helps to reduce the response time of ZR nanocomposites of PCH5 as compared to pure PCH5 at low C_{ZR} (0.01 wt% and 0.02 wt%). Reduction in the ionic impurities may also be one of the reasons for the reduction of response time. However, the value of τ increases with further increase in C_{ZR}= 0.05 as compared to pure NLC.

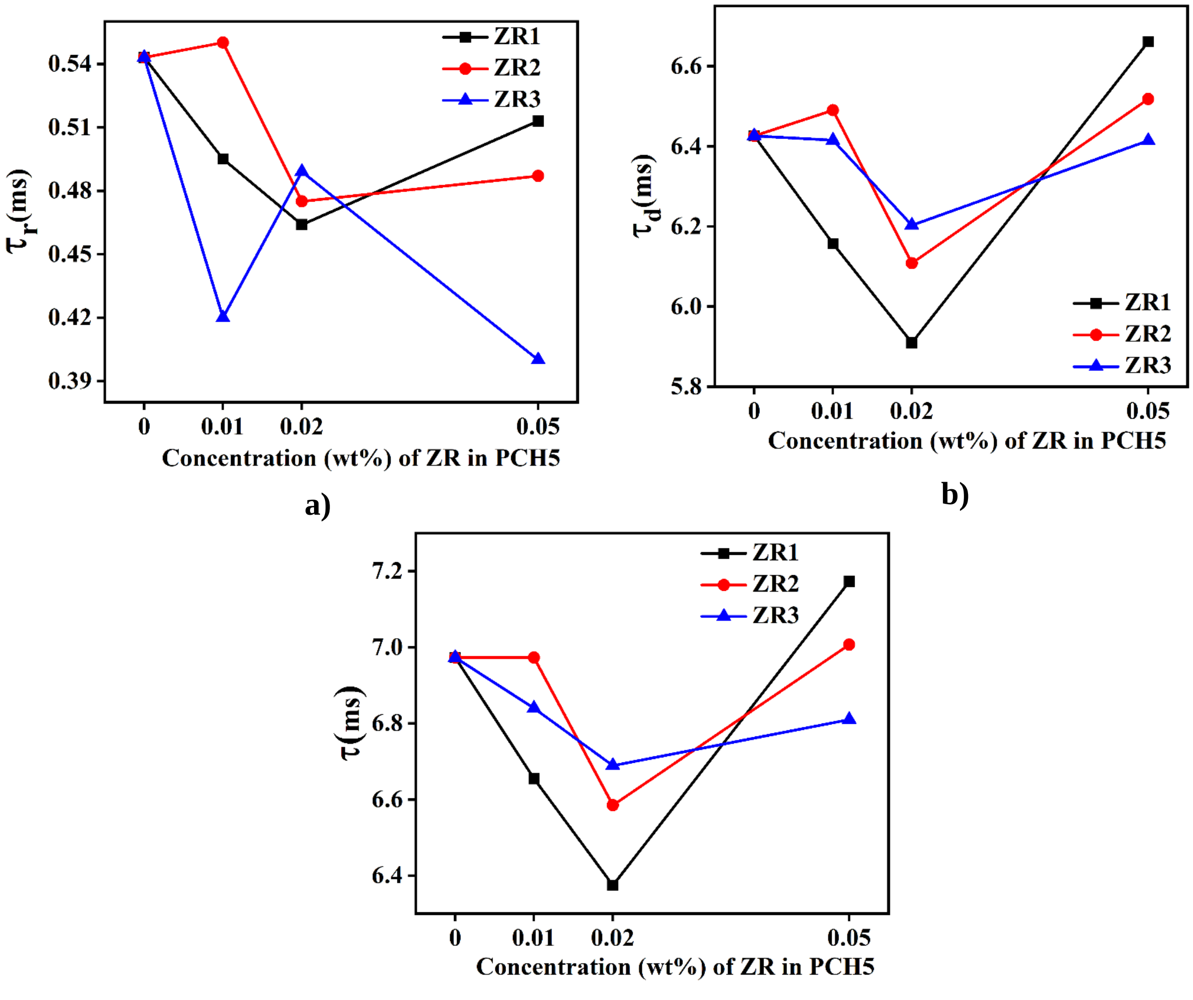

a)

b)

c)

Figure 6-8 Variation of (a) rise time (τ_r); (b) decay time (τ_d); (c) total response time (τ) ; for pure and ZR nanocomposites of PCH5 with varying concentration of ZR at $T - T_{IN} = -15$℃

Variation of bulk ac conductivity (σ_{ac}) of the pure and ZR nanocomposites of PCH5 as a function of temperature are shown in Fig 6-9. The variation of σ_{ac} with variation of C_{ZR} and size of ZR at T-T_{IN} = -15°C is shown in Fig 6-10d. ZnO nanorods are observed to trap the ionic impurities efficiently. With increasing C_{ZR}, value of σ_{ac} increases but is still less than that of the pure PCH5 for the C_{ZR} under investigation. Maximum ionic adsorption is observed for 0.01 wt% ZR nanocomposites of PCH5 viz., 78%, 82% and 77% for ZR1, ZR2 and ZR3, respectively.

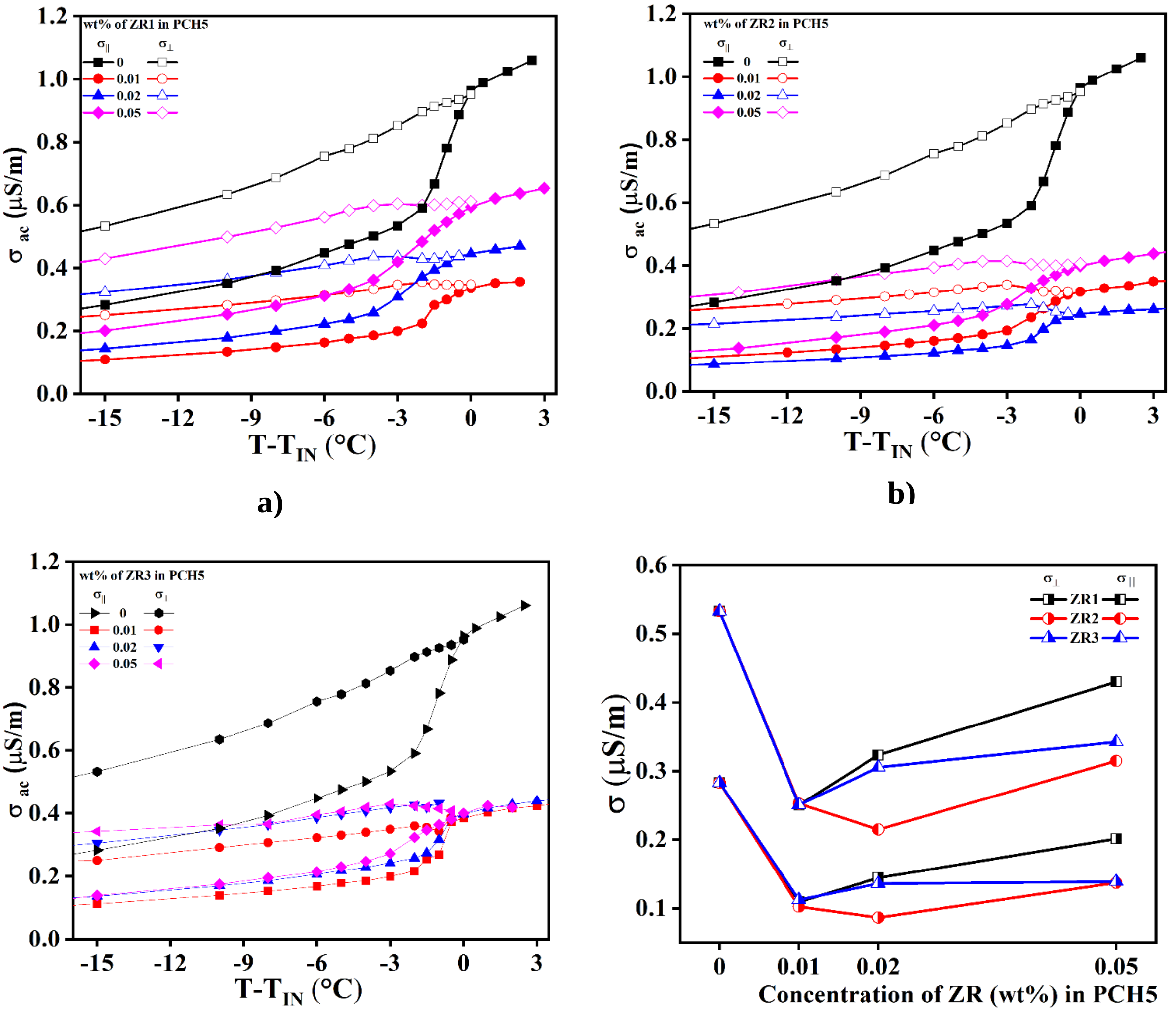

a)

b)

c)

d)

Figure 6-9 Variation of bulk ac conductivity (σ_{ac}) as a function of temperature for pure and ZR nanocomposites of PCH5; variation of parallel ($\sigma_{\parallel}$) and perpendicular ($\sigma_{\perp}$) components of conductivity for ZR1 (a), ZR2(b) and ZR3(c) nanocomposites; variation of $\sigma_{\parallel}$ and $\sigma_{\perp}$ as function of concentration of ZR in PCH5 at $T - T_{IN} = -15°C$

To briefly summarize the observed results, the physical properties of the NLC are observed to enhanced with the incorporation of ZnO nanorods at low concentration. Presence of nanorods induces short range nematic order in the isotropic phase of the liquid crystal. Smaller nanorods (ZR1) are expected to form chain like structure owing to orientational order of NLC. Increase in dielectric as well as optical anisotropy which in turn indicates increase in the order parameter of the system is observed. Also, substantial decrease in the value of V_{th}, response time and σ_{ac} whereas increased value of K_{11}, K_{33} and K_{33}/K_{11} are observed in ZR nanocomposites of PCH5 as compared to pure PCH5. Hence, incorporation of nanorods in NLC may help to achieve homogeneous and better alignment, decreased threshold voltage and response time, and can be used for high refresh rate as well as high multiplexing devices. Based on all the measured parameters addition of 0.01 wt% of ZnO nanorods of intermediate size $(50nm: 200\ nm)$ are better suited to incorporate in NLC matrix to enhance physical properties as well as device parameters. The schematic shown in Fig 6-10 depicts the expected behaviour of different size of nanorods in the nematic matrix at different applied voltages.

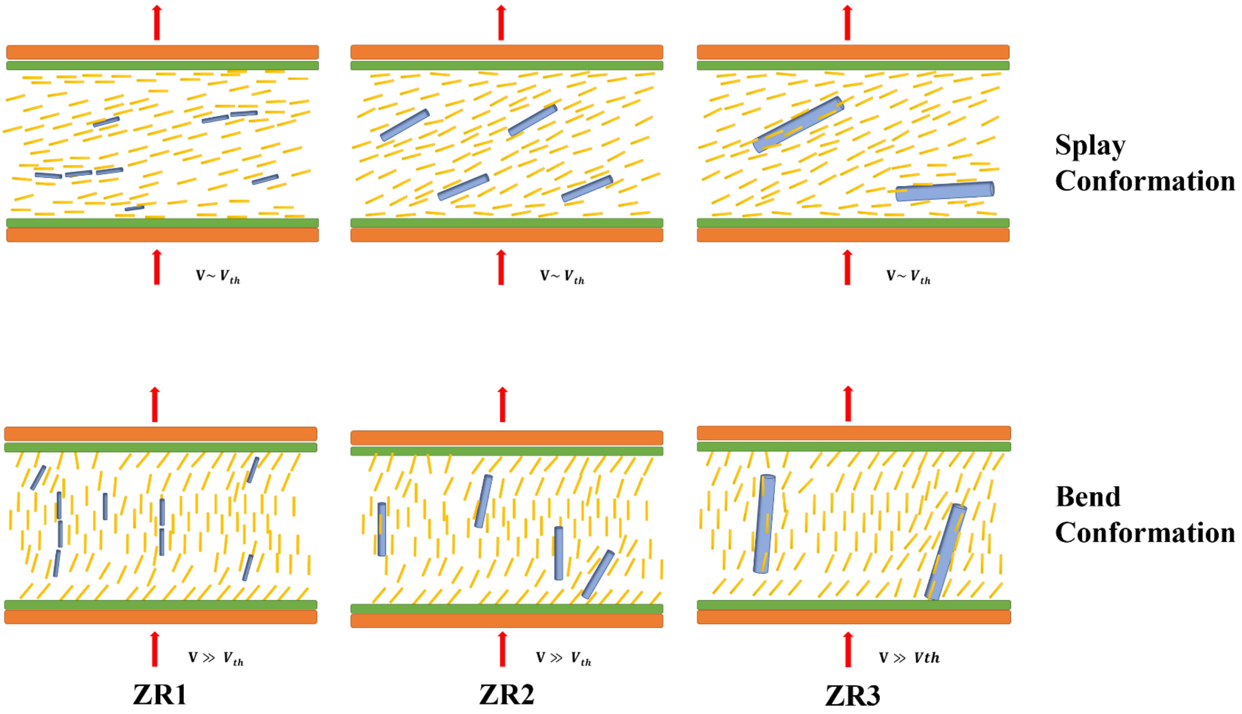

Figure 6-10 Schematic diagram proposed based on the observed results showing the effect of different size of ZnO nanorods on splay and bend deformation at different applied voltages.

6.4 CONCLUSION

As discussed in chapter 5, zinc oxide nanorods are best choice to be incorporated in NLC matrix to enhance physical properties and device parameters, especially, for displays. In this chapter, we presented the results of effect of incorporation of zinc oxide nanorods of different size but similar aspect ratio on physical properties of PCH5. The main findings of the study are:

- The zinc oxide nanorods (ZR) of similar aspect ratio (4-5) but different size (diameter: length) viz., $10: 50\ nm$ (ZR1), $50: 200\ nm$ (ZR2) and $1: 5\ \mu m$ (ZR3) are synthesized.
- Short range nematic order is observed in the isotropic phase of NLC with the incorporation of nanorods.
- The smaller nanorods (ZR1) tend to form chain like structures in host NLC matrix leading to softening of order parameter at the isotropic-nematic transition.
- Incorporation of ZR leads to increase in the dielectric anisotropy of the nanocomposite system as compared to pure PCH5.
- The reduction of threshold voltage, electro-optic response time and conductivity ($\sim 80\%$) of the nanocomposite samples is observed with the incorporation of ZR in host NLC.
- From the results of the study presented in this chapter, the optimization of values of the display device parameters indicates that incorporation of 0.01 wt% of nanorods in the size range of $50\ nm: 200\ nm$ is better suited for display device applications.

CHAPTER 7

CONCLUSION AND FUTURE SCOPE

7.1 CONCLUSION

The primary objective of the thesis is to study the effect of incorporation of 1D nanomaterials on the physical properties, viz., dielectric, and electro-optic properties of calamitic liquid crystals. As predicted by Onsager's theory based on shape anisotropy of molecule, rod-shaped particles can form stable nematic phase. To improve the physical properties of these LCs, it has been proposed that incorporation of 1D nanostructures in LC matrix would be a better choice. To investigate the same, two calamitic LCs, PCH5 having wide nematic temperature range and 8CB showing nematic as well as smectic A phase are selected. Oleic acid functionalized CdS nanowires are obtained from our collaborator Prof. Sandeep Kumar, RRI, Bangaluru. Zinc oxide (ZnO) nanomaterials are synthesised in the laboratory. Zinc oxide has been studied as a potential nanomaterial in various technological fields as sensors, optoelectronics, photovoltaics, drug delivery etc. by researchers worldwide. Synthesis of ZnO NPs of different shapes and aspect ratio with the control over morphology and crystallinity is easy as compared to other nanomaterials. For this thesis work, we have synthesized ZnO NPs of different size and shape in the laboratory.

Brief introduction to the development of theory and applications of liquid crystals is discussed in Chapter1. Synthesis and characterization techniques used for nanomaterials and the preparation and measurement technique of pure and nanocomposite samples of liquid crystals are presented in Chapter 2. The findings of the research work done are discussed in Chapter 3-6. Conclusion and future scope of the research work is presented in Chapter 7.

The results on effect of incorporation of CdS nanowire functionalized with oleic acid on physical properties and behaviour of isotropic-nematic phase transition of nematic liquid crystal, PCH5 are presented in Chapter 3. Incorporation of CdS nanowires ($\leq 0.05\ wt\%$) in nematic matrix shows continuous I-N phase transition on contrary to the weakly first order I-N phase transition of pure PCH5. Also, the conductivity of the nanocomposites is found to increase with the incorporation of CdS nanowires in PCH5 as compared to pure PCH5.

In Chapter 4, we presented the results of effect of zinc oxide nanorods capped with oleic acid (ZOR) on physical properties of 8CB. ZOR is synthesized using reflux method in the laboratory. Results of the study indicate that above a critical concentration of ZOR (0.3 wt% = C^{*}_{ZOR}) 8CB, vertical alignment of host LC molecules is induced in planar/unaligned cells. Systematic investigation of planar to homeotropic alignment of LC by incorporation of ZOR is performed and possible mechanism is discussed. Ionic conductivity is also observed to be reduced in the nanocomposites ($\mathrm{C}_{ZOR} \leq 0.4\, wt\%$) as compared to pure LC. Magnitude of activation energy is observed to be increasing implying reduction in the ion mobility in ZOR nanocomposites as compared to pure LC. Maximum decrease of 57% in the ionic conductivity of the nanocomposite system for $C_{ZOR} < C^{*}_{ZOR}$ is observed due to adsorption of ionic impurities by ZOR.

In chapter 5, we presented the results of effect of shape of nanoparticle on physical properties of PCH5. To carry out a comparative study between the effect of functionalized and unfunctionalized nanomaterials, we synthesized zinc oxide (ZnO) nanoparticles of different shapes, i.e., nanospheres, nanorods and nanowires. Incorporation of 1D nanostructures helps better dispersion, alignment and improved physical properties of nanocomposite samples as compared to pure NLC. Also, isotropic particles tend to self-assemble in chains/strands to minimize the free energy of the nanocomposite system. Pronounced increase in birefringence & dielectric anisotropy and reduction in threshold voltage, response time as well as viscoelastic ratio is observed in NLC nanocomposites of ZR and ZW as compared to ZS nanocomposites of NLC. Based on the results, nanocomposites of PCH5 prepared using ZnO nanorods is found to be the best candidate which offers significant improvement in physical properties.

In continuation to the study presented in Chapter 5, results on effect of size of ZnO nanorods with similar aspect ratio but different size (diameter: length), on physical properties of PCH5 are presented in Chapter 6. Short range nematic order is observed in the isotropic phase of NLC with the incorporation of ZnO nanorods. The smaller nanorods ($10{:}\,50\ nm$) tend to form chain like structures in host NLC matrix leading to softening of order parameter at the isotropic-nematic transition. Incorporation of ZR leads to increase in the dielectric anisotropy of the nanocomposite system as compared to pure PCH5. The important parameters for display devices, i.e., threshold voltage, electro-optic response time and conductivity of the nanocomposite samples are observed to decrease with the incorporation of ZR in host NLC. Results of this study indicates that incorporation of 0.01 wt% of ZnO nanorods in PCH5 yields improved display device properties without observed aggregation or accumulation of nanomaterials in bulk or at interfaces of the LC cell. Based on the results presented in the chapter, ZnO nanorods in the size range of $(50\colon 200\ nm)$ are potential choice as compared to very small rods $(10\colon 50\ nm)$ or very big rods $(1\mu m\colon 5\mu m)$ to incorporate in NLC matrix.

To summarize the thesis work, the effect of size and aspect ratio of nanomaterial on the physical properties of nematic liquid crystal are investigated. The key findings of the thesis are as follows:

- Systematic investigation of functionalized zinc oxide nanorods in LC shows that above critical concentration of 0.3 wt%, homeotropic alignment of LC molecules can be obtained in planar/ unaligned cells. The results of this study indicate that vertical alignment can be induced by incorporation of ZOR in LC without use of any alignment layer. This may be useful for the application related to vertical alignment LCD devices.
- The small nanoparticles (spherical or rod-shaped with $diameter < 50\ nm$) of zinc oxide tend to form chain like structures under the influence of nematic ordering potential. Moderately stiff and long chains of ZnO nanoparticles $(< 50\ nm)$ or functionalized CdS nanowires having long lengths affects the evolution of order parameter at the isotropic-nematic transition.
- Enhancement of the physical properties such as dielectric anisotropy, optical anisotropy, splay and bend elastic constants show that ZnO nanorods are best potential candidates to incorporate in NLC host medium as compared to ZnO nanospheres or nanowires. Incorporation of ZnO nanorods is also observed to reduce the threshold voltage, electro-optic response time and enhance bend to splay elastic constant ratio which are important display device parameters. Hence, nanorod incorporated NLC can be explored for low power and high multiplexing display devices. One of the most important challenges in improvement of display parameters is reduction of ionic impurities. Addition of zinc oxide nanoparticles of any shape at low concentration $(0.01 wt\%)$ are observed to reduce the ionic impurities by $\sim 80\%$. Further, investigation of physical properties of ZnO nanorod of different size incorporated in NLC host shows that nanorods of the size range $\sim 50\colon 200\ nm$ are better alternative for preparing nanocomposite samples. To comprehend the main results, the comparison of various properties of NLC, PCH5 with the incorporation of different shapes and size of zinc oxide nanoparticles at concentration of 0.01 wt% is shown in Fig 7-1.

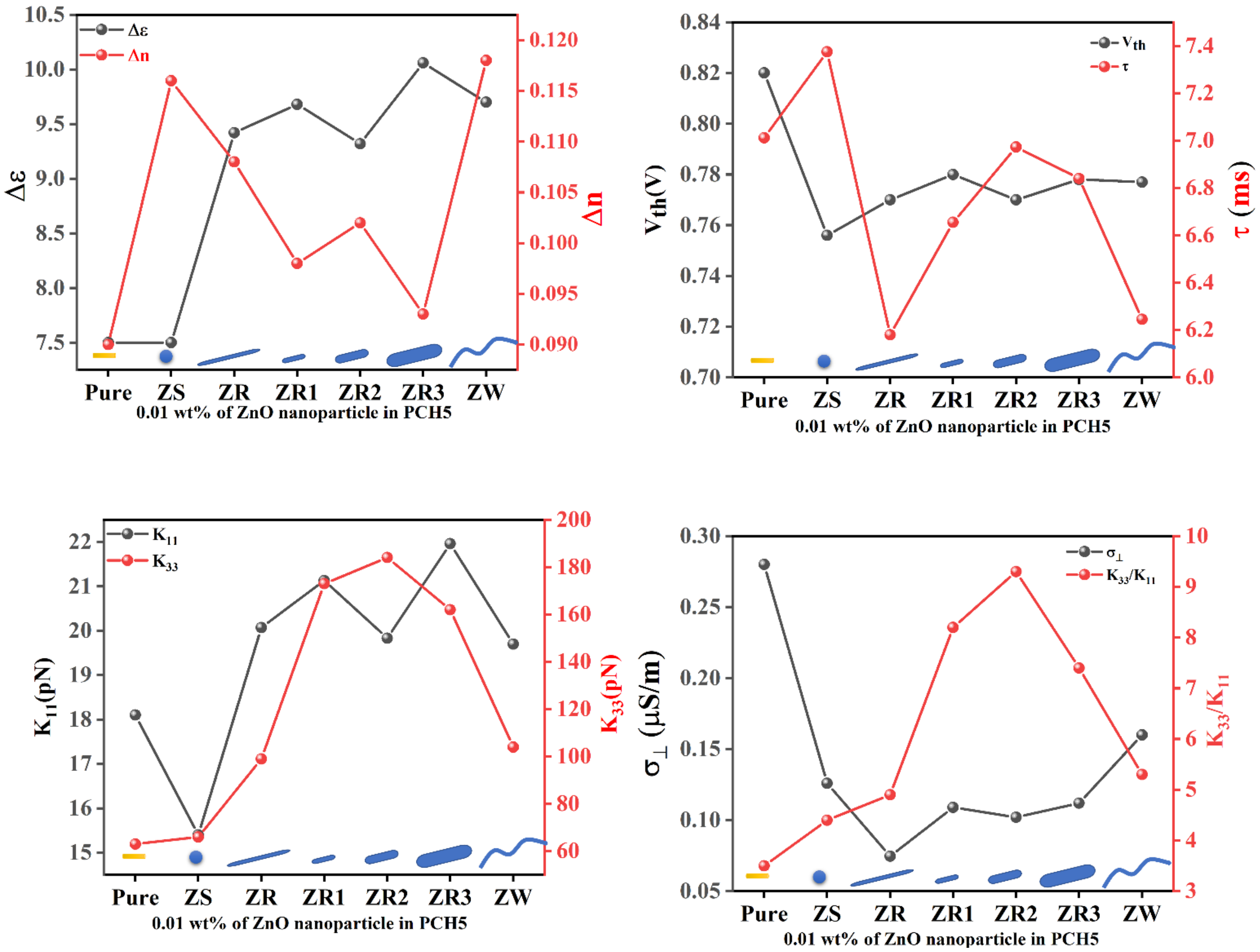

Figure 7-1 Effect of different size and shape of zinc oxide nanoparticles on various physical properties of PCH5 (concentration of nanomaterial in PCH5= 0.01 wt%)

7.2 FUTURE SCOPE

In this thesis work we have presented the studies on effect of incorporation of 1D nanomaterials on phase transition behaviour and physical properties of liquid crystals. However, more studies are required to understand the nanocomposite systems of NLC.

- Polarized spectroscopy studies and/or small angle XRD investigations may be helpful to understand the dipole-dipole interactions between NLC molecules and nanoparticles. This may give better insight to the underlying physics of the dipolar interactions in the system which will be helpful to justify the observed results. The dielectric spectroscopy measurements in low frequency region ($\sim mHz$) will also be useful to understand the ionic relaxation phenomenon.
- The effect of functionalization of nanomaterials on properties of liquid crystals can be investigated and the comparative study of functionalized and non-functionalized NPs can be performed.
- The investigation of composite systems of nematic liquid crystals with different 1D nanomaterials showing different properties such as luminescent NPs, dielectric NPs, magnetic NPs etc. may also be explored.
- As discussed in the thesis, ZnO NMs are observed to minimize the ionic impurities to a great extent. Hence, further device applications of the NLC incorporated with ZnO NMs can be developed. Use of these nanocomposite samples for commercial device applications like twisted nematic display, switchable window or sensors can be explored.

REFERENCES

[1] Reinitzer F. Contributions to the knowledge of cholesterol. Liq Cryst. 1989;5:7–18.

[2] Gennes PG de, J.Prost. The Physics of Liquid Crystals, 2nd Edition. Oxford University Press; 1993.

[3] Lueder E. Liquid Crystal Displays:Addressing Schemes and Electro-Optical Effects. 2nd ed. Lowe AC, editor. Conf. Rec. - Electro. Wiley-SID Series in Display Technology; 1981.

[4] Kumar M, Kumar S. Liquid crystals in photovoltaics: A new generation of organic photovoltaics. Polym J [Internet]. 2017;49:85–111. Available from: http://dx.doi.org/10.1038/pj.2016.109.

[5] Sun K, Xiao Z, Lu S, et al. A molecular nematic liquid crystalline material for high-performance organic photovoltaics. Nat Commun [Internet]. 2015;6:1–9. Available from: http://dx.doi.org/10.1038/ncomms7013.

[6] Gregg BA, Fox MA, Bard AJ. Photovoltaic effect in symmetrical cells of a liquid crystal porphyrin. J Phys Chem. 1990;94:1586–1598.

[7] Hogan BT, Kovalska E, Craciun MF, et al. 2D material liquid crystals for optoelectronics and photonics. J Mater Chem C. 2017;5:11185–11195.

[8] Kelker H. History of Liquid Crystals. Mol Cryst Liq Cryst. 1973.

[9] Kelker H, Knoll PM. Plenary lecture: Some pictures of the history of liquid crystals. Liq Cryst. 1989;5:19–42.

[10] Fréedericksz V, Zolina V. Forces causing the orientation of an anisotropic liquid. Trans Faraday Soc. 1933;29:919–930.

[11] Onsager L. the Effects of Shape on the Interaction of Colloidal Particles. Ann N Y Acad Sci. 1949;51:627–659.

[12] H. HG. LIQUID-CRYSTAL DISPLAY DEVICES. Sci Am. 1970;222:100–107.

[13] Chandrasekhar S, Sadashiva BK, Suresh KA. Liquid crystals of disc-like molecules. Pramana. 1977;9:471–480.

[14] Magnuson ML, Fung BM, Bayle JP. On the temperature dependence of the order

parameter of liquid crystals over a wide nematic range. Liq Cryst. 1995;19:823–832.

[15] Tough RJA, Bradshaw MJ. Determination of the Order Parameters of Nematic Liquid Crystals By Mean Field Extrapolation. J Phys Paris. 1983;44:447–454.

[16] Maier W Von, Meier G. A simple theory of the dielectric properties of homogeneously oriented crystalline liquid phases of the nematic type. Zeitschrift fur Naturforsch - Sect A J Phys Sci. 1961;16:262–267.

[17] Kremer F. Dielectric spectroscopy - Yesterday, today and tomorrow. J Non Cryst Solids. 2002;305:1–9.

[18] Ward AA. State of the Art Dielectric Materials for Advanced Applications. 2015;1–70.

[19] Kundu SK, Okudaira S, Kosuge M, et al. Broadband dielectric spectroscopy of a nematic liquid crystal in benzene. J Chem Phys. 2008;129:1–7.

[20] Havriliak S, Negami S. A complex plane representation of dielectric and mechanical relaxation processes in some polymers. Polymer (Guildf). 1967;8:161–210.

[21] Havriliak S, Negami S. A complex plane analysis of α-dispersions in some polymer systems. J Polym Sci Part C Polym Symp. 2007;14:99–117.

[22] Iglesias TP, Vilão G, Reis JCR. An approach to the interpretation of Cole-Davidson and Cole-Cole dielectric functions. J Appl Phys [Internet]. 2017;122. Available from: http://dx.doi.org/10.1063/1.4985839.

[23] Meier G, Saupe A. Dielectric Relaxation in Nematic Liquid Crystals. Mol Cryst. 1966;1:515–525.

[24] Oseen C W. The Theory of Liquid Crystals. 1932;

[25] Frank FC. LIQUID CRYSTALS :On the theory of liquid crystals. 1958;19–28.

[26] Bisoyi HK, Kumar S. Liquid-crystal nanoscience: An emerging avenue of soft self-assembly. Chem Soc Rev. 2011;40:306–319.

[27] Kulkarni SK. Nanotechnology - Principles and Practices 3rd ed (Springer, CP, 2015).pdf. 3rd ed. Springer; 2014.

[28] Ersoz M, Isitan A, Balaban M. Nanotechnology 1: fundamentals of nanotechnology. UNINANO Univers. Nanotechnol. Ski. Creat. Motiv. Dev. 2018.

[29] Hong NH. Introduction to Nanomaterials: Basic Properties, Synthesis, and Characterization [Internet]. Nano-sized Multifunct. Mater. Elsevier Inc.; 2019. Available from: http://dx.doi.org/10.1016/B978-0-12-813934-9.00001-3.

[30] Ealias AM, Saravanakumar MP. A review on the classification, characterisation, synthesis of nanoparticles and their application. IOP Conf Ser Mater Sci Eng. 2017;263.

[31] Baig N, Kammakakam I, Falath W, et al. Nanomaterials: A review of synthesis methods, properties, recent progress, and challenges. Mater Adv. 2021;2:1821–1871.

[32] Liang Q, Zou X, Chen H, et al. High-performance formaldehyde sensing realized by alkaline-earth metals doped In2O3 nanotubes with optimized surface properties. Sensors Actuators, B Chem [Internet]. 2020;304:127241. Available from: https://doi.org/10.1016/j.snb.2019.127241.

[33] Salam MA, Burk R. Synthesis and characterization of multi-walled carbon nanotubes modified with octadecylamine and polyethylene glycol. Arab J Chem [Internet]. 2017;10:S921–S927. Available from: http://dx.doi.org/10.1016/j.arabjc.2012.12.028.

[34] Wiley B, Sun Y, Xia Y. Synthesis of silver nanostructures with controlled shapes and properties. Acc Chem Res [Internet]. 2007;40:1067–1076. Available from: http://dx.doi.org/10.1021/ar7000974.

[35] Liu Q, Tang J, Zhang Y, et al. Shape-dependent dispersion and alignment of nonaggregating plasmonic gold nanoparticles in lyotropic and thermotropic liquid crystals. Phys Rev E - Stat Nonlinear, Soft Matter Phys. 2014;89:1–10.

[36] Cheon S, Lee WW, Park W Il, et al. Fabrication of arrangement-controlled and vertically grown ZnO nanorods by metal nanotransfer printing. J Ind Eng Chem [Internet]. 2020;81:385–392. Available from: https://doi.org/10.1016/j.jiec.2019.09.029.

[37] Cerrón-Calle GA, Aranda-Aguirre AJ, Luyo C, et al. Photoelectrocatalytic decolorization of azo dyes with nano-composite oxide layers of ZnO nanorods decorated with Ag nanoparticles. Chemosphere. 2019;219:296–304.

[38] Feng X, Huang Y, Li C, et al. Controllable synthesis of porous NiCo2O4/NiO/Co3O4 nanoflowers for asymmetric all-solid-state supercapacitors. Chem Eng J [Internet]. 2019;368:51–60. Available from: https://doi.org/10.1016/j.cej.2019.02.191.

[39] Peng L, Xiong P, Ma L, et al. Holey two-dimensional transition metal oxide nanosheets

for efficient energy storage. Nat Commun. 2017;8.

[40] Hadia NMA, Mohamed HAH. Characteristics and optical properties of MgO nanowires synthesized by solvothermal method. Mater Sci Semicond Process [Internet]. 2015;29:238–244. Available from: http://dx.doi.org/10.1016/j.mssp.2014.03.049.

[41] Kumar S, Ojha AK. Synthesis, characterizations and antimicrobial activities of well dispersed ultra-long CdO nanowires. AIP Adv. 2013;3:1–6.

[42] Zhao S, Shen Y, Li A, et al. Effects of rare earth elements doping on gas sensing properties of ZnO nanowires. Ceram Int [Internet]. 2021;47:24218–24226. Available from: https://doi.org/10.1016/j.ceramint.2021.05.133.

[43] McLellan JM, Li ZY, Siekkinen AR, et al. The SERS activity of a supported ag nanocube strongly depends on its orientation relative to laser polarization. Nano Lett. 2007;7:1013–1017.

[44] Li N, Zhao P, Astruc D. Anisotropic gold nanoparticles: Synthesis, properties, applications, and toxicity. Angew Chemie - Int Ed. 2014;53:1756–1789.

[45] Singh JP, Singh V, Sharma A, et al. Approaches to synthesize MgO nanostructures for diverse applications. Heliyon [Internet]. 2020;6:e04882. Available from: https://doi.org/10.1016/j.heliyon.2020.e04882.

[46] Garbovskiy YA, Glushchenko A V. Liquid crystalline colloids of nanoparticles: Preparation, properties, and applications. Solid State Phys. - Adv. Res. Appl. 2010.

[47] Zhang Y, Liu Q, Mundoor H, et al. Metal nanoparticle dispersion, alignment, and assembly in nematic liquid crystals for applications in switchable plasmonic color filters and E-polarizers. ACS Nano. 2015;9:3097–3108.

[48] Singh UB, Dhar R, Dabrowski R, et al. Enhanced electro-optical properties of a nematic liquid crystals in presence of BaTiO3 nanoparticles. Liq Cryst [Internet]. 2014;41:953–959. Available from: http://dx.doi.org/10.1080/02678292.2014.894209.

[49] Ayushi Rastogi , Fanindra Pandey RM, Singh S. Effect of Doping of Cd1−xZnxS/ZnS Core/Shell Quantum Dots in Negative Dielectric Anisotropy Nematic Liquid Crystal p-Methoxybenzylidene p-Decylaniline. crystals. 2021;11.

[50] Kundu S, Hill JP, Richards GJ, et al. Ultranarrow PbS nanorod-nematic liquid crystal

blend for enhanced electro-optic properties. ACS Appl Mater Interfaces. 2010;2:2759–2766.

[51] Wu KJ, Chu KC, Chao CY, et al. CdS nanorods imbedded in liquid crystal cells for smart optoelectronic devices. Nano Lett. 2007;7:1908–1913.

[52] Mishra S, Manjuladevi V, Gupta RK, et al. Experimental evidence of continuous isotropic-nematic phase transition in CdS nanowire nanocomposites of a nematic liquid crystal. Liq Cryst [Internet]. 2020;00:1–11. Available from: https://doi.org/10.1080/02678292.2020.1849833.

[53] Li F, Buchnev O, Cheon C Il, et al. Orientational coupling amplification in ferroelectric nematic colloids. Phys Rev Lett. 2006;97:5–8.

[54] Hayes CF. Magnetic Platelets in a Nematic Liquid Crystal. Mol Cryst Liq Cryst. 1976;36:245–253.

[55] Kopčanský P, Tomašovičová N, Koneracká M, et al. Structural changes in the 6CHBT liquid crystal doped with spherical, rodlike, and chainlike magnetic particles. Phys Rev E - Stat Nonlinear, Soft Matter Phys. 2008;78:4–8.

[56] Basu R, Iannacchione GS. Carbon nanotube dispersed liquid crystal: A nano electromechanical system. Appl Phys Lett. 2008;93:2–5.

[57] Lisetski L, Soskin M, Lebovka N. Carbon nanotubes in liquid crystals: Fundamental properties and applications. Springer Proc. Phys. 2015.

[58] Singh DP, Duponchel B, Lin Y, et al. Orientation of 4-: N -octyl-4′-cyanobiphenyl molecules on graphene oxide surface via electron-phonon interaction and its applications in nonlinear electronics. J Mater Chem C. 2019;7:2734–2743.

[59] Zhai F, Feng Y, Zhou K, et al. Graphene-based chiral liquid crystal materials for optical applications. J Mater Chem C. 2019;7:2146–2171.

[60] Kumar A, Singh DP, Singh G. Recent progress and future perspectives on carbon-nanomaterial-dispersed liquid crystal composites. J Phys D Appl Phys. 2022;55.

[61] Mishra S, Sontakke AM, Gupta RK, et al. Dielectric spectroscopy studies of silver nanorod doped nematic liquid crystal. Mater Today Proc [Internet]. 2021;50:2587–2591. Available from: https://doi.org/10.1016/j.matpr.2021.12.244.

[62] S J S, Mishra S, Dutta K, et al. Frequency dependence of dielectric permittivity and conductivity of functionalized carbon nanotube-nematic liquid crystal nanocomposite. J Mol Liq [Internet]. 2022;349:118168. Available from: https://doi.org/10.1016/j.molliq.2021.118168.

[63] Patro CK, Verma R, Garg A, et al. Boost in the thermal stability, ionic conductivity and director relaxation frequency in the composite of liquid crystal and functionalised multi-walled carbon nanotubes. Liq Cryst [Internet]. 2020;00:1–16. Available from: https://doi.org/10.1080/02678292.2020.1783588.

[64] Liu Y, Lim YJ, Kundu S, et al. Super-fast switching of twisted nematic liquid crystals with a single-wall-carbon-nanotube-doped alignment layer. J Korean Phys Soc. 2015;66:952–958.

[65] Schymura S, Scalia G. On the effect of carbon nanotubes on properties of liquid crystals. Philos Trans R Soc A Math Phys Eng Sci. 2013;371.

[66] Gorkunov M V., Osipov MA. Mean-field theory of a nematic liquid crystal doped with anisotropic nanoparticles. Soft Matter. 2011;7:4348–4356.

[67] Egorov SA, Milchev A, Virnau P, et al. A new insight into the isotropic-nematic phase transition in lyotropic solutions of semiflexible polymers: Density-functional theory tested by molecular dynamics. Soft Matter. 2016;12:4944–4959.

[68] Orlandi S, Benini E, Miglioli I, et al. Doping liquid crystals with nanoparticles . A computer simulation of the effects of nanoparticle shape. 2016;2428–2441.

[69] Viamontes J, Tang JX. Continuous isotropic-nematic liquid crystalline transition of F-actin solutions. Phys Rev E - Stat Physics, Plasmas, Fluids, Relat Interdiscip Top. 2003;67:4.

[70] Singh DP, Gupta SK, Yadav SP, et al. Guest – host interaction in ferroelectric liquid crystal – nanoparticle. 2014;37:511–518.

[71] Chen HY, Lee W, Clark NA. Faster electro-optical response characteristics of a carbon-nanotube- nematic suspension. Appl Phys Lett. 2007;90.

[72] S J S, Gupta RK, Kumar S, et al. Enhanced electro-optical response of nematic liquid crystal doped with functionalised silver nanoparticles in twisted nematic configuration. Liq Cryst [Internet]. 2020;00:1–13. Available from:

https://doi.org/10.1080/02678292.2020.1755901.

[73] Yadav SP, Singh S. Carbon nanotube dispersion in nematic liquid crystals: An overview [Internet]. Prog. Mater. Sci. Elsevier Ltd; 2016. Available from: http://dx.doi.org/10.1016/j.pmatsci.2015.12.002.

[74] Scalia G, Lagerwall JPF, Schymura S, et al. Carbon nanotubes in liquid crystals as versatile functional materials. Phys Status Solidi Basic Res. 2007;244:4212–4217.

[75] Sivaranjini B, Mangaiyarkarasi R, Ganesh V, et al. Vertical Alignment of Liquid Crystals over a Functionalized Flexible Substrate. Sci Rep [Internet]. 2018;8:1–13. Available from: http://dx.doi.org/10.1038/s41598-018-27039-3.

[76] Umadevi S, Feng X, Hegmann T. Large area self-assembly of nematic liquid-crystal-functionalized gold nanorods. Adv Funct Mater. 2013;23:1393–1403.

[77] Sridevi S, Prasad SK, Nair GG, et al. Enhancement of anisotropic conductivity , elastic , and dielectric constants in a liquid crystal-gold nanorod system Enhancement of anisotropic conductivity , elastic , and dielectric constants in a liquid crystal-gold nanorod system. Appl Phys Lett. 2015;151913:2013–2016.

[78] Acharya S, Kundu S, Hill JP, et al. Nanorod-driven orientational control of liquid crystal for polarization-tailored electro-optic devices. Adv Mater. 2009;21:989–993.

[79] Osipov MA, Gorkunov M V. Effect of nanoparticle chain formation on dielectric anisotropy of nematic composites. 2015;032501:1–8.

[80] Kumar J. Effect of Nanomaterial Dopants on the Physical Properties of Liquid Crystals. 2016;

[81] Frenkel D. Onsager’s spherocylinders revisited. J Phys Chem. 1987;91:4912–4916.

[82] Van Roie B, Leys J, Denolf K, et al. Weakly first-order character of the nematic-isotropic phase transition in liquid crystals. Phys Rev E. 2005;72:1–8.

[83] ALBEN R. Pretransition effects in nematic liquid crystals: Model calculations. Mol Cryst. 1971;13:193–231.

[84] Helfrich W. Effect of electric fields on the temperature of phase transitions of liquid crystals. Phys Rev Lett. 1970;24:201–203.

[85] Basappa G, Madhusudana N V. Effect of Strong Electric Fields on Phase Transitions in

Some Liquid Crystals. Mol Cryst Liq Cryst. 1996;288:37–41.

[86] Cuesta JA, Frenkel D. Monte Carlo simulation of two-dimensional hard ellipses. Phys Rev A. 1990;42:2126–2136.

[87] Chen ZY. Continuous isotropic-nematic transition of partially flexible polymers in two dimensions. Phys Rev Lett. 1993;71:93–96.

[88] Petridis L, Terentjev EM. Nematic-isotropic transition with quenched disorder. Phys Rev E - Stat Nonlinear, Soft Matter Phys. 2006;74:1–11.

[89] Disch S, Schmidt C, Finkelmann H. Nematic elastomers beyond the critical point. Macromol Rapid Commun. 1994;15:303–310.

[90] Lebar A, Kutnjak Z, Žumer S, et al. Evidence of supercritical behavior in liquid single crystal elastomers. Phys Rev Lett. 2005;94:1–4.

[91] Allender DW. Continuous Nematic-Isotropic Transition in Submicron-Size Liquid-Crystal Droplets. Phys Rev Lett. 1965;207:1238.

[92] Kityk A V., Wolff M, Knorr K, et al. Continuous paranematic-to-nematic ordering transitions of liquid crystals in tubular silica nanochannels. Phys Rev Lett. 2008;101:1–4.

[93] Sheng P. Boundary-layer phase transition in nematic liquid crystals. Phys Rev A. 1982;26:1610–1617.

[94] Acharya S, Panda AB, Efrima S, et al. Polarization properties and switchable assembly of ultranarrow ZnSe nanorods. Adv Mater. 2007;19:1105–1108.

[95] Peterson MSE, Georgiev G, Atherton TJ, et al. Dielectric analysis of the interaction of nematic liquid crystals with carbon nanotubes. Liq Cryst [Internet]. 2018;45:450–458. Available from: https://doi.org/10.1080/02678292.2017.1346212.

[96] Pagidi S, Manda R, Bhattacharyya SS, et al. Superior electro-optics of nano-phase encapsulated liquid crystals utilizing functionalized carbon nanotubes. Compos Part B Eng [Internet]. 2019;164:675–682. Available from: https://doi.org/10.1016/j.compositesb.2019.01.091.

[97] Singh D, Singh UB, Pandey MB, et al. Enhancement in electro-optical parameters of nematic liquid crystalline material with SWCNTs. Opt Mater (Amst) [Internet].

2018;84:16–21. Available from: https://doi.org/10.1016/j.optmat.2018.06.045.

[98] Shivanandareddy AB, Kumar M, Gowda A, et al. Trapping of inorganic nanowires in supramolecular organic nanoribbons. J Mol Liq [Internet]. 2017;244:1–6. Available from: http://dx.doi.org/10.1016/j.molliq.2017.08.099.

[99] Shivaraja SJ, Gupta RK, Kumar S, et al. Effect of functionalised silver nanoparticle on the elastic constants and ionic transport of a nematic liquid crystal. Liq Cryst [Internet]. 2019;46:1868–1876. Available from: https://doi.org/10.1080/02678292.2019.1611964.

[100] Li J, Gauza S, Wu ST. Temperature effect on liquid crystal refractive indices. J Appl Phys. 2004;96:19–24.

[101] Sen S, Kali K, Roy SK, et al. Refractive Indices and Dielectric Studies of Three Phenylcyclohexane Liquid Crystals in the Nematic Phase. Mol Cryst Liq Cryst. 1985;126:269–279.

[102] Kumar J, Gupta RK, Kumar S, et al. Electro-optic and dielectric studies on quantum dot doped nematic liquid crystal. Macromol Symp. 2015;357:47–51.

[103] Uchida T, Takahashi Y. New Method To Determine Elastic Constants of Nematic Liquid Crystal From C-V Curve. Mol Cryst Liq Cryst. 1981;72 Lett:133–137.

[104] Baik IS, Jeon SY, Lee SH, et al. Electrical-field effect on carbon nanotubes in a twisted nematic liquid crystal cell. Appl Phys Lett. 2005;87:1–3.

[105] Kumar P, Jaggi C, Sharma V, et al. Advancements of vertically aligned liquid crystal displays. Micron [Internet]. 2016;81:34–47. Available from: http://dx.doi.org/10.1016/j.micron.2015.11.001.

[106] Oh-E M, Yokoyama H, Kim D. Mapping molecular conformation and orientation of polyimide surfaces for homeotropicliquid crystal alignment by nonlinear optical spectroscopy. Phys Rev E - Stat Physics, Plasmas, Fluids, Relat Interdiscip Top. 2004;69:11.

[107] Lee SH, Lee SL, Kim HY. Electro-optic characteristics and switching principle of a nematic liquid crystal cell controlled by fringe-field switching. Appl Phys Lett. 1998;73:2881–2883.

[108] Shirota K, Yaginuma M, Sakai T, et al. Surface orientation of cyanobiphenyl liquid

crystal monolayer and pretilt angle under various rubbing strengths. Japanese J Appl Physics, Part 1 Regul Pap Short Notes Rev Pap. 1996;35:2275–2279.

[109] Haba O, Hiratsuka D, Shiraiwa T, et al. Homeotropic orientation of nematic liquid crystals induced by dissolving polypropyleneimine dendrimer having peripheral mesogens. Opt Mater Express. 2014;4:934.

[110] Van Aerle NAJM, Barmentlo M, Hollering RWJ. Effect of rubbing on the molecular orientation within polyimide orienting layers of liquid-crystal displays. J Appl Phys. 1993;74:3111–3120.

[111] Yoon Jung Lee, Yong Woon Kim, Jae Du Ha JMO and MHY. Synthesis and characterization of novel polyimides with 1-octadecyl side chains.pdf. Polym Adv Technol. 2007;18:226–234.

[112] Moon J, Kang C, Kang H. Derivatives Structurally Similar to LC Molecules. 2022;

[113] Chen SH, Chou TR, Chiang Y Te, et al. Nanoparticle-induced vertical alignment liquid crystal cell with highly conductive PEDOT:PSS films as transparent electrodes. Mol Cryst Liq Cryst [Internet]. 2017;646:107–115. Available from: https://doi.org/10.1080/15421406.2017.1284552.

[114] Fang G, Shi Y, Maclennan JE, et al. Photo-reversible liquid crystal alignment using azobenzene-based self-assembled monolayers: Comparison of the bare monolayer and liquid crystal reorientation dynamics. Langmuir. 2010;26:17482–17488.

[115] Yi Y, Farrow MJ, Korblova E, et al. High-sensitivity aminoazobenzene chemisorbed monolayers for photoalignment of liquid crystals. Langmuir. 2009;25:997–1003.

[116] Jeng SC, Kuo CW, Wang HL, et al. Nanoparticles-induced vertical alignment in liquid crystal cell. Appl Phys Lett. 2007;91:1–4.

[117] Koenig GM, Gettelfinger BT, De Pablo JJ, et al. Using localized surface plasmon resonances to probe the nanoscopic origins of adsorbate-driven ordering transitions of liquid crystals in contact with chemically functionalized gold nanodots. Nano Lett. 2008;8:2362–2368.

[118] Qi H, Hegmann T. Formation of periodic stripe patterns in nematic liquid crystals doped with functionalized gold nanoparticles. J Mater Chem. 2006;16:4197–4205.

[119] Zhao D, Zhou W, Cui X, et al. Alignment of liquid crystals doped with Nickel nanoparticles containing different morphologies. Adv Mater. 2011;23:5779–5784.

[120] Kinkead B, Hegmann T. Effects of size, capping agent, and concentration of CdSe and CdTe quantum dots doped into a nematic liquid crystal on the optical and electro-optic properties of the final colloidal liquid crystal mixture. J Mater Chem. 2010;20:448–458.

[121] Qi H, Hegmann T. Liquid crystal-gold nanoparticle composites. Liq Cryst Today. 2011;20:102–114.

[122] Kim KH, Park BW, Choi SW, et al. Vertical alignment of liquid crystals without alignment layers. Liq Cryst. 2013;40:391–395.

[123] Hwang SJ, Jeng SC, Yang CY, et al. Characteristics of nanoparticle-doped homeotropic liquid crystal devices. J Phys D Appl Phys. 2009;42.

[124] Ma H, Lu S, Xie Q, et al. A stable liquid crystals sensing platform decorated with cationic surfactant for detecting thrombin. Microchem J. 2021;170.

[125] Luan C, Luan H, Luo D. Application and technique of liquid crystal-based biosensors. Micromachines. 2020;11.

[126] Sawamura M, Kawai K, Matsuo Y, et al. Stacking of conical molecules with a fullerene apex into polar columns in crystals and liquid crystals. Nature. 2002;419:702–705.

[127] Kuo CW, Jeng SC, Wang HL, et al. Application of nanoparticle-induced vertical alignment in hybrid-aligned nematic liquid crystal cell. Appl Phys Lett. 2007;91:2005–2008.

[128] Goodby JW, Saez IM, Cowling SJ, et al. Transmission and amplification of information and properties in nanostructured liquid crystals. Angew Chemie - Int Ed. 2008;47:2754–2787.

[129] Li Y, Zhang W Bin, Hsieh IF, et al. Breaking symmetry toward nonspherical janus particles based on polyhedral oligomeric silsesquioxanes: Molecular design, “click” synthesis, and hierarchical structure. J Am Chem Soc. 2011;133:10712–10715.

[130] Mishra S, Manjuladevi V, Gupta RK, et al. Investigation on physical properties of silver nanorod doped nematic liquid crystal. AIP Conf Proc. 2021;2369.

[131] Basu R, Atwood LJ. PHYSICAL REVIEW E 102 , 022701 (2020) Homeotropic liquid

crystal device employing vertically aligned carbon nanotube arrays as the alignment agent (a) (c) (d). Phys Rev E [Internet]. 2020;102:22701. Available from: https://doi.org/10.1103/PhysRevE.102.022701.

[132] Dhar R, Pandey AS, Pandey MB, et al. Optimization of the display parameters of a room temperature twisted nematic display material by doping single-wall carbon nanotubes. Appl Phys Express. 2008;1:1215011–1215013.

[133] Manohar R, Srivastava AK, Tripathi PK, et al. Dielectric and electro-optical study of ZnO nano rods doped ferroelectric liquid crystals. J Mater Sci. 2011;46:5969–5976.

[134] Yin M, Gu Y, Kuskovsky IL, et al. Zinc oxide quantum rods. J Am Chem Soc. 2004;126:6206–6207.

[135] Li C, Li Y, Wu Y, et al. Synthesis of zinc oxide nanocrystals by thermal decomposition of Zn-oleate in organic medium. Sci China, Ser E Technol Sci. 2008;51:2075–2079.

[136] Urbanski M. On the impact of nanoparticle doping on the electro-optic response of nematic hosts. Liq Cryst Today [Internet]. 2015;24:102–115. Available from: http://dx.doi.org/10.1080/1358314X.2015.1059586.

[137] Su H, Zhang J, Wang C, et al. Vertical Alignment of Liquid-Crystal Molecules due to Unilateral Anchoring from Charge Accumulation at the Semiconductor Interface. Phys Rev Appl [Internet]. 2019;12:1. Available from: https://doi.org/10.1103/PhysRevApplied.12.064029.

[138] Urbanski M, Mirzaei J, Hegmann T, et al. Nanoparticle doping in nematic liquid crystals: Distinction between surface and bulk effects by numerical simulations. ChemPhysChem. 2014;15:1395–1404.

[139] Cseh L, Mehl GH. Structure-property relationships in nematic gold nanoparticles. J Mater Chem. 2007;17:311–315.

[140] Chinky, Kumar P, Sharma V, et al. Nano particles induced vertical alignment of liquid crystal for display devices with augmented morphological and electro-optical characteristics. J Mol Struct [Internet]. 2019;1196:866–873. Available from: https://doi.org/10.1016/j.molstruc.2019.06.045.

[141] Choudhary A, George TF, Li G. Theoretical analysis of nanoparticle-induced homeotropic alignment in nematic liquid crystals. 2015; Available from:

https://arxiv.org/abs/1510.08166v1.

[142] Garbovskiy Y. Kinetics of Ion-Capturing/Ion-Releasing Processes in Liquid Crystal Devices Utilizing Contaminated Nanoparticles and Alignment Films. Nanomaterials. 2018;8:59.

[143] Lebovka N, Dadakova T, Lysetskiy L, et al. Phase transitions, intermolecular interactions and electrical conductivity behavior in carbon multiwalled nanotubes/nematic liquid crystal composites. J Mol Struct. 2008;887:135–143.

[144] Soichi Hayashi, Kazumi Kurita, Noriyuki Kimura JU, Takena T. FT-IR Studies on Molecular Structure and Orientation of a Liquid Crystal, 4’-n-Octyl-4-cyanobiphenyl. Bull Inst Chem Res. 1985;63.

[145] Smela E, Martínez-miranda LJ. X-Ray Study of Liquid Crystal Alignment: Evidence for an Alternate Mesophase at the Free Surface? Mol Cryst Liq Cryst. 1991;203:1–8.

[146] Schweicher G, Gbabode G, Quist F, et al. Homeotropic and planar alignment of discotic liquid crystals: The role of the columnar mesophase. Chem Mater. 2009;21:5867–5874.

[147] Van Aerle NAJM. Anchoring of 4-n-alkyl-4’-cyanobiphenyl liquid crystal molecules on rubbed polyimides. Liq Cryst. 1994;17:585–588.

[148] Mishra R, Hazarika J, Hazarika A, et al. Dielectric properties of a strongly polar nematic liquid crystal compound doped with gold nanoparticles. Liq Cryst [Internet]. 2018;45:1661–1671. Available from: https://doi.org/10.1080/02678292.2018.1478995.

[149] Tang CY, Huang SM, Lee W. Electrical properties of nematic liquid crystals doped with anatase TiO2 nanoparticles. J Phys D Appl Phys. 2011;44.

[150] Singh S. Impact of dispersion of nanoscale particles on the properties of nematic liquid crystals. Crystals. 2019;9.

[151] Sakai Y, Nishida N, Shiraki H, et al. Dielectric properties of twisted nematic liquid crystal displays fabricated by doping Ag-Pd metal nanoparticles having a long term stability. Mol Cryst Liq Cryst. 2005;441:143–152.

[152] Shiraishi Y, Toshima N, Maeda K, et al. Frequency modulation response of a liquid-crystal electro-optic device doped with nanoparticles. Appl Phys Lett. 2002;81:2845–2847.

[153] Kobayashi S, Miyama T, Nishida N, et al. Dielectric spectroscopy of metal nanoparticle doped liquid crystal displays exhibiting frequency modulation response. IEEE/OSA J Disp Technol. 2006;2:121–128.

[154] Shivakumar U, Mirzaei J, Feng X, et al. Nanoparticles: Complex and multifaceted additives for liquid crystals. Liq Cryst. 2011;38:1495–1514.

[155] Ouskova E, Buchnev O, Reshetnyak V, et al. Dielectric relaxation spectroscopy of a nematic liquid crystal doped with ferroelectric Sn2P2S6 nanoparticles. Liq Cryst. 2003;30:1235–1239.

[156] Prakash J, Khan S, Chauhan S, et al. Metal oxide-nanoparticles and liquid crystal composites: A review of recent progress. J Mol Liq [Internet]. 2020;297:112052. Available from: https://doi.org/10.1016/j.molliq.2019.112052.

[157] Chandran A, Prakash J, Naik KK, et al. Preparation and characterization of MgO nanoparticles/ferroelectric liquid crystal composites for faster display devices with improved contrast. J Mater Chem C. 2014;2:1844–1853.

[158] Eskalen H, Öz↓an, Alver, et al. Electro-optical properties of liquid crystals composite with zinc oxide nanoparticles. Acta Phys Pol A. 2015;127:756–760.

[159] Venkataraman A, Amadi EV, Chen Y, et al. Carbon Nanotube Assembly and Integration for Applications. Nanoscale Res Lett. 2019;14.

[160] Podgornov F V., Wipf R, Stühn B, et al. Low-frequency relaxation modes in ferroelectric liquid crystal/gold nanoparticle dispersion: impact of nanoparticle shape. Liq Cryst [Internet]. 2016;43:1536–1547. Available from: http://dx.doi.org/10.1080/02678292.2016.1186754.

[161] Sugisawa H, Toriumi H, Watanabe H. Time-Resolved FT-IR Analysis of Electric Field-Induced Reorientation Dynamics in Nematic 4-Pentyl-(4-cyanophenyl)-Cyclohexane Liquid Crystals. Mol Cryst Liq Cryst Sci Technol Sect A Mol Cryst Liq Cryst. 1992;214:11–22.

[162] Osipov MA, Ostrovskii BI. Study of the orientational order in liquid crystals by x-ray scattering. Crystallogr Rev. 1992;3:113–152.

[163] Basu R, Iannacchione GS. Evidence for directed self-assembly of quantum dots in a nematic liquid crystal. Phys Rev E - Stat Nonlinear, Soft Matter Phys. 2009;80:3–6.

[164] Gruler H. The Elastic Constants of a Nematic Liquid Crystal. Zeitschrift fur Naturforsch - Sect A J Phys Sci. 1975;30:230–234.

[165] Gruler H. Elastic Constants of Nematic Liquid Crystals. Z Naturforsch. 1972;28a:765–770.

[166] ALFRED S Von. Temperaturabhängigkeit und Größe der Deformationskonstanten nematischer Flüssigkeiten. Z Naturforsch. 1960;15a:810–814.

[167] Blinov LM, Chigrinov VG, Patel JS. Electro-Optic Effects in Liquid Crystal Materials. Phys. Today. 1995.

[168] Kim YB, Hur IK. High speed response time of nematic liquid crystal mixtures for lcd monitor and tv applications. J Inf Disp. 2001;2:32–38.

[169] Lisetski LN, Minenko SS, Fedoryako AP, et al. Dispersions of multiwalled carbon nanotubes in different nematic mesogens: The study of optical transmittance and electrical conductivity. Phys E Low-Dimensional Syst Nanostructures. 2009;41:431–435.

[170] Bates MA. Nematic-isotropic transition in polydisperse systems of infinitely thin hard platelets. J Chem Phys. 1999;110:6553–6559.

[171] Cheng B, Samulski ET. Hydrothermal synthesis of one-dimensional ZnO nanostructures with different aspect ratios. Chem Commun. 2004;4:986–987.

[172] Mishra S, Manjuladevi V, Gupta R. Effect of shape of ZnO nanoparticle on electro-optic and dielectric properties of nematic liquid crystal. J Mol Liq [Internet]. 2023;386:122482. Available from: https://doi.org/10.1016/j.molliq.2023.122482.

BRIEF BIOGRAPHY OF SUPERVISOR

Prof. V. Manjuladevi is Professor in the Department of physics, Birla Institute of Technology & Science (BITS Pilani), Pilani Campus. Prof. V. Manjuladevi completed her PhD from Raman Research Institute (RRI), Bangaluru, India in 2004. She was a postdoctoral fellow at Trinity College, Dublin, Ireland during 2004-2006.

The major research interests of Prof. V. Manjuladevi include experimental soft condensed matter, especially, the investigation of fundamental properties and applications of liquid crystals and composites of liquid crystals with nanomaterials. The research includes measurement of electro-optic switching and dielectric properties of pure and nanocomposites of liquid crystals, V-shaped switching properties of ferroelectric liquid crystals, properties of liquid crystal in bulk and at interfaces, thin films of liquid crystals and applications of liquid crystals in displays, switchable windows, sensors etc. She has completed several research projects funded by DST-SERB as principal investigator or co-principal investigator. She has authored/co-authored 60+ research articles in international journals of repute. And is also a reviewer of high impact international journals such as Nature Comm, Nanoscale letters, Journal of molecular liquids etc. Till date, 3 PhD students have graduated under the guidance of Prof Manjuladevi V and she is currently guiding 4 PhD students.

BRIEF BIOGRAPHY OF STUDENT

Ms. Mishra Shweta Ravindra has completed her M.Sc. in Physics from University of Pune, Pune, India in 2016. She is currently pursuing her PhD under the guidance of Prof. Manjuladevi V, Department of Physics, BITS Pilani, Pilani Campus, India. Her current research interest includes experimental condensed matter physics, viz., synthesis and characterization of nanomaterials, electro-optic and dielectric properties of liquid crystals and investigation of physical properties of composite systems of nanomaterials with liquid crystals. She has published four research articles in international journals of repute and few manuscripts are under review/ preparation. She has also attended several national and international conferences and presented her work and received awards.

PUBLICATIONS

➢ Articles

- Experimental evidence of continuous isotropic-nematic phase transition in CdS nanowire nanocomposites of a nematic liquid crystal, **S Mishra**, V Manjuladevi, RK Gupta, S Kumar, Liquid Crystals 48 (8), 1151-1161, 1, 2021
- Frequency dependence of dielectric permittivity and conductivity of functionalized carbon nanotube-nematic liquid crystal nanocomposite, SJ Shivaraja, **S Mishra**, K Dutta, RK Gupta, V Manjuladevi, Journal of Molecular Liquids 349, 118168, 2022 *(not a part of this thesis)*
- Zinc Oleate Nanorod-Induced Vertical Alignment of Nematic Liquid Crystal, **Shweta Mishra**, Manjuladevi V, Raj Kumar Gupta, ACS Omega, 7, 50, 46466–46474, 2022, https://doi.org/10.1021/acsomega.2c05196
- Effect of shape of ZnO nanoparticle on electro-optic and dielectric properties of nematic liquid crystal, **Shweta Mishra**, Manjuladevi V, Raj Kumar Gupta, J Mol Liq; 386:122482, 2023. https://doi.org/10.1016/j.molliq.2023.122482.
- Effect of size of ZnO nanorods on electro-optic and dielectric properties of nematic liquid crystal, **Shweta Mishra**, Manjuladevi V, Raj Kumar Gupta (in preparation)

➢ Conference Proceedings

- Investigation on physical properties of silver nanorod doped nematic liquid crystal, **S Mishra**, V Manjuladevi, RK Gupta, S Kumar, AIP Conference Proceedings 2369 (1), 020065,1,2021
- Dielectric spectroscopy studies of silver nanorod doped nematic liquid crystal, **S Mishra**, AM Sontakke, RK Gupta, S Kumar, V Manjuladevi, Materials Today: Proceedings 50, 2587-2591,2022

CONFERENCES & WORKSHOPS

- 4th International Conference on Soft Materials, MNIT Jaipur, India, Dec 2020
  Title of the talk: Dielectric spectroscopy studies of silver nanorod doped nematic liquid crystal

- National Conference on Physics and Chemistry of Materials (NCPCM), Govt Holkar Science College, Indore, India, Dec 2020
  Title of the talk: Investigation on physical properties of silver nanorods doped nematic liquid crystal **(Best Paper Award)**

- International Conference on Liquid Crystals, Liquid Crystalline Polymers and Nanosystems (ICLCPN), MG University, Kottayam, India, Dec 2019
  Title of the talk: Nematic liquid crystal doped with CdS nanowires: an experimental investigation **(2nd Prize in short invited talks)**

- National Conference on Liquid Crystals (NCLC), 2019, 2020, India

- Workshop on ‘SOFT AND ACTIVE MATTER’, School of Physics, University of Hyderabad, India, February 2018